DOCTOR OF PHILOSOPHY

AC electrokinetic bioassays

development of electrorotation assay for detection of viable and non-viable bacteria and macromolecules

Mitchell, Clare

Award date:
2001

Awarding institution:
Bangor University

A THESIS SUBMITTED TO THE UNIVERSITY OF WALES

IN CANDIDATURE FOR THE DEGREE OF

DOCTOR OF PHILOSOPHY

A.C. ELECTROKINETIC BIOASSAYS. DEVELOPMENT OF ELECTROROTATION ASSAY FOR DETECTION OF VIABLE AND NON-VIABLE BACTERIA AND MACROMOLECULES.

BY

Clare Mitchell

B.Eng. Electronics Engineering

School of Electronic Engineering Science and Computer Systems

University of Wales, Bangor, Gwynedd. U.K.

10th May 2001

ACKNOWLEDGEMENTS

I would like to take this opportunity to thank the many people who have assisted me during the course of this work.

I am particularly grateful to my two supervisors, Dr. Stephen Bone and Professor Ron Pethig, for their encouragement and advice during this project.

I am grateful to Dr Gerard Markx and Mr. John Kerslake for assisting with the transition into the multidisciplinary nature of this work. I would also like to express my thanks to Drs Andrew Goater, Julian Burt, Mark Talary, Xiao-Feng Zhou, Sally Cotterill and Richard Lee of Bangor University, and to Dr Mike Arnold of the Industrial Research Labs, Lower Hutt, New Zealand. My thanks also go to my colleagues Gary Lock, Colin Dalton and John Tame.

I would also like to gratefully acknowledge the award of an EPSRC-CASE research studentship in collaboration with Severn Trent Water Ltd..

Finally, I would like to thank my husband David, for his support and understanding.

SUMMARY

The work described is primarily concerned with the understanding of the induced AC electrokinetic properties of latex particle complexes. The assays are based on the electrorotational response of elliptical latex particles to the binding of bacteria or biomacromolecular species.

Two coliform bacteria systems were investigated, gram-negative *E. coli* and gram-positive *B. subtilis*. Latex particles were coated in antibodies against these two bacteria and this resulted in adhesion of the bacteria to the latex particles when placed together in an aqueous suspension. The electrorotational response of both viable and non-viable *E.coli* and *B. Subtilis* bound to particles was investigated. The resulting assay proved to be sufficiently sensitive to be able to detect at the single organism level and it was possible to measure the bound bacterial concentration. In addition, the bacteria possessed distinct electrorotational properties and it proved possible to distinguish between the two species. This section of the work is likely to be of benefit to the water and food industries.

The effect of binding antibodies and nucleic acids to the surface of latex particles was also investigated. It was found possible to detect the presence of nucleic acid on the particle surface using electrorotation measurements. For antibody-coated particles, it was possible to distinguish between primary, secondary and tertiary antibody coating. In addition, binding of gold conjugated antibodies was found to elicit a considerably greater change in the electrorotational characteristics of the system. These findings have potential benefits in medical diagnostic applications.

Contents

Chapter 1

Introduction

1.1 Introduction

The foods that we eat are rarely, if ever, sterile, they contain microbes[1]. The micro-organisms present will originate from the natural microflora of the raw material and those organisms introduced during the harvesting/slaughtering, processing, storage and distribution. In most cases these microbes have no discernible effect and can be consumed with no adverse effects. In some instances, these microbes can manifest themselves in the following ways:

- they can cause spoilage;
- they can cause foodborne illness.

It has been estimated that the average loss in cereals and legumes exceeds 10 %. For more perishable items the figure is more than 20 %, increasing to an estimated 25 % for highly perishable items like fish. The US Academy of Sciences has estimated that the losses of legumes and cereals in developing countries as 100 million tonnes, enough to feed 300 million people.

Despite our increased food hygiene knowledge today, 'Foodborne diseases is perhaps the most widespread health problem in the world and an important cause of reduced economic productivity'[2]. The bacteria investigated in this study were *E. coli* (K12) and *B. subtilis*. Between 1980 and 1995 the number of *Bacillus* food poisoning cases reached a high of 418 cases in 1988.

Most *E. coli* that are found in the human intestine are harmless but Vero cytotoxin-producing *E. coli* produce potent toxins that can cause severe disease in humans. One such example is *E. coli* O157 VTEC. This disease is being increasingly found, see figure 1.1.

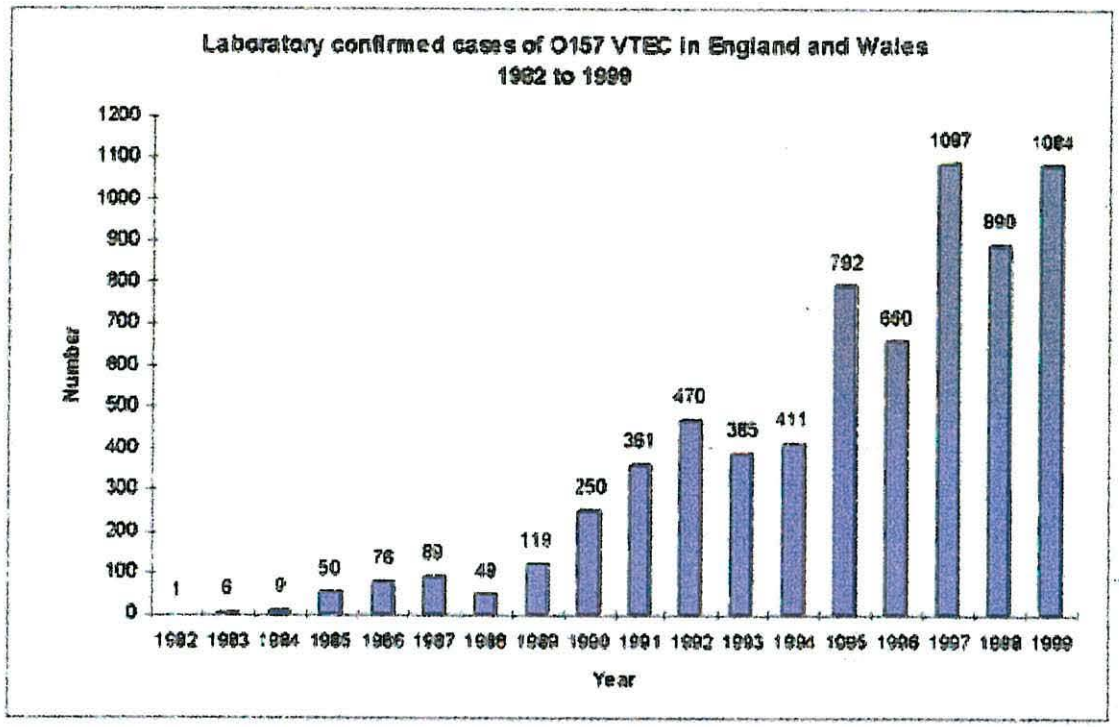

Figure 1.1 Public Health Laboratory figures on the rising number of confirmed cases of *E. coli* O157 VTEC[3].

Since *E. coli* is a coliform bacteria it may also be found in our water supplies, which may have been contaminated with sewage. The presence of coliform bacteria, in particular *E. coli*, is the principle micro-biological parameter used to determine the sanitary quality of drinking water[4]. For regulatory purposes tests must be able to detect low levels of contamination, one target organism per 100 ml. In a report by the Standing Committee of Analysts, presence-absence tests for coliform organisms and *Escherichia coli* were evaluated. They high-lighted some problems with the tests which were the number of false positives that the tests yielded and the length of time to obtain a result, averaging at 28 hours. There is a clearly a need for improved testing for coliform bacteria against these outbreaks and to help reduce food spoilage.

In addition to the observations that it is necessary to detect the presence of harmful microbes, there is also an increasing awareness that the early detection of diseases is of great importance. For example, two relatively common heritable cancer risk genes have recently been located. Among people with colon cancer, it appears that up to 10% carry an altered germline copy of a gene called *MSH2*[5, 6, 7]. Individuals with an altered *MSH2*

gene face approximately an 80% risk of colon cancer. Women also have an elevated risk of uterine and ovarian cancer. Intense medical surveillance, including annual colonoscopy beginning in the third decade, may be beneficial in preventing colon cancer deaths in this high- risk group[8].

Similarly, approximately 5% of women with breast cancer have inherited an altered copy of the *BRCA1* gene, which has been pinpointed to a small region of chromosome 17. As the gene itself has not yet been identified, *BRCA1* mutation carriers currently can only be identified by linkage analysis, which requires DNA samples from several affected relatives. A woman with an inherited *BRCA1* mutation faces approximately an 85% lifetime risk of breast cancer and an elevated risk of ovarian cancer[9]. Medical or surgical interventions may be effective in reducing the risk of cancer death for these women[10, 11].

The National Advisory Council for Human Genome Research, the advisory body to the National Center for Human Genome Research, found that despite the promise of these discoveries for benefiting humankind, it is premature to offer testing of either high-risk families or the general population as part of general medical practice until a series of crucial questions has been addressed[12]. Of the questions they identified, they included the necessity of wide-spread testing, across all risk groups, and the issue of quality control of results. There clearly exists a requirement for reliable, cheap methods of testing for blood analytes, such as DNA.

Latex agglutination tests were invented in 1956 when Singer and Plotz developed a rheumatoid factor test[13]. Particles are now used as supports for sandwich tests, e.g. used in particle capture enzyme linked immunosorbent tests and assays (ELISA's). Dyed microspheres now function as the colour tags in commercially available sandwich-type pregnancy tests as well as laboratory tests for drug abuse[14]. Uniform latex particles have been used, since 1956, as solid supports for antibody-antigen interactions. In this study, a uniform latex particle will be used as a solid support upon which the affects of these interactions will be monitored using electrorotation.

1.2 The Electrorotation Assay

Pohl[15] described that non-uniform fields can sometimes induce a torque on a particle, causing it to rotate. The term electrorotation was first used to describe the motion of particles in rotating electric fields by Arnold and Zimmerman[16] and Mischel et al[17]. Electrorotation has been reviewed in several journal articles (Arnold and Zimmermann[18], Pethig[19], Schnelle et al[20]) and has been described in texts (Jones[21], Pethig[22, 23]). The electrorotation force on a particle depends on the dielectric properties of the particle and the suspending medium, for further details see the Theory chapter.

In brief, the magnitude and direction of the electrorotation force on a particle suspended in a dielectric medium depends on a number of factors including, the particle permittivity and conductivity, the medium permittivity and conductivity as well as the field strength and frequency. The fact that the electrorotation force is dependent on such a variety of parameters makes electrorotation a powerful tool for particle characterisation, especially biological particles.

1.3 Overview of research in Electrorotation

A great deal of work has been carried out to elucidate the nature of the electrorotation force, in connection with dielectrophoresis (Wang *et al*[24, 25]) and travelling wave dielectrophoresis (Huang, *et al*[26], Wang *et al*[27]). Specifically designed electrorotation electrodes have been used to characterise the dielectric properties of cells, starting with Arnold & Zimmerman's work on isolated plant cells[16]. Further work has been carried out on prokaryotic (Hodgson & Pethig[28]) as well as other eukaryotic cells, including the indirect examination of protozoal particles through *Plasmodium falciparum* infected erythrocytes (Gascoyne *et al*[29]) as well as direct examination of fungal cells (Asami & Yonezawa[30]) algae (Gimsa *et al*[31]) an invertebrate cell line (Freitag *et al*[32]) as well as mammalian cell lines (Gascoyne[33]) lymphocytes (Ziervogel *et al*[34]) and platelets (Egger

& Donath[35]). Acellular particles have also been investigated, as with *Plasmodium falciparum*, virus particles have been studied indirectly through their interactions with erythrocytes. Electrorotation data from non-biological particles such as artificial liposomes (Chan *et al*[36]) have been of use in verifying the theoretical nature of the electrorotation force, as these are simple membraned cellular particles. Latex micro-particles have similarly been of use in probing the effects of surface groups and charges on the electrorotation spectra (Arnold, et al[37], Maier[38]).

Arnold and Zimmerman[18] have demonstrated that electrorotation measurements provide a very sensitive method for monitoring the physiological state of cells and determining their sensitivity to exposure to chemicals and other agents. Diagnosis of bacterial contamination using electrorotation has several advantages. Firstly, it is non-invasive, allowing it to become part of a series of simultaneous investigations. Secondly, it functions at the single organism level, which can be extremely important when accurate viability information for low numbers of organisms is required, as is the case for water testing (one target organism per 100 ml).

The information gained from such studies includes particle characterisation and monitoring of changes in the physiological state of the cell. Finally, particle viability information can be obtained (Gundel et al[39], Zhou *et al*[40], Dalton *et al*[41]). The use of electrorotation for particle characterisation and for determining viability are explored in this thesis, using coliform bacteria *Escherichia coli* and *Bascillus subtilis*.

So far, there has not been a comprehensive analysis of the affect of antibody attachment to latex particles of the electrorotation properties of the particles. The use of electrorotation for determining antibody attachment and the affects of subsequent bindings of antibody to the spectra of latex particles is investigated in this work. In addition, the affect of gold conjugates is also explored.

1.4 Thesis outline

Chapter Two contains a review of dielectric theory and the electric field manipulation techniques used in this thesis. Chapter Three contains a review of the materials and methods used in this work. It reviews the theory behind the main reagents used in this work, including polystyrene latex particles, bacteria, nucleic acids and antibodies. The methods, such as the antibody attachment protocol are also discussed in this section. Chapter Four presents electrorotation results for uncoated latex particles and shows how the particles are sensitive to changes in their environment. Chapter Five presents electrorotation results for antibody coated beads with bacteria attached, highlighting the sensitivity to be achieved using this assay for detecting low concentrations of bacteria. Chapter Six describes the affect of antibody attachment on the electrorotation spectra of latex particles, and the subsequent attachment of unconjugated and gold-conjugated antibodies.

1.5 References

[1] Adams MR and Moss MO. Food Microbiology. 1995. The Royal Society of Chemistry.

[2] World Health Organisation. WHO Commission of Health and Environment. Report of the Panel on Food and Agriculture. 1992, WHO/EHE/92..2: 191.

[3] PHLS Vero Cytotoxin-Producing *Escherichia coli* O157 Fact Sheet. Updated: 22 March 2000

[4] Standing Committee of Analysts. An evaluation of presence-absence tests for coliform organisms and *Escherichia coli*. 1996. HMSO Publications.

[5] Fishel R, Lesco MK, Rao MRS, et al. The human mutator gene homolog MSH2 and its association with hereditary nonpolyposis colon cancer. *Cell*. 1993;75:1027-1038.

[6] Leach FS, Nicolaides NC, Papadopoulos N, et al. Mutations of a muts homolog in hereditary non-polyposis colorectal cancer. *Cell*. 1993;75:1215-1225.

[7] Parsons R, Li GM, Longley MJ, et al. Hypermutability and mismatch repair deficiency in rer+ tumor cells. *Cell*. 1993; 75:1227-1236.

[8] Lynch HT, Smyrk TC, Watson P, et al. Genetics, natural history, tumor spectrum, and pathology of hereditary nonpolyposis colorectal cancer: an updated review. *Gastroenterology*. 1993;104:1535-1549.

[9] Easton DF, Bishop DT, Ford D, et al. Genetic linkage analysis in familial breast and ovarian cancer: results from 214 families. *Am J Hum Genet*. 1993; 52:678-701.

[10] Biesecker BB, Boehnke M, Calzone K, et al. Genetic counselling for families with inherited susceptibility to breast and ovarian cancer. *JAMA*. 1993; 269:1970-1974.

[11] King MC, Rowell S, Love S. Inherited breast and ovarian cancer: what are the risks? what are the choices? *JAMA*. 1993; 269:1975-1980.

[12] National Advisory Council for Human Genome Research, National Center for Human Genome Research, National Institutes of Health, U.S. Department of Health and Human Services. Published in the *Journal of the American Medical Association* 1994; 271:785.

[13] Singer JM and Plotz CM. The latex fixation test. 1. Application to the serologic diagnosis of rheumatoid arthritis. *Am. J. Med.* 1956; 21: 888.

[14] Bangs LB. New developments in particle-based tests and immunoassays. 1993. The Latex Course. Bangs Laboratories, Inc.

[15] Pohl HA. Dielectrophoresis. 1978. Cambridge University Press, Cambridge.

[16] Arnold, W.M. & Zimmermann, U. Rotating-field-induced rotation and measurement of the membrane capacitance of single mesophyll cells of *Avena sativa. Zeitschrift fur Naturforsch.* 1982; 37c: 908-915.

[17] Mischel, M., Voss, A. & Pohl, H.A. Cellular spin resonance in rotating electric fields. *Journal of Biological Physics.* 1982; 10: 223-226.

[18] Arnold, W.M. & Zimmermann, U. Electrorotation : development of a technique for dielectric measurements on individual cells and particles. *Journal of Electrostatics* 1988; 21: 151-191.

[19] Pethig, R. Biological electrostatics - Dielectrophoresis and Electrorotation. *Institute of Physics Conference Series.* 1991; 118: 13-26.

[20] Schnelle, T, Glasser, H. & Fuhr, G. Opto-electronic technique for automatic detection of electrorotational spectra of single cells. *Cellular Engineering.* 1997; 2: 33-41.

[21] Jones, T.B. *Electromechanics of Particles.* Cambridge University Press, Cambridge. 1995. p 212.

[22] Pethig, R. Application of AC electrical fields to the manipulation and characterisation of cells. *In: Automation in Biotechnology.* (Ed. I., Karube), 1991, pp. 159-185. Elsevier, Amsterdam.

[23] Pethig, R. Dielectric and A.C. Electrodynamic properties of cells. In: *Bioelectrodynamics and biocommunication.* (Eds. M.W. Ho, F-A. Popp & U. Warnke) 1994. Ch. 9, pp. 229-249.

[24] Wang, X-B, Pethig, R. & Jones, T.B. Relationship of dielectrophoretic and electrorotational behaviour exhibited by polarised particles. *Journal of Physics D-Applied Physics.* 1992; 25: 905-912.

[25] Wang, X-B., Huang, Y., Holzel, R., Burt, J.P.H. & Pethig, R. Theoretical and experimental investigations of the interdependence of the dielectric , dielectrophoretic and electrorotational behaviour of colloidal particles. *Journal of Physics D-Applied Physics.* 1993; 26: 312-322.

[26] Huang, Y., Wang, X-B, Tame, J. & Pethig, R. Electrokinetic behaviour of colloidal particles in travelling electric fields: Studies using yeast cells. *Journal of Physics D-Applied Physics.* 1993; 26: 1528-1535.

[27] Wang, X-B., Huang, Y., Becker, F.F. & Gascoyne P.R.C. A unified theory of dielectrophoresis and travelling wave dielectrophoresis. *Journal of Physics D-Applied Physics.* 1994; 27: 1571-1574.

[28] Hodgson, C.E. & Pethig, R. Determination of the viability of *Escherichia coli* at the single organism level by electrorotation. *Clinical Chemistry.* 1998; 44: 2049-2051.

[29] Gascoyne, P., Pethig, R., Satayavivid, J., Becker, F.F. & Ruchirawat, M. Dielectrophoretic detection of changes in erythrocyte membranes following malarial infection. *Biochimica et Biophysica Acta-Biomembranes.* 1997; 1323: 240-252.

[30] Asami, K. & Yonezawa, T. Dielectric behaviour of wild-type yeast and vacuole deficient mutant over a frequency range of 10kHz to 10GHz. *Biophysical Journal* 1996; 71: 2192-2200.

[31] Gimsa, J., Marszlatek, P., Loewe, U. & Tsong, T.Y. Dielectrophoresis and electrorotation of *Neurospora* slime and murine myeloma cells. *Biophysical Journal* 1991; 60: 749-760.

[32] Freitag, R., Schügerl, K., Arnold, W.M. & Zimmermann, U. The effect of osmotic and mechanical stress and enzymatic digestion on the electrorotation of insect cells (*Spodoptera frugiperda*). *Journal of Biotechnology.* 1989; 11: 325-336.

[33] Gascoyne, P.R.C., Wang, X-B., Huang, Y. & Becker, F.F. Dielectrophoretic separation of cancer cells from blood. *IEEE Transactions on Industry Applications.* 1997; 33: 670-678.

[34] Ziervogel, H., Glaser, R., Schadow, D. & Heymann, S. Electrorotation of lymphocytes, the influence of membrane events and nucleus. *Bioscience reports.* 1986; 6: 973-982.

[35] Egger, M. & Donath, E. Electrorotation measurements of diamide-induced platelet activation changes. *Biophysical Journal.* 1995; 68: 364-372.

[36] Chan, K.L., Gascoyne, P.R.C., Becker, F.F. & Pethig, R. Electrorotation of liposomes: verification of dielectric multi-shell model for cells. *Biochimica et Biophysica Acta-Lipids and Lipid metabolism.* 1997; 1349: 182-196.

[37] Arnold, W.M., Schwan, H.P. & Zimmermann, U. Surface conductance and other properties of latex particles measured by electrorotation. *Journal of Physical Chemistry.* 1987; 91: 5093-5098.

[38] Maier, H. Electrorotation of colloidal particles and cells depends on surface charge. *Biophysical Journal.* 1997; 73: 1617-1626.

[39] Gundel, J., Wicher, D., & Matthies, H. Electrorotation as a Viability Test for Isolated Single Animal-Cells. *Studia Biophysica.* 1989; 133: 5-18.

[40] Zhou, X.F., Markx, G.H., Pethig, R. & Eastwood, I.M. Differentiation of viable and nonviable bacterial biofilms using electrorotation. *Biochimica et Biophysica Acta-General Subjects.* 1995; 1245: 85-93.

[41] Dalton C, Goater AD, Pethig R and Smith HV. Viability of Giardia intestinalis Cysts and Vaibility and Sporulation State of Cyclospora cayetanensis Oocysts Determined by Electrorotation. Appl. Environ. Microbiol. 2001; 67(2): 586-590.

Chapter 2

Theory

2.1 Introduction

If a particle is exposed to an external electric field, it becomes electrically polarized. A.C. electrokinetics describes how this externally applied alternating electric field can induce motion on a particle.

Microelectrodes, fabricated on glass microscope slides using photolithography[1, 2, 3], can be used to create various forms of localised electric fields having frequencies covering the range from around 100 Hz to 10 MHz. They can generate various types of electric field and have motional influences on a particle. For this work electrorotation was chosen as the method of investigation. Electrorotation produces a rotational torque on a particle by producing a rotating electric field. This is generated by energising four electrodes with sinusoidal voltages of 90° phase separation. This results a rotational movement of the particle. The rate and direction of the resulting motion is dependent on the dielectric properties of the dielectric particle and its suspending medium.

Using a suitable mathematical model for the particle and analysing the response of a particle to an applied electric field, information can be obtained about the nature of the dielectric particle upon which motion is imparted.

2.2 Dielectric Properties of Materials

Consider a capacitor system, which consists of two electrodes separated by an insulating material, known as a *dielectric*. When an electric field is applied across the capacitor, the dielectric becomes polarized, which, very simply, means it has formed positive and negative charges at the surface of the dielectric.

An important property of the dielectric is its *resistivity* which is a measure of the resistance, R, a charge experiences travelling through the material. The inverse of the resistance is known as the *conductance*, G, which is the ease with which charge is transported through a medium. Another important property of the dielectric is its charge storage capability, known as its *capacitance*, C. Both the capacitance and conductance are dependent on the frequency of the applied field, and the variation of C and G with frequency describe a materials dielectric properties. The mathematical equations relating these factors are given below:

$$G = \frac{1}{R} = \frac{\sigma A}{d} \text{ and } C = \frac{Q}{V} = \frac{\varepsilon_o \varepsilon_r A}{d} \qquad (1)$$

where A is the capacitor plate surface area and is d distance between the plates, σ is the electrical conductivity of the material, Q is the charge on the charge on the capacitor, V the voltage between the plates, ε_o and ε_r are the *permittivity of free space*, which is a constant, and the *relative permittivity* of the material.

The relative permittivity is a ratio of the capacitance with the appropriate dielectric compared to that of a capacitance filled with a vacuum. Therefore, the action of a dielectric is to increase the charge storage capability of a capacitor. It manages to do so because at the surfaces of the dielectric charges appear which are of opposite sign to the charges on the electrodes. The surface charges on the dielectric offset the mutual repulsion's of the charges on the plates, enabling greater charges to accumulate there. The capacitance increases by a factor equal to the relative permittivity of the dielectric.

Thus, it can be said that the relative permittivity is a representation of the polarizability of the material.

Some molecules, in a given dielectric, may possess permanent dipoles because of a non-homogeneous charge distribution[10]. When an electric field is applied the positive and negative elements of the dipole experience opposite forces and will be displaced relative to each other. These moving charges, on the application of an external electric field, constitute a transient current, known as the *displacement current*. How successfully a dipole can move in synchronization with an alternating field depends on the size of the molecule, the viscosity of the medium and the frequency of oscillation. At relatively high frequencies the dipoles will find it more difficult to keep up with the alternating field. This results in losses in the amount of current able to cross the dielectric and is known as the *dielectric loss*, ε'', and is sometimes expressed as $\tan \delta$, see section 2.2.1 for further details. The changes in the relative permittivity and the dielectric loss with frequency are discussed, in more detail, in the following section.

2.2.1 Complex Permittivity and the Debye Equation

If a sinusoidal alternating electric field of relatively low frequency is applied to the dielectric, the dipoles will try to align themselves along the field lines with the same frequency. If the electric field and the dipole moment are sufficiently large the dipoles will align themselves along the field lines and the displacement current, that is, the electromagnetic energy, is transmitted through the material without any loss. As the frequency increases, the dipoles find it harder to orientate themselves to the field. At this stage, some of the electromagnetic energy is lost as it is converted into Joule heating of the dielectric and this is the dielectric loss. In addition, the amount of charge stored by the capacitor decreases, as the dipoles are no longer polarized to a maximum extent, resulting in a decrease in the permittivity. At very high frequencies the dipoles are unable to respond to the alternating field, therefore no displacement current can flow through the medium. This results in no dielectric losses occurring and the charge storage capability of the dielectric becomes equivalent to that of a non-polar dielectric.

In order to picture this situation clearly it may be useful to describe this in terms of tan δ. The diagram below is an equivalent circuit for a real capacitor, that is, a capacitor that has losses.

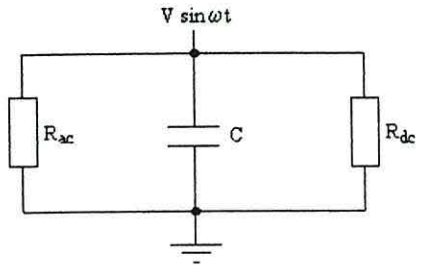

Figure 2.1 Equivalent circuit of a real capacitor.

If the dipoles dissipate energy on oscillation it can be thought that there is a resistance to their movement represented by a resistor, R_{ac}, in parallel with a perfect capacitor, C. Thus, the power loss is due to the current through the resistor. In a 'real' dielectric some charge transport will also occur, thus resulting in the resistor, R_{dc}. However, for simplicity, it is assumed that the dielectric is a perfect insulator against D.C. current so R_{dc} is infinitely large and can be ignored. So, just the parallel RC combination is to be considered.

The currents through the resistor and capacitor are displayed in the phasor diagram below. In this diagram the resultant current is not in phase with the capacitor current but is displaced by a small angle δ.

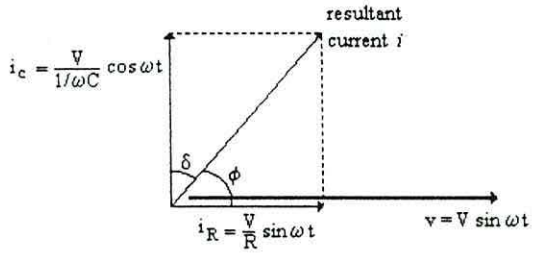

Figure 2.2 Phasor diagram for the equivalent circuit of a 'real' capacitor.

In the situation where the dipoles experience no lag with the alternating field, R_{ac} is considered infinitely large, resulting in no current flow through the resistor. As there is no i_R component, the resultant current is in phase with the capacitor current, that is, the

current is 90° out of phase with the voltage. Thus, the product $V * i = 0$, that is, all the electromagnetic energy is transmitted without loss. As the frequency increases, a component i_R develops, thus the resultant current is no longer 90° out of phase with the voltage and the product $V * i > 0$. At the high frequencies where the dipoles can no longer respond to the applied field i_R becomes zero and a loss-less situation is reached again.

By mathematical analysis of the energy held by the perfect capacitor at any instant of time and the instantaneous power dissipated through R_{ac}, tan δ can be described as the following ratio, where ω is the angular frequency:

$$\tan\delta = \frac{energy\_lost\_per\_cycle}{2\pi \times \max imum\_energy\_stored} = \frac{1}{\omega C R_{ac}} \qquad (2)$$

For a material exhibiting a dielectric loss process, a typical response of dielectric loss and permittivity with frequency are illustrated in the diagram below.

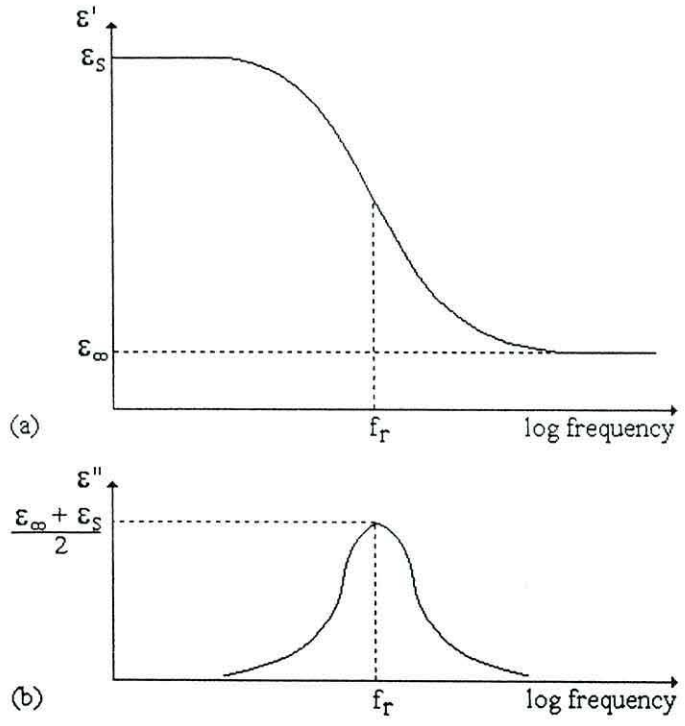

Figure 2.3 Graphs illustrating typical (a) dielectric permittivity and (b) loss with frequency.

The permittivity, ε', and the dielectric loss, ε'', are related by a complex equation, known as the *Debye Equation*[11]:

$$\varepsilon^*(\omega) = \varepsilon' - \varepsilon'' = \varepsilon_\infty + \left(\frac{\varepsilon_s - \varepsilon_\infty}{1 + j\omega\tau}\right) \tag{3}$$

Where $\varepsilon^*(\omega)$ is the *complex permittivity*, ε_s is the low-frequency relative permittivity, ε_∞ is the high-frequency relative permittivity and τ is the relaxation time and is described by the following equation:

$$\tau = \frac{1}{2\pi f_r} \tag{4}$$

Where f_r is known as the *relaxation frequency*. The real and imaginary parts can be equated to give the permittivity and dielectric loss as:

$$\varepsilon'(\omega) = \varepsilon_\infty + \frac{(\varepsilon_s - \varepsilon_\infty)}{1 + \omega\tau} \tag{5}$$

and

$$\varepsilon''(\omega) = \frac{(\varepsilon_s - \varepsilon_\infty).(\omega\tau)}{1 + \omega^2\tau^2} \tag{6}$$

The equations above are Debye equations and describe the rotational relaxation for a system with a single relaxation time, the *dielectric dispersion* having a half-height frequency width of 1.14 decades. The width of the dispersion increases if a distribution of relaxation times exists. The Debye equation is modified in the following way:

$$\varepsilon^*(\omega) = \varepsilon_\infty + \frac{\varepsilon_s - \varepsilon_\infty}{1 + (j\omega\tau)^\beta} \tag{7}$$

Where $0 < \beta \leq 1$. When a system demonstrates a single relaxation time, $\beta = 1$ and approaches zero when an infinite distribution of relaxation times is demonstrated.

2.2.2 Relaxation Time

The *relaxation time* is the time taken for the dipole to orientate itself in the applied field. Debye based the relaxation process on a simple physical model whereby the dipoles are assumed to be spheres whose movement is opposed by the microscopic viscosity of the medium. Debye relaxations occur in homogeneous media. The relaxation time for this model is given as:

$$\tau = \frac{3V\eta}{kT} = \frac{4\pi\eta r^3}{kT} \qquad (8)$$

Where V is the volume and r is the radius of the sphere, η is the viscosity of the medium, k is Boltzman's Constant and T is the absolute temperature.

2.3 Polarization Mechanisms

In general, polarization is the distortion of charge distribution, giving rise to one end having an excess positive charge and the other end having an excess negative charge. This system is then said to posses a *dipole*. The dipole is expressed as the *dipole moment, m*, and is given by:

$$m = q.d \qquad (9)$$

Where q is the magnitude of the charge and d is the separation of the charge.

The ease with which a material is polarized is expressed as the *polarizability*. The total polarizability, α_T, of a material is the sum of the electronic, atomic and orientational type polarizabilities:

$$\alpha_T = \alpha_E + \alpha_A + \alpha_O \qquad (10)$$

The different types of polarisations will be discussed in the following sections. The main type of interest is orientational induced polarisations, which includes interfacial polarization. For completeness, electronic, atomic and dipolar polarisations will be described too.

2.3.1 Gauss's Law

In a system that contains various dielectrics, the total charge Q within the system is given by:

$$Q = Q_f + Q_b \tag{11}$$

Where Q_f is the total free charge and Q_b is the total bound charge. When there are no surface charges in the system then Gauss's Law relates the outward flux of the electric field E through the surface area A to the net enclosed charge Q by:

$$\int_A E.d\hat{\mathrm{A}} = \frac{Q}{\varepsilon_0} \tag{12}$$

Where $d\hat{A}$ is the vector normal to a small element of the surface and ε_0 is the permittivity of free space. In the case where the system is inside the dielectric Gauss's Law can be expressed in the differential format:

$$\nabla.E = \frac{\rho}{\varepsilon_0} \tag{13}$$

Where $\rho = \rho_f + \rho_b$ is the total charge density.

2.3.2 Electronic Polarization

In electronic polarization, the electric field displaces the symmetrical distribution of electrons around the nucleus. This action is described in the diagrams below.

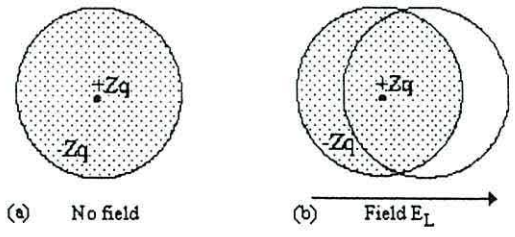

Figure 2.4 Diagram to describe the action of an electric field on an atom, electronic polarization.

A molecule can be considered to be a collection of atomic nuclei, which are positively charged, surrounded by a symmetrically distributed 'cloud' of negatively charged electrons, figure 2.4a. In an electric field the nuclei and electrons are displaced in opposite directions, figure 2.4b. Consequently, the atom has an excess of negative charge at one end and the other has an excess of positive charge. This resonance process is constant for applied alternating electric fields with frequencies up to 10^{15} Hz.

2.3.3 Atomic Polarization

When an electric field causes the atomic nuclei to move relative to each other, *atomic polarization* is said to have occurred. This type of polarization is apparent in ionic compounds. This process is described in the diagram below.

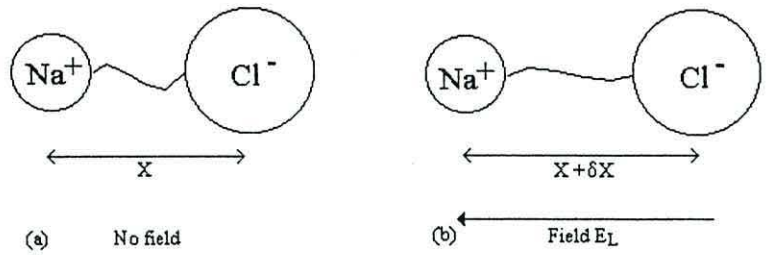

Figure 2.5 Action of an electric field on an ionic molecule.

Without the influence of an electric field the atoms are at an equilibrium distance apart, figure 2.5a. Under the influence of an electric field a displacement of the relative positions of the atoms occurs, figure 2.5b. This resonance process is constant for applied frequencies up to 10^{13} Hz.

2.3.4 Dipolar Orientational Polarization

Polar materials consist of molecules that possess a permanent dipole, such as the asymmetrical water molecule, figure 2.6a, whereas molecules like carbon dioxide, which are symmetrical, have no overall charge asymmetry and therefor have no net charge, figure 2.6b.

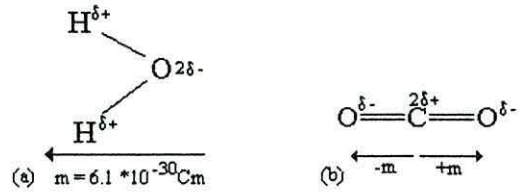

Figure 2.6 Examples of the overall dipole moments possessed by (a) a non-symmetrical molecule and (b) a symmetrical molecule.

If no electric field is present the polar molecules are randomly aligned in all directions. In an electric field the dipoles experience a torque and will try to orientate themselves with the field. The frequency range over which dipolar polarisations occur is dependent on the size of the molecule, from 10^5 Hz for large molecules to approximately 10^{10} Hz for smaller molecules. The amount of orientation depends on the Langevin function, *L(x)* where *x*:

$$x = \frac{mE_1}{kT} \tag{14}$$

m is the dipole moment and E_1 is the local electric field acting on the molecule. Where $x << 1$, *L(x)* can be simplified to:

$$L(x) = \frac{x}{3} = \frac{mE_1}{3kT} \tag{15}$$

2.3.5 Induced Orientational Polarisations

The orientational polarisations depend on the immediate environment of the molecular dipole, as described by Debye[4] type relaxations. These are characterised by the Debye equations given in section 2.2.1. If a particle carrying a net electrical charge is introduced into an electrolyte counter ions will form a weakly attracted ion 'cloud' around the particle, this is known as an electrical double layer. Under the influence of an electric field, the double layer is displaced to give an asymmetrical distribution of counter ions and charge. An induced dipole is therefore formed. This new equilibrium

will be determined by the magnitude of the field but will be opposed by a restoring force, which will try to reduce the concentration gradient to its random symmetrical distribution. This electrical double layer polarisation affect is relevant up to 50 kHz. A quantitative analysis of this effect is still under development[5] and is only of relevance to the development of the electrorotation assay when frequencies below around 1 kHz are to be employed.

2.3.5.1 Maxwell-Wagner Interfacial Polarisation

Maxwell-Wagner interfacial polarization is an example of field-induced accumulation of ions at non-conducting boundaries. This type of polarization is common in biological heterogeneous systems, which are composed of molecules exhibiting many different permittivities and conductivities. The mobility of charge carriers, such as ions, is dependent on the viscosity of its constituent phase. Therefore, when under the influence of an electric field, charge migration can occur at varying rates, for example, migration is faster in the aqueous phase rather than the lipid phase. This gives rise to a build up of charge at non-conducting boundaries resulting in a distortion in the charge in certain regions[6]. This system often exhibits dispersions and dielectric properties that are different from the constituent phases.

The magnitude of the charges involved is small, however, the large distance between the oppositely charged poles is large, which results in a large dipole moment. For example, if the charge involved were equivalent to one electronic charge, for a cell of diameter 5 μm, the dipole moment would be around 2.5 $x10^5$ Debye units (c.f. 1.84 for a water molecule). Dipole moments associated with Maxwell-Wagner interfacial polarisations can exert their influence up to frequencies of 50 MHz and beyond[7].

These heterogeneous systems can be modelled as a parallel plate capacitor that consists of two parallel different dielectrics, see figure 2.7.

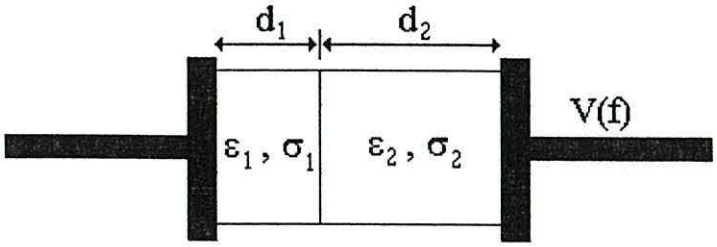

Figure 2.7. Parallel plate capacitor with an applied voltage of frequency, *f*. The plates are of surface area *A*. The gap is filled by two dielectrics of thickness d_1 and d_2, with permittivities ε_1 and ε_2 and conductivity's σ_1 and σ_2.

The mechanism by which interfacial polarisation occurs can be explained in terms of the non-uniform distribution of charges across the interface between the two differing dielectrics. The build up of charge at the interface causes polarisation in the dielectric system. This polarisation is frequency dependent.

By assuming that σ_2 is negligibly small and that ε_1, σ_2 and ε_2 are frequency independent, it is possible to obtain a simple expression for the behaviour of the dielectric system. The system can be regarded as two capacitors in series, for which the total capacitance can be found[8]:

$$\frac{1}{C} = \frac{1}{C_1} + \frac{1}{C_2} \tag{16}$$

The capacitance of the two capacitors are given by:

$$C_1 = \frac{A\varepsilon_0\left(\varepsilon_1 - \frac{j\sigma_1}{\omega\varepsilon_0}\right)}{d_1} \tag{17}$$

and

$$C_2 = \frac{A\varepsilon_0\varepsilon_2}{d_2} \tag{18}$$

Giving a total capacitance:

$$C = \frac{A\varepsilon_0\varepsilon_2\left(\varepsilon_1 - \frac{j\sigma_1}{\omega\varepsilon_0}\right)}{d_2\left(\varepsilon_1 - \frac{j\sigma_1}{\omega\varepsilon_0}\right) + d_1\varepsilon_2} \tag{19}$$

From which it can be seem that in the low frequency limit, $\omega \to 0$, the effective permittivity, ε_l, can be given by:

$$\varepsilon_l = \frac{\varepsilon_2 d}{d_2} \tag{20}$$

Where $d = d_1 + d_2$. While for the high frequency limit, $\omega \to \infty$, the effective permittivity, ε_∞, is given by:

$$\varepsilon_\infty = \frac{\varepsilon_1\varepsilon_2 d}{d_2\varepsilon_1 + d_1\varepsilon_2} \tag{21}$$

from which it can be seen that $\varepsilon_l > \varepsilon_\infty$ indicating that the system exhibits a dielectric dispersion. From an analysis of the two layer system it can be shown that the dielectric dispersions of a two layer system can be described in terms of Debye equations (5) and (6)[9] with:

$$\varepsilon_l = \frac{d(\varepsilon_1 d_1\sigma_2^2 + \varepsilon_2 d_2\sigma_1^2)}{(\sigma_1 d_2 + \sigma_2 d_1)^2} \tag{22}$$

and

$$\varepsilon_\infty = \frac{d\varepsilon_1\varepsilon_2}{\varepsilon_1 d_2 + \varepsilon_2 d_1} \tag{23}$$

and

$$\tau = \frac{\varepsilon_0(\varepsilon_1 d_1 + \varepsilon_2 d_2)}{\sigma_1 d_2 + \sigma_2 d_1} \tag{24}$$

The conductivity of the interfacial system as a whole is given by[9]:

$$\sigma = \frac{d\sigma_1\sigma_2}{\sigma_1 d_2 + \sigma_2 d_1} \qquad (25)$$

2.4 Manipulation of particles using non-uniform electric fields

The polarisation of a particle can be depicted very simply, see figure 2.8. This shows how the dipole moment is developed in a particle in a field generated by a parallel plate electrode. The field between the two plates would be uniform in the absence of the particle. As a result, no net electrical force is exerted on the particle. For example, in figure 2.8a, the forces of attraction to the anode and cathode are equal at each side of the particle, as are the forces of repulsion, in figure 2.8b, hence, there is no movement. This is not the case for particles exposed to non-uniform fields.

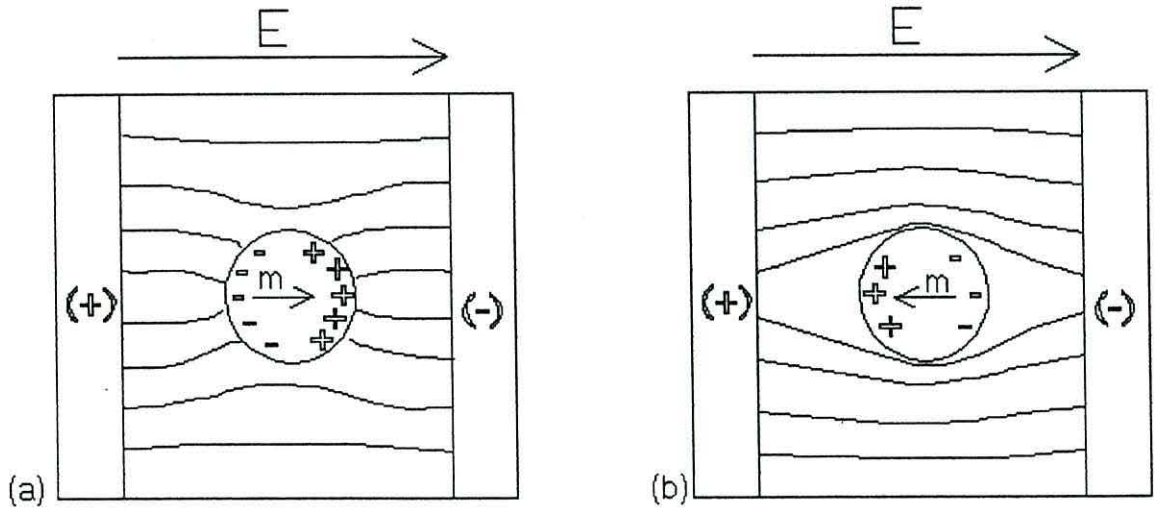

Figure 2.8. The distribution of electric charges induced at the surface of a particle and the direction of the resulting dipole moment, m. (a) Where the polarisability of the particle is greater than the surrounding medium, and (b) where the polarisability of the particle is less than the surrounding medium.

The magnitude of the dipole moment for the induced interfacial charges produced for a spherical particle of radius r, following the theories of Maxwell and Wagner, can be shown to be given by[7, 10]:

$$m = 4\pi\varepsilon_s \left(\frac{\sigma_p^* - \sigma_s^*}{\sigma_p^* + 2\sigma_s^*} \right) r^3 E \qquad (26)$$

Where ε_s is the finite dielectric permittivity of the suspending medium, E is the electric field strength and σ_p^* and σ_s^* are the complex conductivities of the particle and suspending medium.

The complex conductivity takes account of the fact that the particle and suspending medium exhibit both conduction and dielectric properties when exposed to electrical fields, and have the mathematical form:

$$\sigma^* = \sigma + j\omega\varepsilon \qquad (27)$$

Where ω is the angular frequency of the applied field and j ($=\sqrt{-1}$) indicates that the dielectric displacement current leads the conduction current by a phase angle of 90°. This equation can be rearranged to give:

$$\varepsilon^* = \varepsilon - j(\sigma/\omega) \qquad (28)$$

From this manipulation the magnitude of the dipole moment can also be written as:

$$m = 4\pi\varepsilon_s \left(\frac{\varepsilon_p^* - \varepsilon_m^*}{\varepsilon_p^* + 2\varepsilon_m^*} \right) r^3 E \qquad (29)$$

The relaxation time of this Maxwell-Wagner system can be characterised by the following equation:

$$\tau = \left(\frac{\varepsilon_p - 2\varepsilon_m}{\sigma_p + 2\sigma_m} \right) \qquad (30)$$

The frequency dependence of the effective dipole moment is described by:

$$K(\omega) = \frac{\varepsilon_p^* - \varepsilon_m^*}{\varepsilon_p^* + 2\varepsilon_m^*} = \frac{\sigma_p - \sigma_m}{\sigma_p - 2\sigma_m} \tag{31}$$

This expression is known as the Clausius-Mossotti factor. The Clausius-Mossotti factor is correct under conditions where the characteristic size of the electric field is large compared to the size of the particle, and the particle is sufficiently far away from other dielectric objects to not be influenced by their dipole moments.

Equations 26 and 27 describe the magnitude, polarity and time response of the dipole moment induced in a particle by an electric field. They provide the basis for understanding how various forms of A.C. fields may be used to selectively manipulate bioparticles. Three phenomena will be discussed, dielectrophoresis, electrorotation and travelling wave. The area of interest is electrorotation, however, the others have been included for completeness.

2.4.1 Dielectrophoresis

When a polarisable particle is suspended in a dielectric medium and exposed to an electric field the particle polarises. In a non-uniform electric field, the forces will not be balanced (unlike in a uniform field) and the particle will experience a force. Pohl termed this induced force dielectrophoresis[11, 12, 13, 14]. Particles that are more polarisable than their suspending medium experience a dielectrophoretic force that attracts them to the high field region. Particles of lower polarisability, than their suspending medium, are repelled from high field areas. See figure 2.9.

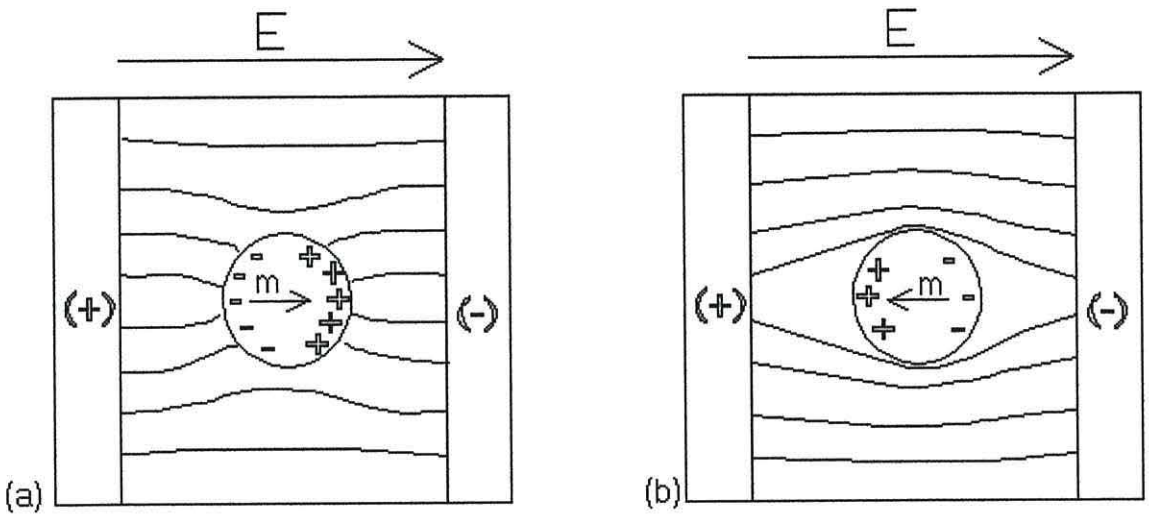

Figure 2.9. Two particles in a non-uniform field. The particle on the left is more polarisable than its suspending medium and is attracted to the high field region, at the pin electrode. The particle of low polarisability, on the left, is repelled from the high field area.

2.4.1.1 Dielectrophoretic force acting on a particle

When a particle is subjected to conditions that causes it to experience a net dipole moment, it will have centres of positive and negative charges that are equally separated by distance *d*, see figure 2.10.

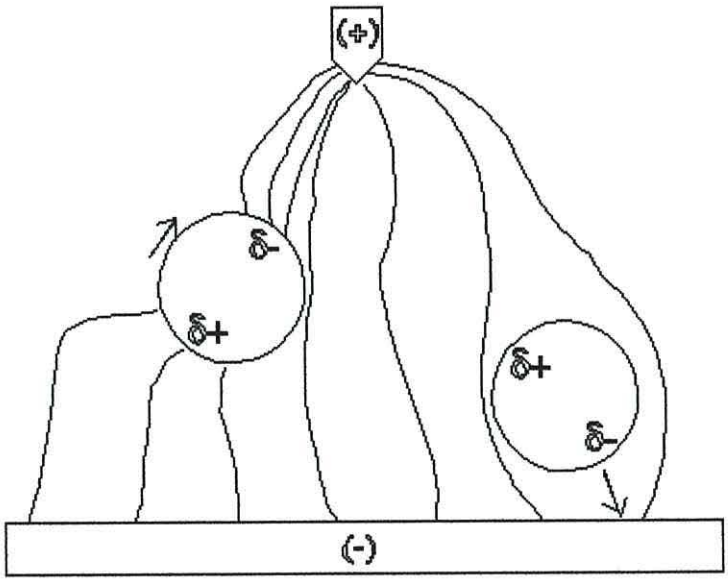

Figure 2.10. The net force on a dipole given by $m = qd$ in a non-uniform field. The electric field vectors show the direction and magnitude of the electric field at the positive and negative charges.

In a non-uniform field, E, the total electric force acting on a particle, of net charge Q, with radius r, is:

$$F = QE(r+d) - QE(r) \tag{32}$$

For the case where d is small compared to the non-uniformity of the field:

$$F = QE + \delta qE(r_+) - \delta qE(r_-) = QE + (m.\nabla).E \tag{33}$$

Where ∇ is the del vector operator. If the particle is uncharged, i.e. $Q = 0$, or for frequencies above approximately 1kHz, where electrophoretic affects are negligible, the term on the right-hand side of the above equation, involving the dipole moment and field gradient, will dominate, resulting the time-averaged force becoming:

$$F(\omega) = \mathrm{Re}\{m(\omega)\}\nabla E^2 / 2E \tag{34}$$

Where Re denotes that the *real* part of the dipole moment is involved. It can be seen that the dielectrophoretic force is directed along the gradient of the electric field. Substituting for m, from equation 29:

$$F(\omega) = 2\pi\varepsilon_1 r^3 \,\mathrm{Re}[K(\omega)]\nabla E^2 / 2E \tag{35}$$

Where $K(\omega)$ is the Clausius-Mossotti factor described in equation 31. For positive dielectrophoresis to occur $K(\omega)$ must be greater than 0, that is $\varepsilon_2 > \varepsilon_1$. In this case the particles are attracted to electric field maxima and are repelled from the minima. For negative dielectrophoresis $K(\omega)$ must be less than 0, that is $\varepsilon_2 < \varepsilon_1$. In this case, the particles are attracted to electric field minima and are repelled from the maxima.

2.4.2 Electrorotation

Pohl[12] described that non-uniform fields can sometimes induce a torque on a particle, causing it to rotate. However, the controlled way to induce particle rotation is to subject it to a rotating electric field, the first reports of this were given by Arnold and Zimmerman[15] and Mischel et al[16]. By changing the electrical connections to give 90° phase difference between adjacent electrodes, see figure 2.11, a rotating electric field is generated.

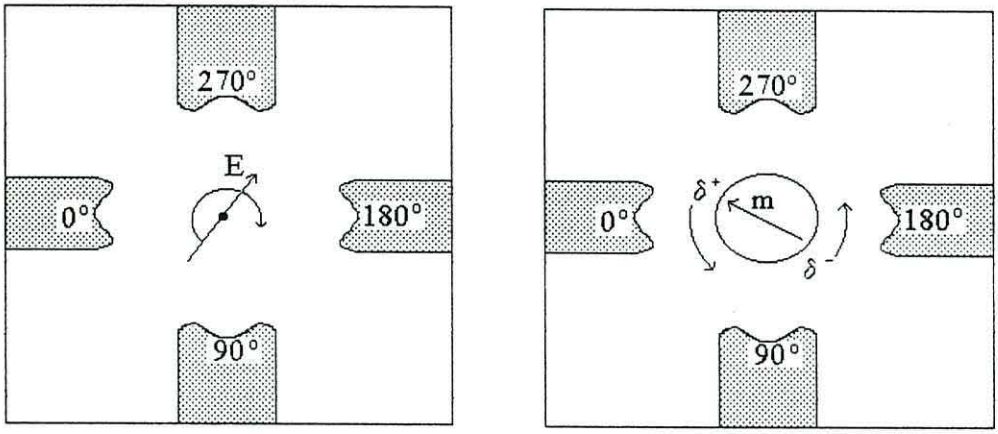

(a) (b)

Figure 2.11. Bone electrode structure, with illustration of rotating electric field. (a) Co-field electrorotation of a particle. (b) Anti-field electrorotation of a particle.

Both co-field and anti-field rotation, in the same sense and opposite sense of the field, can be observed. In practical terms, anti-field rotation occurs when the polarizability of the particle appears to be less than that of the suspending medium and as will be the case, for example, for viable micro-organisms who have a resistive cytoplasmic membrane. Co-field rotation occurs for particles having polarizabilities greater than that of the surrounding medium, for example carboxylated latex particles.

2.4.2.1 Electrorotational Force on a Particle

Consider a particle that is exposed to an externally applied electric field that causes the particle to have centres of positive and negative charge equal in magnitude but separated by distance *d* giving rise to a dipole moment, see figure 2.12. Initially, this

dipole moment will not be aligned with the field, causing the dipole to experience a torque. The torque is caused by the positive and negative charges experiencing a force ($F = qE$) that are equal in magnitude but that act in opposite directions. These forces result in the dipole experiencing a rotational torque to try to align with the field.

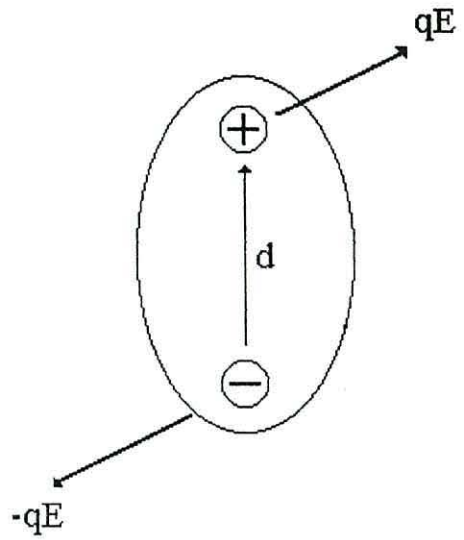

Figure 2.12. Force components creating a net torque on a dipole, $m = qd$, in an electric field. The positive and negative charges generate forces in opposite directions, these generate a torque as the dipole tries to align itself with the electric field.

The net torque exerted by an applied electric field on a dipole can be found by considering the net force acting about the centre of a small dipole[17]. Each of the charges contributes to the torque:

$$\Gamma = \frac{d}{2} \times qE + \frac{-d}{2} \times (-qE) = qdE \qquad (35)$$

From which the instantaneous torque on a dipole due to an applied electric field can be found:

$$\Gamma_{dipole} = mE \qquad (36)$$

The above derivation is accurate for calculations of the torque on particles in an electric field where dimensions of the electrode are much larger than that of the dielectric particle. From the expression of the torque it can also be seen that the torque does not depend on the gradient of the electric field.

2.4.2.2 Time Averaged Torque

If the torque depends on time, as a result of the electric field being time varying of the form:

$$E = E_0 e^{j\omega t} \tag{37}$$

Where E_0 depends on position only, then the dipole moment will rotate at the same angular velocity as the electric field. However, the dipole moment and the electric field will be separated by angle θ. The time-averaged torque can be found using[17]:

$$\langle \Gamma \rangle = \frac{1}{2} \mathrm{Re}[mE^*] \tag{38}$$

Where E^* indicates the complex conjugate of E. Using the expressions for the dipole moment, equation 29, and the Clausius-Mossotti Factor, equation 31, the magnitude of the time-averaged force becomes:

$$\Gamma = 4\pi\varepsilon_m r^3 |K(\omega)| E_0^2 \sin\theta \tag{39}$$

Where θ is given by:

$$\sin\theta = -\frac{\mathrm{Im}\{K(\omega)\}}{|K(\omega)|} \tag{40}$$

It can be shown that the time averaged torque is given by[18]:

$$\Gamma = -4\pi\varepsilon_m r^3 \,\mathrm{Im}\{K(\omega)\}E_0^2 \qquad (41)$$

Expanding this we get the following equation for the time averaged rotational torque[19, 20, 21]:

$$\Gamma(\omega) = -4\pi\varepsilon_m \, r^3 \,\mathrm{Im}\left(\frac{\varepsilon_p^* - \varepsilon_m^*}{\varepsilon_p^* + 2\varepsilon_m^*}\right)E^2 \qquad (42)$$

where ε_p^* and ε_m^* are the complex permittivities of the particle and suspending medium. Thus it can be seen that the dipole moment is dependent on the dielectric properties of the total particle suspension[14]. The resulting rotational torque exerted on a particle is given by:

$$\Gamma(\omega) = -\mathrm{Im}\{m(\omega)\}E \qquad (43)$$

The symbol *Im* indicates that it is the *imaginary* component of the dipole moment that determines the rate and sense of the induced electrorotation. If the imaginary component of the Clausius-Mossotti factor is positive the torque exerted will be negative and the particle rotates in a direction that is opposite to the rotating field. If the imaginary component of the Clausius-Mossotti factor is negative the torque exerted will be positive and the particle rotates in the same sense as the electric field.

The sense and magnitude of the rotation, as seen from equation 42, are dependent on the relative dielectric properties of the particle and the suspending medium and the frequency of the applied field. These affect the phase angle of the field induced dipole moment. When the dipole moment lags the electric field by an angle of 0 to 180° co-field rotation is observed, however, if the dipole moment lags the field by more than 180° anti-field rotation takes place[22].

2.4.3 Travelling Wave

For symmetrical electrodes the rotating electric field is uniform over the central inter-electrode gap and the electrorotation behaviour is described by equation (42). However, near the electrode edges both the dielectrophoretic force and rotational torque influences the kinetic behaviour of the particle. In other words, the electrokinetic properties of the particle are influenced by both the real and imaginary parts of the dipole moment.

An electrode geometry and applied voltage arrangement where the interplay between dielectrophoretic and electrorotation affects are manipulated produces interesting electrokinetics, see figure 2.13. An electric "wave" travelling from left to right is produced by electrodes of this design if energised by cosine voltages of the indicated phase relationships. This geometry results in a particle rotating as well as directional motion. This phenomenon is termed 'travelling wave'.

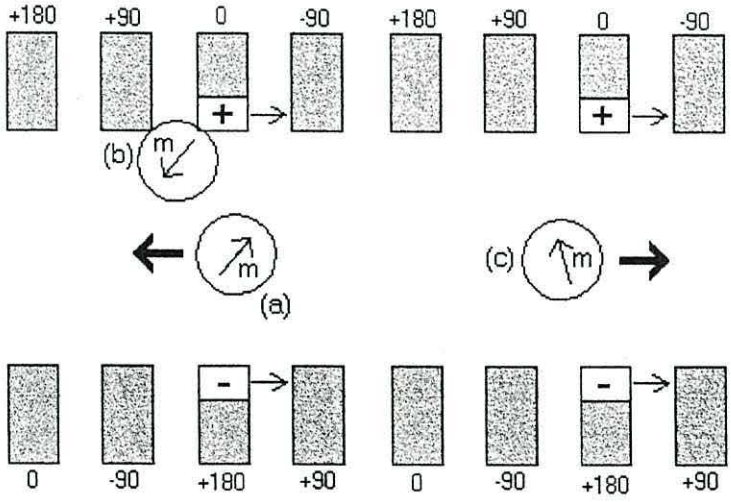

Figure 2.13. (a) Motion expected for a particle that is more polarisable than its suspending medium. (b) A cell trapped by positive dielectrophoresis. (c) Motion expected for a particle that is less polarisable than its suspending medium.

The time-averaged force acting on a particle in the centre of the channel formed in the above electrode arrangement, figure 2.13, is given by[23]:

$$F(\omega) = -\frac{\pi}{\lambda}\mathrm{Im}\{m(\omega)\}E \qquad (44)$$

Where E is the field strength across the channel and λ is the wavelength of the travelling field of value equal to the repeat distances between the electrodes of the same phase.

From equations 34, 43 and 44 we can see that the unifying link between dielectrophoretic, electrorotation and travelling wave field effects is the magnitude, polarity, and time response of the dipole moment induced in a particle. In a bioparticle, that is, a biological entity, this dipole moment represents the overall net response of the ions, polar species and the interfacial polarisations associated with its physico-chemical properties. It is also dependent on the dielectric properties of the suspending medium and frequency of the applied field. The dependence on the frequency means that we are dealing with a type of spectroscopy, where each type of particle exhibits its own unique 'identity'.

2.5 Surface Conductivity and Zeta Potential

The surface conductivity represents the charge of all ionized groups on the particle surface while the zeta potential, ζ, is the potential on the shear plane of the electrical double layer, a distance away from the surface, see figure 2.14. According to the Gouy-Chapman-Stern model for double layers the zeta potential is the potential, ψ, at the position of the Shear Plane[24].

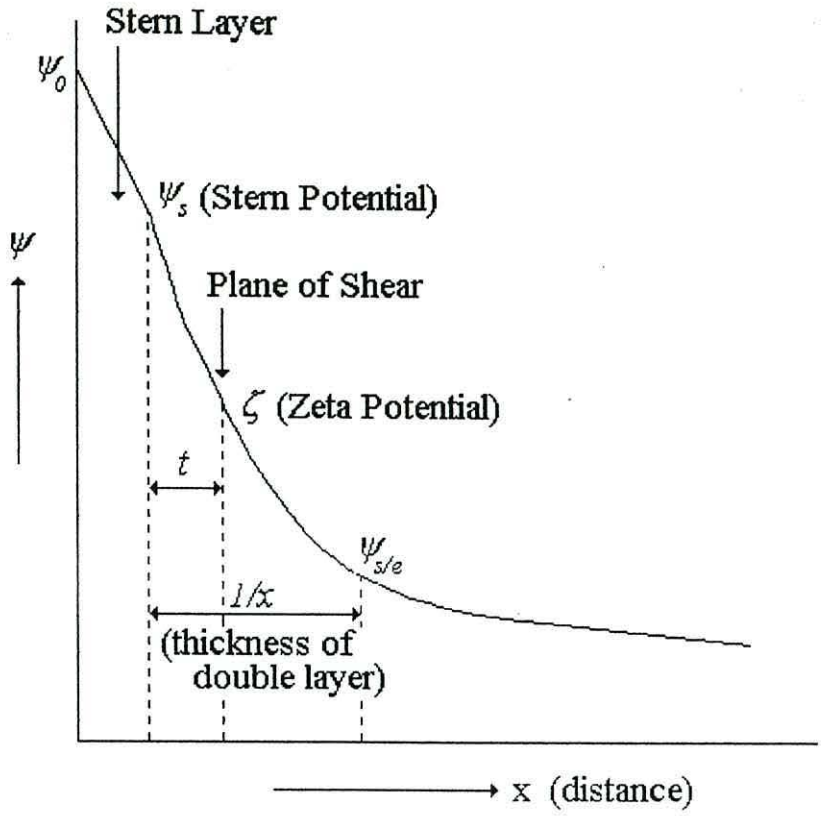

Figure 2.14. Potential distribution for the Gouy-Chapman-Stern model of the electrical double layer as a function of the distance from the solid-liquid interface.

Figure 2.14 shows the potential distribution in this double layer model as a function of the distance from the solid-liquid interface, where ψ_0 is the surface potential. The position, t, of the shear plane was estimated by the treatment of Eversole and Boardman[25], who expressed the dependence of the zeta potential on the electrolyte concentration:

$$\ln\tanh(ze\zeta / 4kT) = \ln\tanh(ze\Psi_s / 4kT) - \kappa t \qquad (45)$$

Where z is the valence of the ions, e, the charge on an electron, k, the Boltzmann Constant, T, the absolute temperature, ψ_s, the Stern potential, and κ is the Debye-Huckel parameter. For 1:1 electrolyte, the equation can be written for water solutions at 25°C:

$$\ln\tanh(9.727\times10^{-3}\zeta) = \ln\tanh(9.727\times10^{-3}\Psi_s) - 0.3285\sqrt{c}t \qquad (46)$$

Thus the position of the shear plane can estimated from the slope of the straight line equation that equation 46 provides. The zeta potential can be calculated by evaluating the equation.

2.6 Mathematical modelling

2.6.1 Single Shell

The polystyrene latex particle is a homogeneous system. It can be represented by the single shell model. Arnold et al[26] concluded that the effective conductivity, σ_p, was strongly influenced by a surface conductance K_s:

$$\sigma_p = \sigma_b + 2\frac{K_s}{r} \qquad (47)$$

Where σ_b is the bulk conductivity of the bead. This describes the expected single peak expected for single shell systems[27]. However, as will be seen in the work in this study, polystyrene latex particles exhibit two co-field peaks. One centred around 400kHz, which can be attributed to the Maxwell-Wagner effect, which the above equation (47) describes, and another below 1kHz. This behaviour, which Arnold et al[26] also observed, is considered to be anomalous since it cannot be understood using conventional theory[14, 26]. To accommodate this anomalous peak, the total conductivity of the beads becomes:

$$\sigma_p = \sigma_b + 2\frac{K_s}{r} + \frac{A}{1+(j\omega t)^{\alpha}} \qquad (48)$$

Where A and t define the magnitude and mean characteristic time constant, respectively, of the anomalous conductivity dispersion that gives rise to the low frequency anomalous peak. α is an empirical parameter describing the distribution of

relaxation times around t^{28}. These equations, along with that that describes the electrorotation rate, equation 42, can be used in the mathematical modelling program, MatLab (The Math Works Inc.) to analyse the results obtained. The MatLab program for the single shell model is contained in Appendix A.

2.6.2 Multi-Shell Model

A model that takes into account the makeup of a particle can describe a heterogeneous particle. Biological cells often consist of different components that have distinct dielectric properties. Cells might consist of a nucleus, a nuclear membrane, the cytoplasm, cytoplasmic membrane and cell membrane, see section on *E. coli* bacteria for further details.

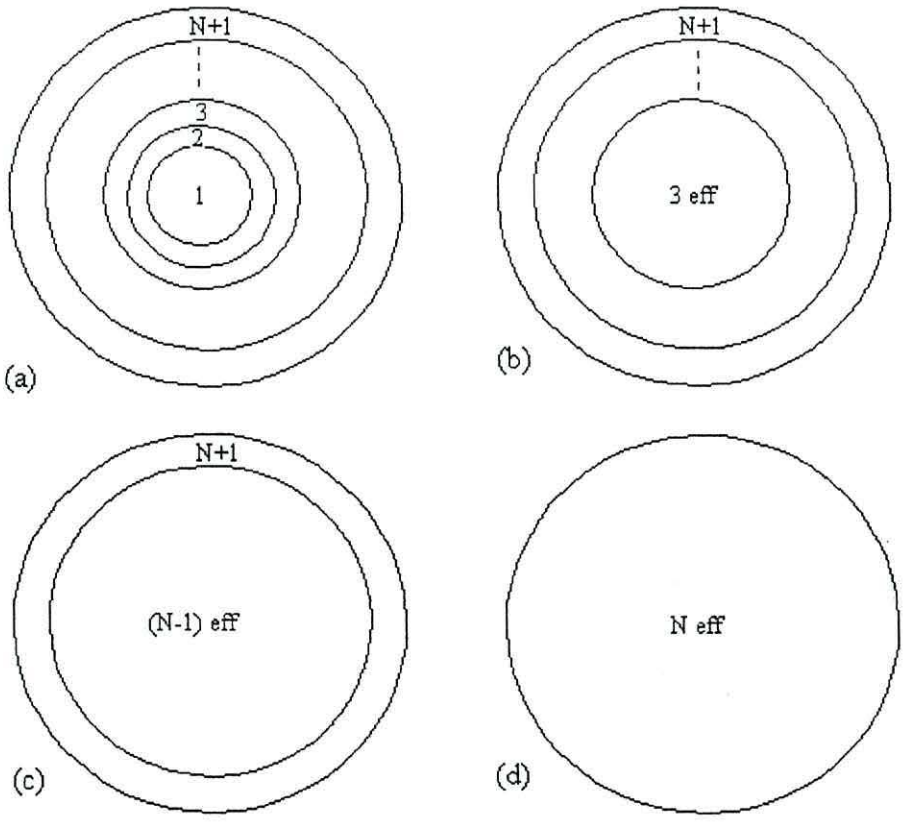

Figure 2.15. A smeared out spherical shell approach to determine the effective permittivity of a sphere consisting on *N* shells. (a) to (d) represent the effect of smearing the shells.

Such a system can be considered to consist of several layers of concentric spherical shells, see figure 2.15a. Each of the shells has a distinct complex permittivity given by:

$$\varepsilon_i^* = \varepsilon_i - j\frac{\sigma_i}{\omega} \tag{49}$$

And a distinct radius a_i, where i is 1, 2, ..., $N+1$, with $i = 1$ corresponding to the inner most layer. A smeared out can be used to describe the effective complex permittivity of such a particle[29, 30]. It was later adapted[31] for the calculation of electrorotation torque on a cell in a rotating electric field. The effective complex permittivity of a particle composed of $N-1$ concentric spheres[1]:

$$\varepsilon_{peff}^* = \varepsilon_{N+1}^* \frac{\left[\left(\frac{a_{N-1}}{a_N}\right)^3 + 2f(\varepsilon_{(N-1)eff}^* \varepsilon_{N+1}^*)\right]}{\left[\left(\frac{a_{N-1}}{a_N}\right)^3 - f(\varepsilon_{(N-1)eff}^* \varepsilon_{N+1}^*)\right]} \tag{50}$$

Where ε_{N-1}^* is the complex permittivity of the outer-most shell and $\varepsilon_{(N-1)eff}^*$ represents the effective complex permittivity of the inner-most N spheres after they have been 'smeared' together.

In this study, bacteria were attached to the surface of the particle using antibody attachment. Although the bacteria did not cover the surface of the particle, they can be modelled in the same way as described in figure 2.15. Equation 50 can be simplified:

$$\varepsilon_{eff}^* = \varepsilon_2^* \frac{\left[a^3 + 2\left(\frac{\varepsilon_1^* - \varepsilon_2^*}{\varepsilon_1^* + 2\varepsilon_2^*}\right)\right]}{\left[a^3 - \left(\frac{\varepsilon_1^* - \varepsilon_2^*}{\varepsilon_1^* + 2\varepsilon_2^*}\right)\right]} \tag{51}$$

Where subscripts '1' and '2' represent the antibody coated bead and the bacteria respectively. This equation, along with that that describes the electrorotation rate, equation 42, can be used in the mathematical modelling program, MatLab to analyse the results obtained. The MatLab program for the multi shell model is contained in Appendix B.

2.7 References

[1] Huang Y, Hölzel R, Pethig R and Wang X-B. Differences in the AC electrodynamics of viable and non-viable yeast cells determined through combined dielectrophoresis and electrorotation studies. *J. Phys. Med. Biol.* 1992; 37: 1499-1517.

[2] Zhou X-F, Markx GH and Pethig R. Effect of biocide treatment on electrorotation spectra of yeast cells. *Biochim. Biophys. Acta* 1996; 1281: 60-64.

[3] Zhou X-F, Burt JPH and Pethig R. Automatic cell electrorotation measurements: studies of the biological effects of low-frequency magnetic fields and of heat shock. *J. Phys. Med. Biol.* 1998; 43: 1075-1090.

[4] Debye P. Polar Molecules. 1947. New York: Dover.

[5] Zhou, X.F., Markx, G.H., Pethig, R. & Eastwood, I.M. Differentiation of viable and nonviable bacterial biofilms using electrorotation. *Biochimica et Biophysica Acta-General Subjects.* 1995; 1245: 85-93.

[6] K. Asami, Y. Takahashi and S. Takashima. Dielectric-properties of mouse lymphocytes and erythrocytes. *Biochim. Biophys. Acta* 1989; 1010: 49-55.

[7] Pethig R. In Automation in Biotechnology, (ed.I. Karube) Elsevier, 159-185.

[8] Pethig R. Dielectric and Electronic Properties of Biological Materials. 1979. Chichester: John Wiley and Sons.

[9] Berk LKHV. Dielectric Behaviour of Heterogeneous Systems, in Progress in Dielectrics, JB Birks, Editor. 1960. Haywood: London.

[10] Wagner KW. Arch. Elektrotech. 1914. 2:371-87.

[11] Pohl HA. J. Appl. Phys. 1958. 29:1182-1188.

[12] Pohl HA. Dielectrophoresis. Cambridge: Cambridge University Press.

[13] Wang XB, Pethig R and Jones TB. Relationship of dielectrophoretic and electrorotation behaviour exhibited by polarised particles. *J. Phys. D:Appl. Phys.* 1992; 25: 905-912.

[14] Wang XB, Huang Y, Hözel R, Burt J and Pethig R. Theoretical and experimental investigations of the interdependence of the dielectric, dielectrophoretic and electrorotational behaviour of colloidal particles. *J. Phys D:Appl. Phys.* 1993; 26: 312-322.

[15] Arnold, W.M. & Zimmermann, U. Rotating-field-induced rotation and measurement of the membrane capacitance of single mesophyll cells of *Avena sativa. Zeitschrift fur Naturforsch.* 1982; 37c: 908-915.

[16] Mischel, M., Voss, A. & Pohl, H.A. Cellular spin resonance in rotating electric fields. *Journal of Biological Physics.* 1982; 10: 223-226.

[17] Jones TB. Electromechanics of Particles. 1995, Cambridge: Cambridge University Press.

[18] Pethig R. Biological electrostatics: dielectrophoresis and electrorotation. *IOP Conference Series.* 1991; 118(1): 13-26.

[19] Fuhr, G. (1985) *Über die Rotation Dielektrischer Körper in Rotierenden*, Feldern PhD Dissertation, Humboldt-Universität, Berlin.

[20] Sauer, F.A., *Interactions Between Electromagnetic Fields and Cells*, ed A Chiabrera (New York: Plenum) 1985. pp203-51.

[21] Pethig, R., Huang, Y., Wang, X.B. and Burt, J. Positive and negative dielectrophoretic collection of colloidal particles using interdigitated castellated microelectrodes. *J. Phys. D:Appl. Phys.*, 1992; 25: 881-8.

[22] Huang, Y., Hölzel, R., Pethig, R., and Wang, X.B. differences in the ac electrodynamics of viable and nonviable yeast-cells determined through combined dielectrophoresis and electrorotation studies. *Phys. Med. Biol.* 1992; 37(7): 1499-1517.

[23] Huang Y., Wang XB, Tame JA and Pethig R. Electrokinetic behaviour of colloidal particles in travelling electric-fields - studies using yeast-cells. *J. Phys. D:Appl. Phys.* 1993; 26:1528-153.

[24] Shirahama H and Suzawa T. Surface characterization of soap-free carboxylated polymer latices. *Polymer Journal.* 1984; 16: 795-803.

[25] Eversole WG and Boardman WW. *J. Chem Phys.* 1941. 9: 798

[26] Arnold WM, Schwan HP and Zimmermann U. Surface conductance and other properties of latex-particles measured by electrorotation. *J. Phys. Chem.* 1987; 91:5093-5098.

[27] Zhou XB, Markx GH, Pethig R and Eastwood IM. Differentiation of viable and non-viable biofilms using electrorotation. *Biochim et Biophys Acta.* 1995; 1245: 85-93.

[28] Takashima S. Electrical Properties of Biopolymers and Membranes. 1989. Adam Hilger. Bristol and Philidelphia.

[29] Huang Y, Hölzel R, Pethig R and Wang XB. Differences in the AC electrodynamics of viable and non-viable yeast cells determined through combined dielectrophoresis and electrorotation studies. *Physics in Medicine and Biology.* 1992; 37(7): 1499-1517.

[30] Irimajiri A, Hanai T, and Inouye A. A dielectric theory of 'multi-stratified shell' model with its application to a lymphoma cell. *Journal of Theoretical Biology*. 1979; 78: 251-269.

[31] Furh G. Über die Rotation dielektrischer Körper in roteirenden Feldern PhD Dissertation. 1985.

Chapter 3

Materials and Methods

The aim of this chapter is to provide the reader with details of the main reagents used within this study. In particular, it provides an overview of theory considered relevant on the latex particles, antibodies, DNA and *E. coli* and *B. subtilis*. In addition, the experimental details are presented here, since the preparations were common to all of the studies. The experimental detail includes the preparation of the latex particles and bacteria, coating of the latex particles with antibody, attachment of the bacteria or antibody to the antibody coated beads and the electrorotation experimental procedure.

3.1 Materials

3.1.1 Latex Particles

Three types of non-spherical polystyrene latex particles were used in this study:

- Elliptical shaped with carboxylate modified surface groups. (Stock: P0041500CN, batch: CA1596A.)
- Elliptical shaped with no-surface group modifications. (Stock: P0043501PN, batch: PS1628B.)
- Peanut shaped with no-surface group modifications. (Stock: P0045500PN, batch: PS1405B.)

The peanut and elliptical shapes are illustrated in figure 3.1. Due to the manufacture of the particles, the particles with no-surface group modifications had sulfate groups present on their surface. The following section contains details of their manufacture. Bangs Laboratories, Inc specially manufactured the particles for this study. Latex particle manufacturers usually make their particles spherical, however, the rotation rates of the non-spherical particles are much easier to measure.

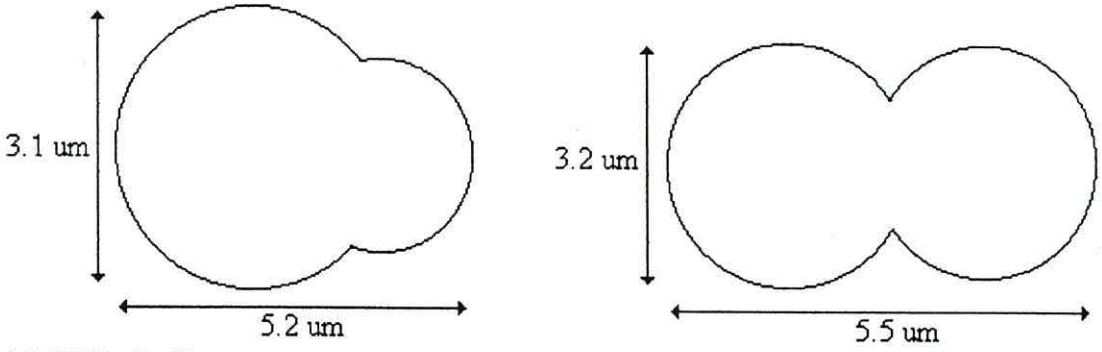

(a) 'Elliptical' **(b) 'Peanut'**

Figure 3.1. Illustration of the latex particles.

The main particles of interest were the carboxylated elliptical particles. Many protein attachment protocols exist for carboxylated latexes whose methods are widely used by manufacturers. In addition, according to the manufacturers, these particles are more stable than others, namely un-modified particles, and are less prone to flocculation problems.

3.1.1.1 Manufacture

The particles are manufactured using radical emulsion polymerisation. The following components are used:

- Water, the dispersing medium.
- Monomer: styrene. This is subject to radical polymerisation and only slightly water-soluble.
- Initiator: potassium persulfate. A water-soluble radical generator
- Emulsifier. A water-soluble molecule with amphiphilic properties, composed of a organophilic end (long-chain alkyl or alkylaryl) and a hydrophilic end (potassium or sodium salt of sulfate, sulfonate or carboxylate groups – depending on the desired surface group).

The creation of the particle can be represented by three stages[1].

- **Stage I**

  This is also known as the nucleation stage. The emulsifier tends to form micelles which are aggregates of emulsifier molecules with their hydrophobic ends directed

towards the micelle centre and their hydrophobic ends pointing out to the aqueous phase. The monomer is mechanically dispersed, forming 1-10 μm droplets stabilised by the emulsifier molecules. Part of the monomer dissolves within the micelles.

Free radicals initiate the polymerisation forming surface active oligomers. The monomer then polymerises and the micelles are gradually transformed into polymer particles. These primary particles, which are evenly sized, become unstable, flocculate and fuse together to produce a relatively polydisperse system of stable particles, see figure 3.2. At the end of this nucleation stage, the number of particles is fixed.

- **Stage II**

  The monomer contained in the droplets diffuse toward the particles and is converted to polymer. The monomer swollen particles grow until the droplets disappear.

- **Stage III**

  The residual monomer within the particle is transformed into polymer.

The technique described is called 'batch' polymerisation. It is valid for particles of small diameter, 0.1 μm to 0.4 μm. To obtain larger diameters the technique of 'seed' polymerisation is used. This involves a small latex particle being introduced at the start of the polymerisation process, thus eliminating the nucleation stage. Monomer and initiator are gradually added in order for polymerisation to proceed within the particles. This is halted once the desired diameter has been achieved. Steam flushing eliminates residual monomer.

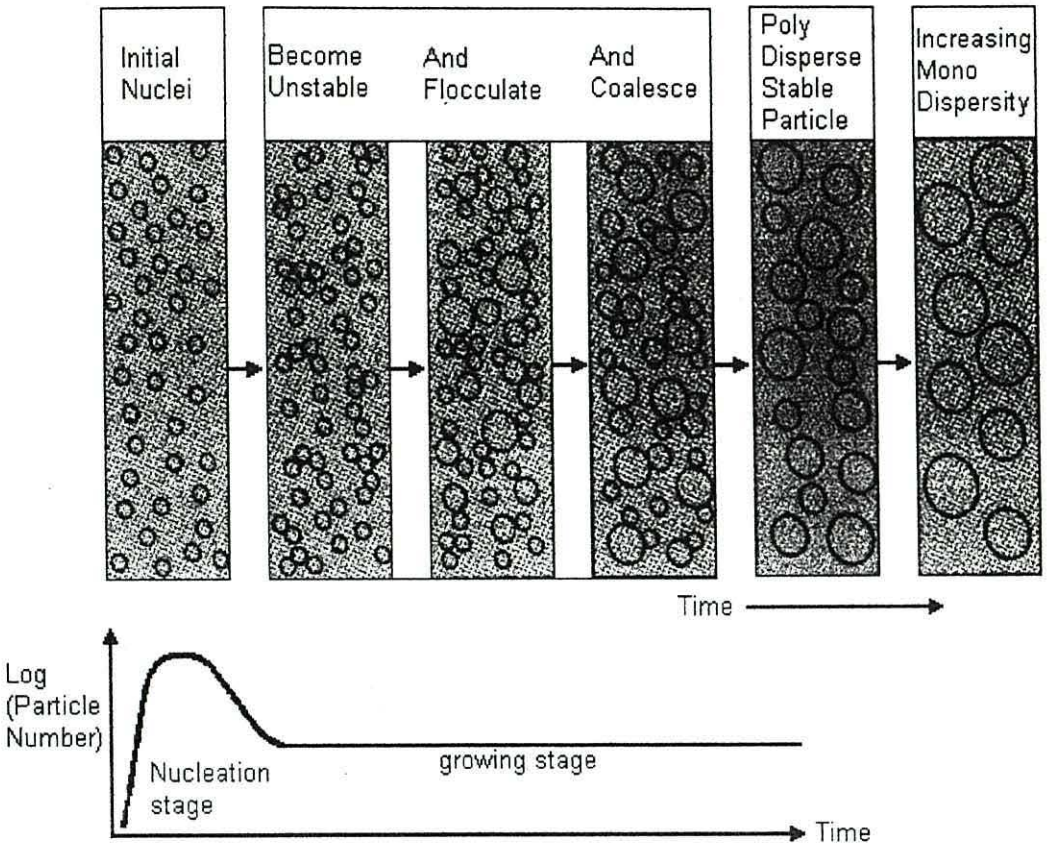

Figure 3.2. Nucleation and growth of the particles.

3.1.1.2 Structure

A typical polystyrene latex particle, after polymerisation, contains approximately 69 % water, 30 % polymer, 0.1 % to 0.5 % surfactant and 0.2 % inorganic salts[2]. Carboxylate modified particles have active hydrophilic groups –COOH, on their surfaces, which aid their stability. The polystyrene particles are made up of 'chains'of polymers, made from styrene ($C_6H_5.CH=CH_2$) monomers. After polymerisation the presence of the pendant phenyl (C_6H_5) groups is key to the properties of polystyrene. These large, ring-shaped groups prevent the polymer chains from packing in to close, crystalline arrangements, so that solid polystyrene is transparent. In addition, the phenyl rings restrict rotation of the chains around the carbon-carbon bonds, thus lending the polymer its noted rigidity, see figure 3.3 for a representation of its chemical structure.

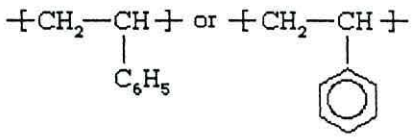

Figure 3.3. Chemical composition of a unit of polystyrene.

The long polymer chains are cross-linked to produce the particle. The cross linking is produced by the sulfate during manufacture, resulting in the formation of sulphur bridges between the chains of polymer. See figure 3.4 for an illustration.

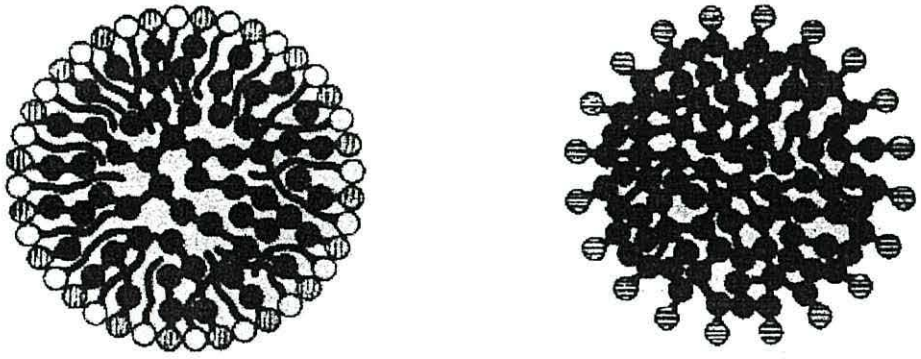

(a) **(b)**

Figure 3.4. Illustration of the latex particle, (a) before ion exchange, with sodium and potassium counter ions in the solution, (b) after ion exchange, with water-soluble electrolyte removed.

After polymerisation the latex particles will have water-soluble polymer, surfactant and sodium and potassium counter ions present. These need to be removed before the particle can be characterised, see methods section for further details.

The particles in this study have either carboxyl or sulfate groups on their surface. Conductometric titration's can be used to find the 'parking area' of a surface charge. That is the charge density of the surface acid group can be calculated from this data, from this, the average area surrounding each titratable group can be found. This is known as the parking area. For un-modified polystyrene particles the sulfate (SO_4) group's parking area is typically 200 – 900 $Å^2$, this compares to the theoretical value of 20 - 25 $Å^2$. For carboxylate-modified polystyrene particles the sulfate group's parking

area is still typically 200 – 900 $Å^2$, whereas the carboxylic acid parking area is in the region of 7-84 $Å^2$.

3.1.2 Antibodies

3.1.2.1 Theory[3]

An antibody is an immunoglobulin, that is, a protective protein produced by the immune system in response to the presence of a foreign substance, called an antigen. In this study antibodies were used to bind antigens, for example biotin, and bacteria. The bacteria are bound because they have antigens on their surface which the antibodies have been produced against.

Both antibodies and antigens are made up from groups of amino acids to form proteins. Functionally, they consist of both amine and carboxyl groups on a carbohydrate structure. They invariably have the general formula $R\text{CH}(\text{NH}_2)\text{COOH}$, where R is a group, varying in composition and structure, called a side chain. Amino acids are joined together to form long chains; most of the common proteins contain more than 100 amino acids.

The basic structure of antibodies consists of two pairs of polypeptide chains (lengths of amino acids linked by peptide bonds) that form a flexible Y shape. The stem of the Y consists of one end of each of two identical heavy chains, while each arm is composed of the remaining portion of a heavy chain and a smaller protein called the light chain. The two light chains also are identical. Within particular classes of antibodies the stem and the bottom of the arms are similar and thus are called the constant region. The tips of the arms, however, are highly variable in sequence. It is these tips that bind antigen. Thus each antibody has two identical antigen-binding sites, one at the end of each arm, see figure 3.5. The antigen-binding sites vary greatly among antibodies.

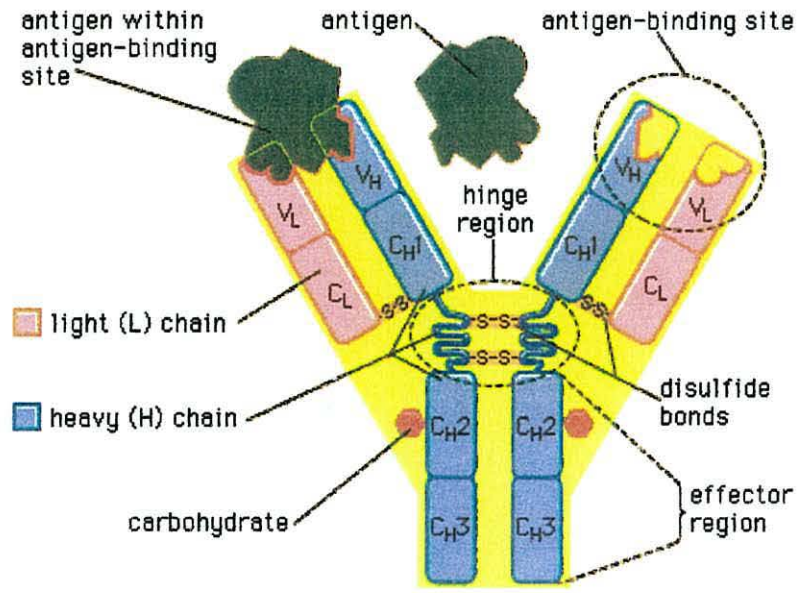

Figure 3.5 The four-chain structure of an antibody, or immunoglobulin, molecule. The basic unit is composed of two identical light (L) chains and two identical heavy (H) chains, which are held together by disulfide bonds to form a flexible Y shape. Each chain is composed of a variable (V) region and a constant (C) region.

Antibodies are grouped into five classes according to their constant region. Each class is designated by a letter attached to an abbreviation of the word *immunoglobulin*: IgG, IgM, IgA, IgD and IgE. The classes of antibody differ not only in their constant region but also in activity. For example, IgG, which was the antibody used in this study, is the most common antibody, is present mostly in the blood and tissue fluids, while IgA is found in the mucous membranes lining the respiratory and gastrointestinal tracts. See figure 3.6 for an illustration of the different forms.

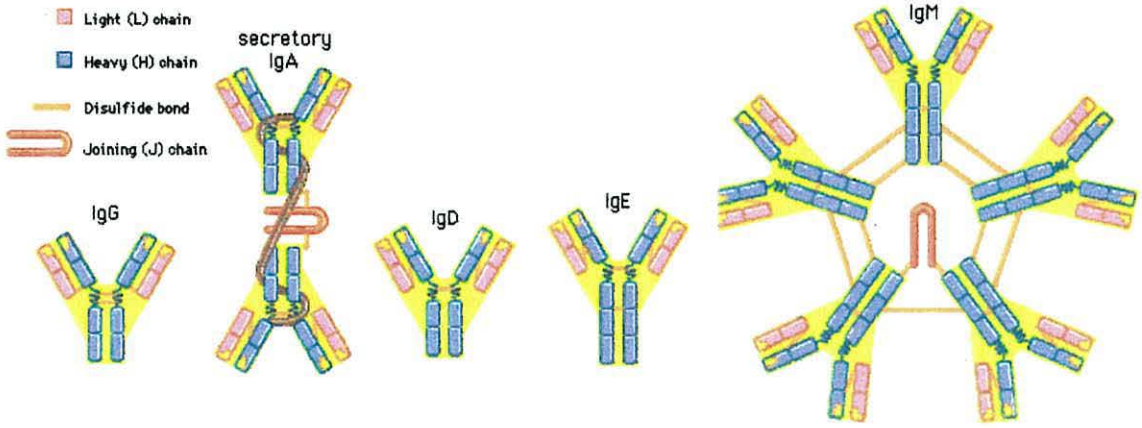

Figure 3.6. The five main classes of antibody (immunoglobulin): IgG, IgA, IgD, IgE, and IgM.

3.1.2.2 Reagents

In the *E. coli* chapter the antibodies used were:

- Polyclonal antibody against 'O' and 'K' antigens (4329-4906), in this case for use with *E. coli*, from Biogenesis.
- FITC conjugated polyclonal antibody against 'O' and 'K' antigens (4329-4916), in this case for use with *E. coli*, from Biogenesis. (Note: this FITC conjugated antibody was found to be unstable over a short period of time, that is, it lost its activity. This was attributed to the FITC conjugate, therefor, the previously described antibody was favored.)
- Monoclonal anti-gram positive antigen antibody (CM11013M), in this case for use with *B. subtilis*, from Biodesign International™.

In the Macromolecules chapter, the main reagents were:

- Monoclonal anti-gram positive antigen antibody (CM11013M), developed in mice, from Biodesign International™, this antibody is often referred to as the primary antibody.
- Anti-Mouse IgG (M-8642), developed in a Goat, is referred to as the secondary antibody, purchased from Sigma® Chemical Company
- FITC Conjugated Rabbit Anti-Goat (F 7367), a tertiary antibody, purchased from Sigma® Chemical Company.
- Gold (10nm) Conjugated Rabbit Anti-Goat (G 7652), another tertiary antibody, purchased from Sigma® Chemical Company.
- FITC Conjugated Sheep Anti-Rabbit (2AB 01F), purchased from Serotec.

3.1.3 Bacteria

Bacteria are prokaryotic single celled organisms. That is, they lack a membrane-bound nucleus and organelles. They can have spherical (coccus), rod-like (bacillus), or curved (vibrio, spirillum, or spirochete) bodies. Two types of bacteria were used in this study:

- *E. coli* (K12) (NCIMB 8797) supplied by National Collection of Industrial and Marine Bacteria Ltd., and was reproduced by growth in a nutritive solution from agar plates.

- *B. subtilis*, (NC006276) supplied by Public Health Laboratory Service, National Collection of Type Cultures, and was reproduced by growth in a nutritive solution from agar plates.

The biology of these bacteria have been comprehensively studied. Neidhardt[4] provides an extensive study of *E. coli*, similarly Sonenshein et al[5] have provided an extensive resource of *Bacillus subtilis*. This section aims to introduce the bacteria of interest.

3.1.3.1 Structure[4, 5, 6, 7]

Prokaryotic cells are fundamentally different from the eukaryotic cells that constitute all other forms of life—namely, plants, animals, fungi, and protists (protozoa and algae). Prokaryotic cells are defined by a much simpler design than is found in eukaryotic cells, most apparent is their lack of any intracellular organelles, a feature characteristically found in all eukaryotic cells. Organelles are discrete membrane-enclosed structures floating in the cytoplasm and include the nucleus. All the activities performed by organelles also take place in bacteria, but they are not carried out by specialized structures. Figure 3.7 illustrates the general structure of a bacterium cell.

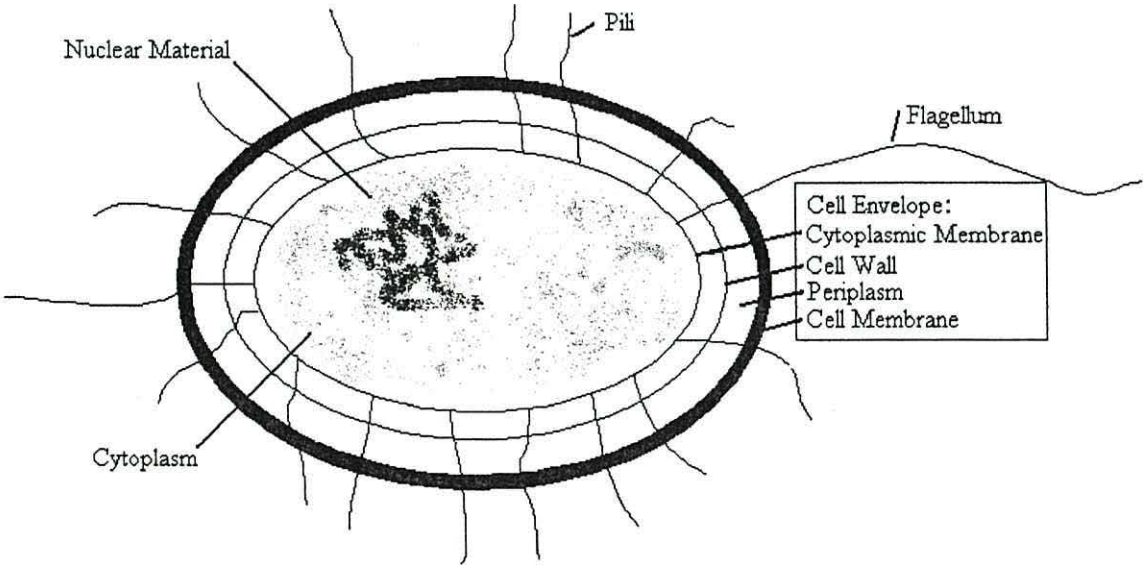

Figure 3.7. General structure of a bacterium[8].

- **Capsules and slime layers**

(Not shown of figure 3.7.) Many bacterial cells secrete some extracellular material in the form of a capsule or slime layer. A slime layer is loosely associated with the bacterium and can be easily washed off, whereas a capsule is more tightly attached and more definite in its boundary. Capsules are usually polymers of simple sugars (polysaccharides). Most capsules are hydrophilic and may help the bacterium avoid desiccation by preventing water loss. Capsules can protect a bacterial cell from ingestion and destruction by white blood cells.

- **Flagella, fimbriae, and pili**

The bacteria in this study are motile, able to swim through a liquid medium or glide or swarm across a solid surface, although not all bacteria are motile. Swimming and swarming bacteria possess flagella, which are the extracellular appendages needed for motility. Flagella are long, helical filaments made of a single type of protein and located either at the ends of rod-shaped cells, as in *Vibrio cholerae* or *Pseudomonas aeruginosa*, or all over the cell surface, as in *Escherichia coli*. The flagellum is attached at its base to a basal body in the cell membrane, which acts like a rotary motor. The protomotive force generated at the membrane is used to turn the flagellar filament, in the manner of a turbine. There can be more than one flagellum per cell, in random tumbling.

Some bacteria, such as *E. coli*, produce straight, rigid, spike-like projections called fimbriae (Latin for threads or fibers) or pili (Latin for hairs). These extend from the surface of the bacterium and attach to specific sugars on other cells, for these strains, intestinal or urinary-tract epithelial cells, respectively. Fimbriae are present only in 'gram-negative' bacteria.

- **Cytoplasm**

Nucleoid - Unlike the DNA in eukaryotic cells, which resides in the nucleus, bacterial DNA is not bound in a membrane-bound organelle but appears as a fibrillar skein distributed through the cytoplasm. In most bacteria, the DNA is present as a single,

circular chromosome. A variable number of smaller, circular DNA molecules, called plasmids, are also found in the cytoplasm and carry auxiliary information.

The amount of DNA in bacterial chromosomes ranges from 840,000 base pairs in *M. pneumoniae* to 4,700,000 base pairs in *E. coli* to 6,400,000 base pairs in the cyanobacterium *Anabaena*. The length of the *E. coli* chromosome is about 1.2 mm, compared to a cell length about 1 μm.

Cytoplasmic structures - The cytoplasm of bacteria contains high concentrations of enzymes, metabolites, and salts. All the proteins of the cell are made on ribosomes scattered throughout the cytoplasm. Granules are present in the cytoplasm, these bodies are never enclosed by a membrane and serve as storage vessels. Glycogen is stored as a reserve of carbohydrate and energy. Volutin, or metachromatic granules, contains polymerised phosphate and represents a storage form for inorganic phosphate and energy. Many bacteria possess lipid droplets. All these granules are produced in cells under favorable growth conditions and are consumed after the nutrients have been depleted from the medium. Many aquatic bacteria produce gas vacuoles, which are protein-bound structures that contain air and allow the bacteria to adjust their buoyancy. Bacteria may have internal membranous structures, which in most cases are outgrowths of the cytoplasmic membrane; mesosomes, for example, appear as whorls of extra membrane material (their function is not known).

- **The Cell Envelope**

Cytoplasmic Membrane - The cytoplasmic membrane separates the inside of the cell from its environment and regulates the flow of nutrients, maintains the proper intracellular milieu, and prevents the loss of the cell's contents. The cytoplasmic membrane carries out a large number of necessary cellular functions, including energy generation, protein secretion, chromosome segregation, and efficient active transport of nutrients. It is a typical unit membrane composed of proteins and lipids, similar to the membrane that surrounds all eukaryotic cells. It appears in electron micrographs as a triple-layered structure of lipids and proteins completely surrounding the cytoplasm, see following section for further details.

Cell Wall - Lying outside this membrane is a rigid wall, whose shape determines that of the bacterial cell. The wall is made of a large molecule called peptidoglycan, or murein. Peptidoglycan is a long-chain polymer of two repeating sugars (N-acetylglucosamine and D-acetyl muramic acid), in which adjacent sugar chains are linked to one another by peptide bridges, conferring rigid stability.

Cell Membrane - In addition, a more complex cell wall structure with multiple layers in which an outer membrane layer lies on top of the thin peptidoglycan layer may also exist. This outer membrane is composed of phospholipids, proteins with unusual properties, and lipopolysaccharides, which are inserted in the outer membrane through their lipid end and have a long chain of sugars extending away from the cell into the medium.

3.1.3.2 Differentiation of Bacteria using Gram staining

Bacteria can be divided into two broad groups on the basis of the structure of their cell envelope, 'gram-positive' and 'gram-negative' bacteria. The Danish physician Hans Christian Gram developed this form of differentiation. He found that bacteria could only be observed when magnified 1,000-times under a light microscope, details of their internal structure can be observed only with the aid of the much more powerful electron microscope. Unless special phase-contrast microscopes are used, bacteria have to be stained with a coloured dye so that they will stand out from their background. This dye is called the Gram Stain.

Bacteria are fixed to a glass slide by brief heating and then exposed to two dyes that combine to form a large blue dye complex within each cell. When the slide is flushed with an alcohol solution, gram-positive bacteria retain the blue colour and gram-negative bacteria lose it. The slide is then stained with a weaker pink dye; the gram-positive bacteria remain blue whereas the gram-negative bacteria become pink. The Gram stain reacts to differences in the structure of the bacterial cell surface, differences that become apparent when the cells are viewed under an electron microscope, see figure 3.8.

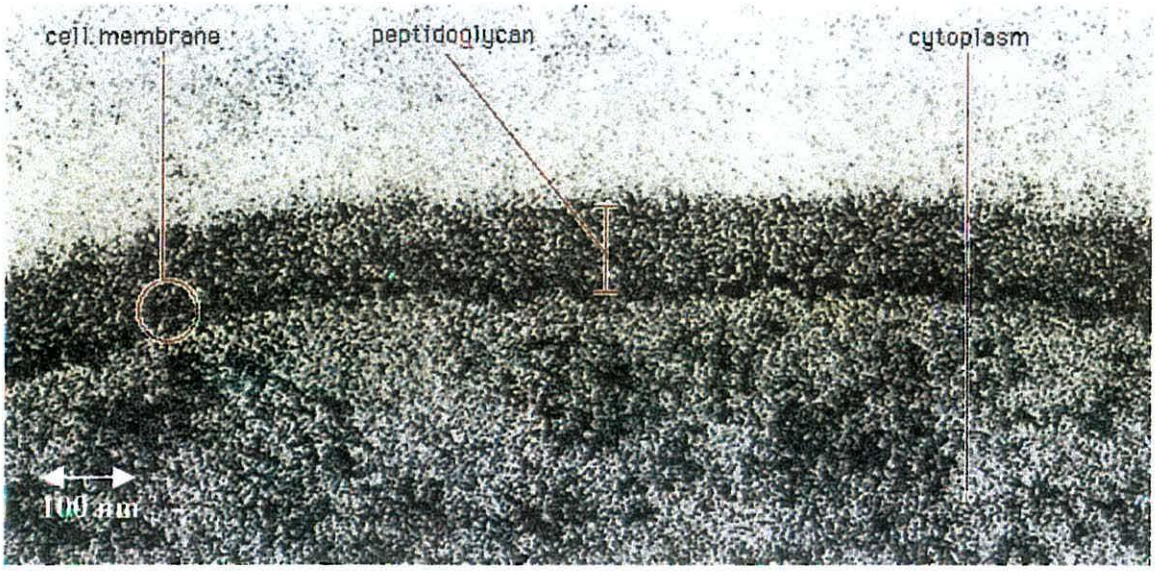

(a)

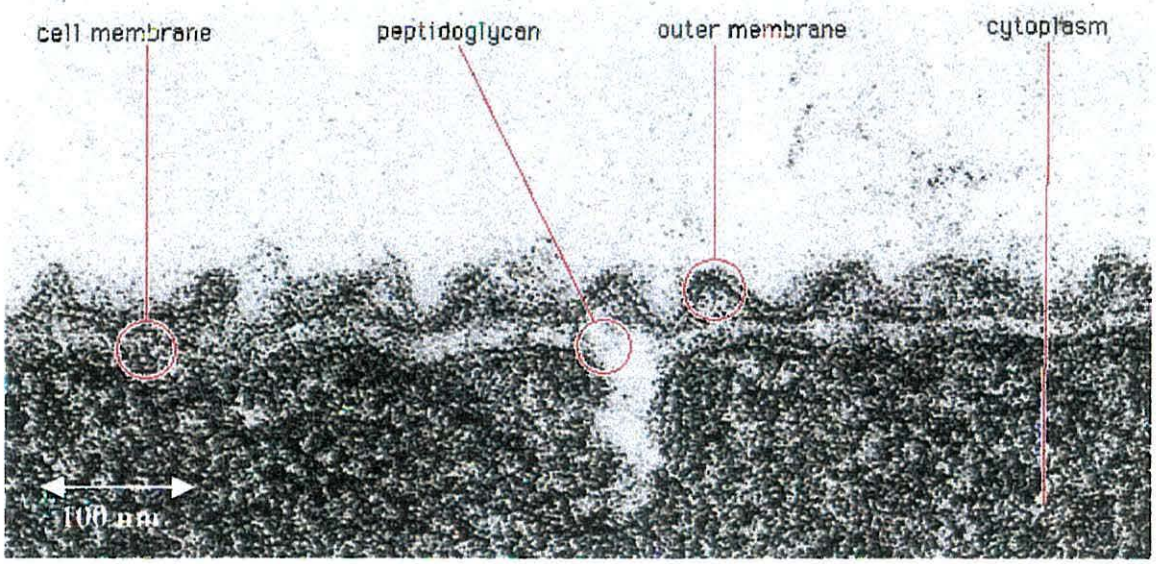

(b)

Figure 3.8. Electronmicrographs of bacterial cell walls. (a) The gram-negative bacterium *Aquaspirillum serpens;* both the cell membrane and the outer membrane are visible. (b) A portion of the gram-positive bacterium *Bacillus coagulans;* note the cell wall's thick peptidoglycan layer immediately surrounding the cell membrane.

The surface of a bacterial cell, the envelope, can vary considerably throughout the bacterial kingdoms. The one feature present in all cells is cytoplasmic membrane. In gram-positive bacteria, the peptidoglycan forms a very thick, mesh-like layer that retains the blue dye of the Gram stain by trapping it. In gram-negative bacteria, the

peptidoglycan layer is very thin (only one or two molecules deep), and the blue dye is washed out easily.

In addition, in the peptidoglycan layer the nature of the peptide bridges differs considerably among species but in general consists of four amino acids. L-alanine is linked to D-glutamic acid, then linked to either diaminopimelic acid in gram-negative bacteria or L-lysine, L-ornithine, or diaminopimelic acid in gram-positive bacteria, and finally linked to D-alanine. In gram-negative bacteria, the peptide bridges connect the D-alanine on one chain to the diaminopimelic acid on another chain. In many gram-positive bacteria, there is an additional peptide chain that extends the reach of the cross-link.

In gram-positive bacteria, the envelope is composed mainly of the thick peptidoglycan meshwork interwoven with other polymers called teichoic acids. Some proteins or lipids may be present but not in organized structures. This is in contrast with gram-negative bacteria that have a more complex cell wall structure with multiple layers in which an outer membrane layer lies on top of the thin peptidoglycan layer.

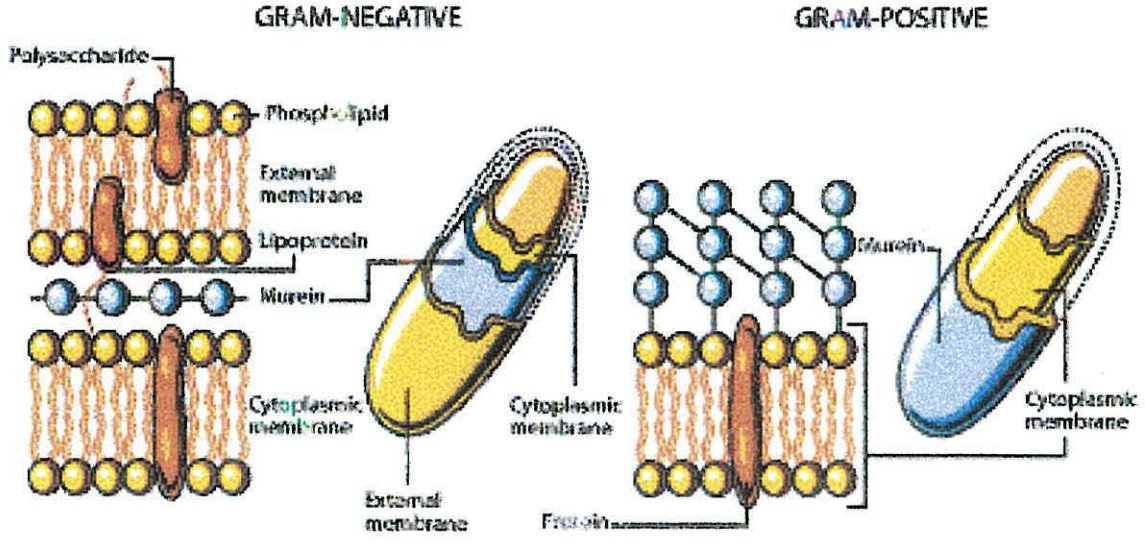

Figure 3.9. Illustration of the structure of the cell envelope in gram-negative and gram-positive bacteria.

Bacteria types can be further distinguished by the presence of specific molecules on their cell surfaces, which are detected with specific antibodies. These molecules are

antigens, see Antibodies section for further details. In the case of *E. coli*, there are hundreds of different strains (serological variants), which differ from one another solely in the antigenic identity of their lipopolysaccharide, flagella, or capsule. Similarly, there are hundreds of types of *Salmonella enteritidis*, differing only in the nature of their lipopolysaccharide sugars chains.

3.1.3.3 Growth, Nutrition and Reproduction[8]

Bacteria differ dramatically with respect to the conditions that allow their optimal growth. In terms of nutritional needs, all cells require carbon, nitrogen, sulfur, phosphorus, numerous inorganic salts (potassium, magnesium, sodium, calcium, and iron), and a large number of other elements called micronutrients (*e.g.*, zinc, copper, manganese, selenium, tungsten, and molybdenum). Carbon is the element required in greatest amount, since hydrogen and oxygen can be obtained from water that must be present as a prerequisite for growth. Also required is a source of energy to fuel the metabolism of the bacterium. The bacteria investigated in this study are examples heterotrophs, that is, they require an organic source of carbon, such as simple sugars, proteins, fats, or amino acids.

Several factors affect the rate of growth:

Oxygen – Bacteria grow well under either aerobic or anaerobic conditions, although obligate aerobes, such as Bacillus subtilis, can grow only in the presence of oxygen
E. coli is an example of a facultative anaerobe. These can alternate their metabolic processes depending on the presence of oxygen, using the more efficient process of respiration in the presence of oxygen and the less efficient process of fermentation under anaerobic conditions.

Temperature - Bacteria have adapted to a wide range of temperatures. The range of temperatures over which optimal growth can occur in any one species is about 20°C. The range in which any growth takes place spans about 40° to 50° C.

pH - Most bacteria grow in the range of neutral pH values, between 5 and 8, although a few bacterial species have adapted to life at more acidic or alkaline extremes. *Bacillus* are alkalophic bacteria, able to grow in alkaline concentration as great as pH 10 to 11.

Water - Water is a fundamental requirement for life. The majority of bacteria need a water concentration greater than 98 percent, similar to seawater.

Bacteria can reproduce using three methods: binary fission, sporulation and budding. The bacteria in this study do not reproduce by budding so it has not been included in this discussion. The two methods of interest are described below.

Binary Fission - Most bacteria reproduce by a process of binary transverse fission, in which the cell grows in volume until it divides in half to yield two identical daughter cells. Each daughter cell can continue to grow at the same rate as its parent. For this process to occur, the cell must grow over its entire surface until the time of cell division, when a new hemispherical pole forms at the division septum in the middle of the cell. *E. coli* use binary fission to reproduce. Generally, in gram-negative bacteria, the walls are flexible, and the division septum forms as the side walls pinch inward, dividing the cell in two.

Sporulation - Many environmental bacteria, including *Bacillus*, are able to produce dormant, or resting, forms as a branch of their life cycle to enhance their survival under adverse conditions. These processes are not an obligate stage of the cell's life cycle but rather an interruption. Such dormant forms are called endospores in *Bacillus* and *Clostridium*, cysts in *Azotobacter*, and heterocysts in some cyanobacteria.

One spore is formed inside each cell in response to nutritional deprivation. First, the cytoplasmic membrane invaginates around a copy of the bacterial chromosome, separating the contents of the smaller cell from the mother cell. The membrane of the mother cell engulfs the smaller cell within its cytoplasm, effectively providing two concentric unit membranes to protect the developing spore. A thin spore membrane and a thick cortex of a peptidoglycan are laid down between the two unit membranes. A rigid spore coat forms outside the cortex, enclosing the entire spore structure; it has

keratin-like properties that may resist staining and noxious chemicals. Endospores have no metabolic activity and exhibit extreme resistance to the lethal effects of heat, desiccation, freezing, chemicals, and radiation. Resistance to heat and radiation may ensue from the extremely low water content inside the spore.

3.1.4 DNA

Nucleic Acids are polymers, long chain molecules, composed of smaller building blocks known as nucleotides. Two types of nucleic acid are found in cells: Deoxyribonucleic Acid, DNA, and Ribonucleic Acid, RNA.

Genes are the units of inheritance, they are composed of DNA and are found in all cells. DNA is a long chain molecule (its molecular weight varying from 10,000 to 5,000,000) and is composed of four different types of nucleotides arranged on a sugar - phosphate backbone. The sequence of bases along the DNA chain codes for amino acids which are the building blocks of proteins. Proteins are present in all living things and are responsible for the structure and function of cells.

3.1.4.1 Structure Of DNA

A nucleotide consists of three molecules linked together: a pentose, a five carbon sugar which is Deoxyribose in DNA, a phosphate group and a nitrogenous base, as illustrated below in figure 3.10.

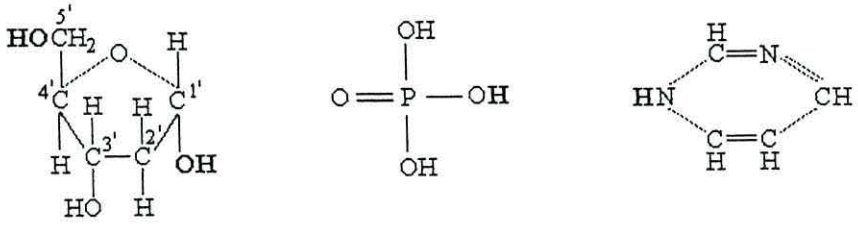

Figure 3.10. Diagram illustrating the three components that make up a nucleotide. The emboldened atoms represent the atoms that are removed in condensation reactions, to form water.

Bonds are formed between these three components by condensation reactions to form a deoxyribonucleotide, as illustrated in figure 3.11.

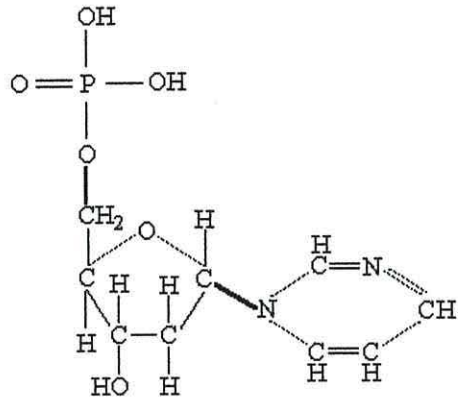

Figure 3.11. Deoxyribonucleotide, formed from its components in figure 3.10 with the resultant bonds in the nucleotide emboldened.

The nucleotides are strung together to form a long polynucleotide chain by further removal of water in *esterification reactions* between the sugar and phosphate groups. These new links are known as *phosphodiester bridges*. The phosphodiester bridges link 3'-hydoxyl of one sugar to the 5'-hydroxyl of the next sugar. Thus, the polynucleotide chain has a backbone consisting of alternating sugar and phosphate groups with the bases projecting out sideways from the sugars, as can be seen in figure 3.12.

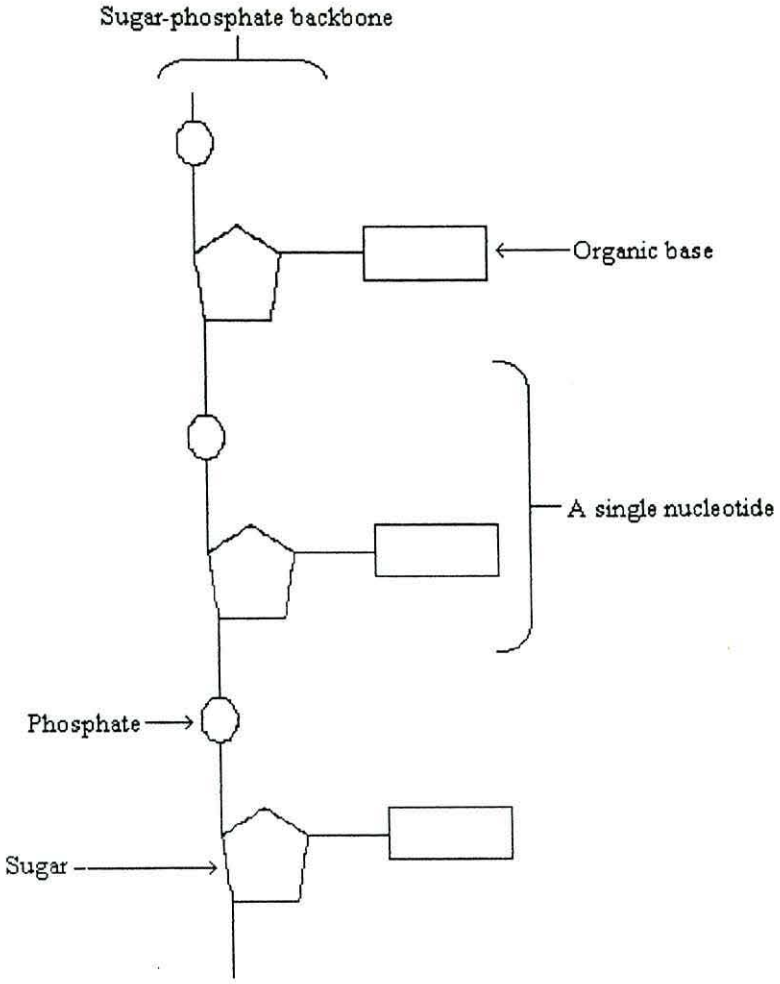

Figure 3.12. Diagram to illustrate the polynucleotide chain.

Two polynucleotide chains run antiparallel and are linked by hydrogen bonding between the nitrogenous bases, this is twisted to form a double helix structure. Note that the bases are normal to the helix axis. The structure of DNA is analogous to that of a *twisted ladder*, the uprights being the backbones and the rungs are pairs of bases, sticking inwards, towards each other, as can be seen in figure 3.13.

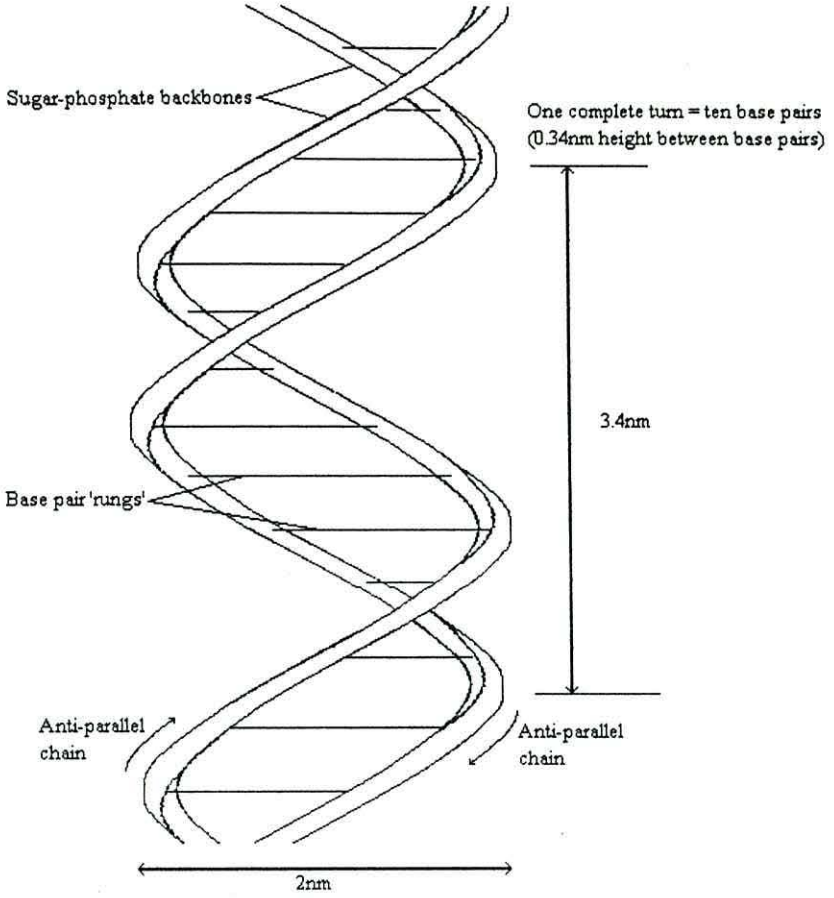

Figure 3.13. Double helix structure of DNA.

DNA has four different kinds of nucleotides, defined by different nitrogenous bases. The four bases in DNA are: adenine and guanine, which are double ring structures belonging to the class known as *Purines*, and cytosine and thymine, which are single ring structures belonging to the class known as *Pyrimidines*, these are illustrated in figure 3.14.

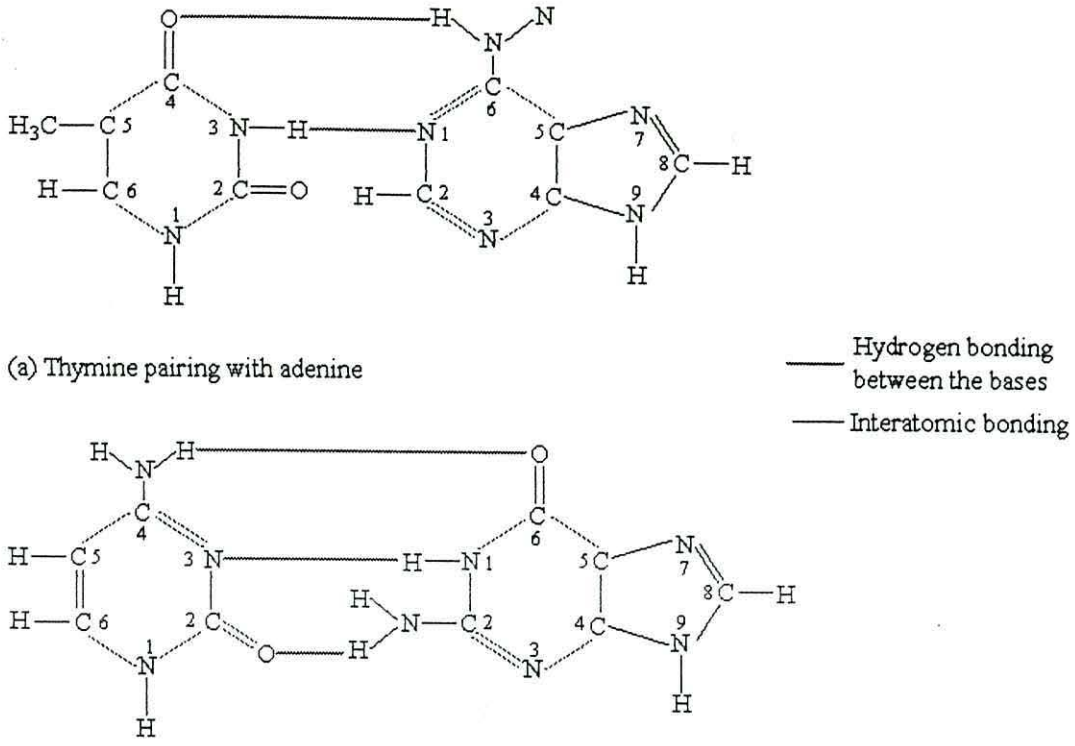

(a) Thymine pairing with adenine

(b) Cytosine pairing with guanine

Figure 3.14. Representations of the base pairs.

Each base 'rung' is composed of a single and a double ringed base, linked by hydrogen bonds. DNA exhibits specificity in the pairing of the bases, adenine always pairing with thymine, using two hydrogen bonds, and cytosine always pairing with guanine, using three hydrogen bonds, this is referred to as *Watson-Crick pairing*, see figure 3.14.

The DNA molecule's structure is stabilized by the hydrogen bonds between the bases and by interactions between stacked bases on the same strand. In a deoxyribonucleotide, the C-1 atom of the deoxyribose is bonded to N-1 of a pyrimidine or N-9 of a purine using a *glycosidic bond.* The overall, planar representation of a section of DNA is shown in figure 3.15, overleaf.

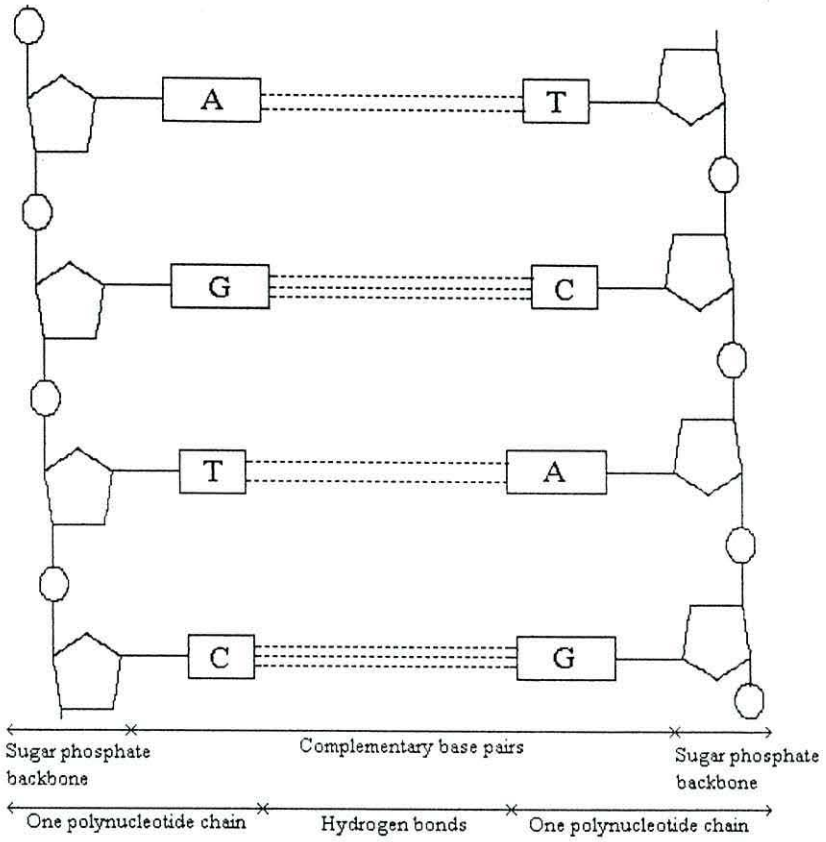

Figure 3.15. Representation of a possible section of DNA.

In 1953, James Watson and Francis Crick developed a model of DNA using the following information[9, 10]:

- Information on the chemical content and that the ratio of C:G and A:T is always one .
- Data on the distances between bonded atoms in molecules, bond angles and sizes of atoms.
- X-Ray diffraction studies on DNA fibers, performed by Maurice Wilkins.

The model developed was that described earlier in this chapter and is known as the *B-DNA helix.* However, DNA is structurally dynamic and can assume a variety of forms. Two other structural forms of DNA exist, the *A-DNA* form, which is dominant in RNA, and *Z-DNA*, a 'zigzagged' structure that is quite rare as its structure is thermodynamically unfavorable.

3.1.4.2 Denaturation

Denaturation of DNA is the loss of its specific 3D conformation, in other words the double helix unwinds and two chains separate into single polynucleotide strands. The hydrogen bonds holding the polynucleotide strands together are relatively weak and can easily be broken. Denaturation can be a reversible or an irreversible process. Irreversible denaturation occurs when the two strands are completely separated. Reversible denaturation occurs when the chain is only partially split into two separate single strands.

If the DNA is permanently denatured it can no longer perform its biological function. Denaturation can be caused by a number of factors such as:

- Exposure to strong acids and alkalis which ionizes the bases;
- Heating, which supplies kinetic energy to the molecule causing its atoms to vibrate violently which may result in the hydrogen bonds breaking;
- Organic solvents may also denature, disrupting the inter-molecular hydrogen bonding;
- Heavy metals, cations, may interrelate between the DNA strands and may disrupt ionic and hydrogen bonds.

The reversal of denaturation is *renaturation*, it is the spontaneous refolding of the DNA into its original structure after denaturation, providing conditions are suitable.

3.1.4.3 Nucleic Acid Reagents

The nucleic acids used in the Macromolecules chapter were supplied by Dr. J.O'Neil, at Leeds University, and was in the form of single stranded primers of 21 bases long, their base sequence are listed below. It should be noted that the primers were not phosphorylated at the 5' end.

Primer One: CAG CTG GCG GCC GTG GAG GCG.
Primer Two: TAC TAC GTC GCC ATC TTC CTC.

3.2 Methods

This section aims to provide the reader with an overview of the techniques used to prepare samples and to describe the experimental technique used.

3.2.1 Latex Particle Preparation.

Polystyrene latex particles were stored at 4°C in phosphate buffered saline (170 mM pH 7.4) with 0.05 % tween-20 (surfactant) and 0.1 % sodium azide (antimicrobial). The particles should not be frozen, since this could result in damage and should be stored in a slightly basic solution.

Cleaning of particles both before and after preparation is required to remove traces of surfactant and any production by-products that may still be present. The manufacturer recommends several methods[11]. The method used, chosen on the basis of access to equipment and ease of use, was cleaning and centrifugation and resuspension in the desired suspending medium at least six times. After centrifuging, the supernatant was removed, fresh suspending medium was introduced and the particles were aspirated in the fresh suspending medium until the sample was considered to be dispersed. Where specified, when time was considered an issue, filtration with a 0.2 μm pore sized filter was used. However, this could lead to coagulation problems and was therefor not used in general. Latex particles were always prepared on the day of their experiment, unless otherwise specified.

The particles were investigated either when uncoated or when coated with antibodies, DNA or antibodies and bacteria. Several methods exist for the attachment of the protein to the surface of carboxylated particles[12, 13, 14, 15]. The two main methods are protein adsorption or covalent coupling to the particle. The adsorption technique was discounted on the basis that evidence suggests that it yields a lower, variable, surface coverage of the particles[16] and covalent coupling binds the protein more securely.

Two main methods exist for covalent coupling the protein to the carboxylated particles. The procedures provide a covalent coupling between the carboxylic acid groups on the latex bead and the amine groups present on the protein. The first is a 'single step'

procedure, which was used initially. The second is a 'two step' procedure, this procedure was favored due to the increased precision of the coating. Unless otherwise specified the two step procedure was used to prepare protein-coated particles. The two methods are described below.

3.2.1.1 Single Step Coupling Procedure

A single step coupling procedure was used to attach DNA to the latex beads, the results are presented in the Macromolecules chapter. This procedure is summarised here and described in detail elsewhere[12, 13, 14, 15].

The beads and the DNA primers were mixed with 2% water soluble carbodiimide solution (1-ethyyl-3-(3-dimethylaminopropyl) carbodiimide), CDI and incubated for twenty minutes at 50°C. The particles were then cleaned by centfugation and suspended in a solution of 170 mM phosphate buffered saline with 0.05 % tween-20, 0.1 % sodium azide and 0.2 % bovine serum albumin (BSA), this was the storage medium for protein coated particles.

This technique appeared to yield variable results for the coating, see Macromolecules chapter for further details. Hence, this technique was only used for the initial experiments on DNA performed for this study.

3.2.1.2 Two Step Coupling Procedure

The two step coupling procedure, saw the first step run at an acid pH during which an intermediate product is formed between the carboxylic acid group on the latex beads and a water soluble carbodiimide (CDI). Excess CDI is removed. The second step is run at a basic pH, during which the antibody is coupled to the bead. An excess of antibody is used to ensure complete coverage of the latex bead. Removal of the CDI prevents cross-coupling between the antibodies and ensures that a single layer of antibody will be present on the bead, see figure 3.16. The antibody coated beads were stored for up to one month, in 170 mM PBS, pH 8.2 with 0.2 % sodium azide, 0.2% BSA and 0.05% tween-20.

Presence, or absence, of the DNA on the surface of the beads was not determined, indirectly, by UV fluorescence. When the attached antibody did not have a fluorescent conjugate attached additional FITC-conjugated antibodies were coupled to the bead-antibody system. Although the test is only qualitative, this coupling protocol has always given a positive fluorescence result, the whole of the bead fluorescing with an even intensity when observed by eye.

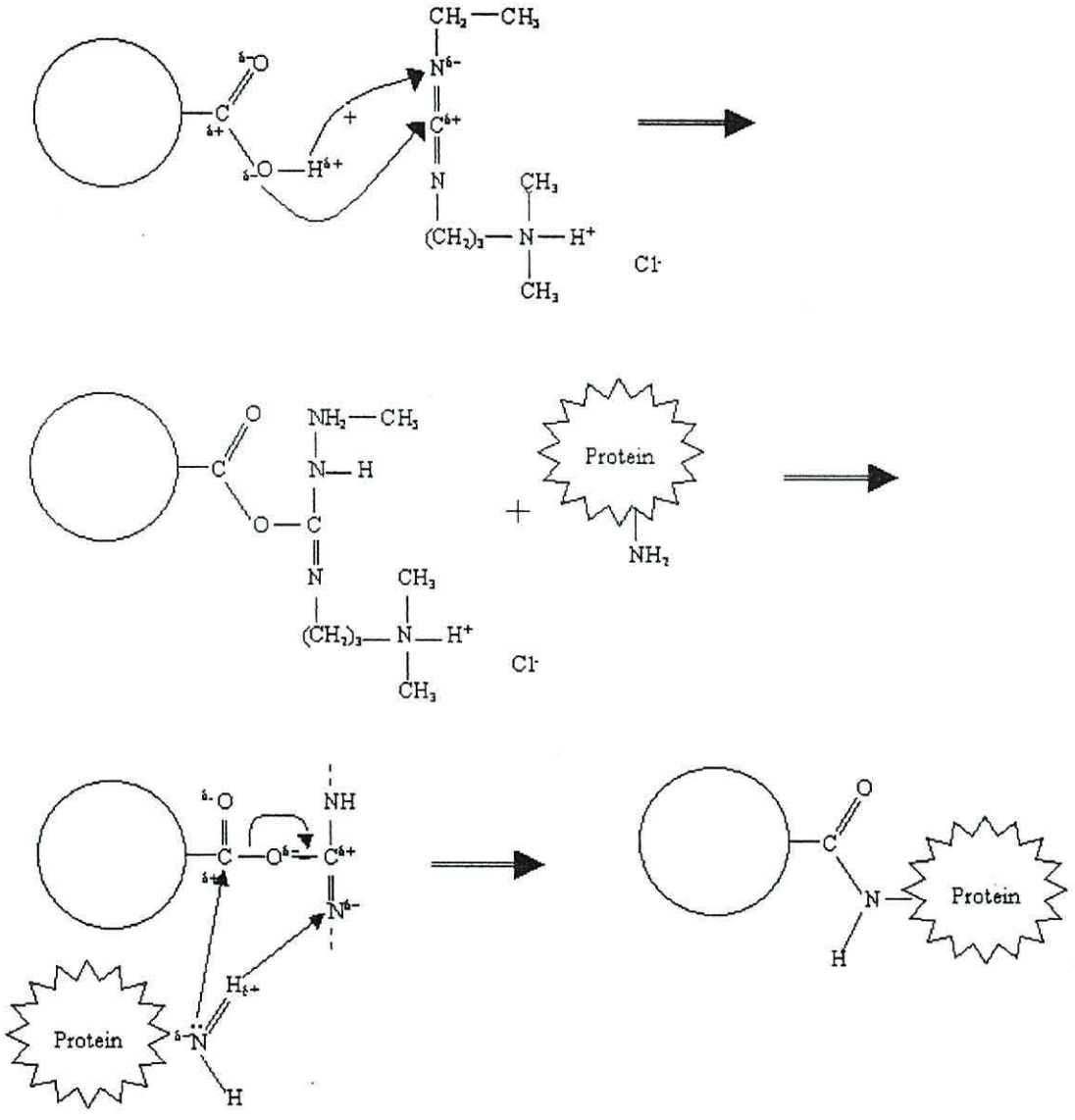

Figure 3.16. Covalent coupling reaction of a protein with a carboxylated latex.

3.2.1.3 Bead Complexes

The aim of this study is to investigate the affect of bacteria, antibodies and DNA on the electrorotation properties of latex particles. Four basic latex particle systems were investigated:

- Uncoated particles.
- Particles coated in antibody, with bacteria subsequently added.
- Particles with short single-stranded nucleic acids attached.
- Particles coated in antibody, with subsequent secondary and either unconjugated or gold-conjugated tertiary antibodies introduced.

Introducing washed (by centrifugation) bacteria into the bead sample and gently rotating for 30 minutes performed attachment of the bacteria to the antibody coated latex bead. After this time, for active antibody, the bacteria were seen to be adhering to the surface of the particle. Up to ten *E. coli* were observed to be attached to the particles.

The same approach was used to adhere the secondary and tertiary antibodies to the antibody coated bead. In this case, it was not possible to directly observe the antibodies attachment. A fourth layer of FITC-conjugated antibody was introduced. If, after cleaning by centrifugation, the beads were observed to fluoresce the attachment of the three antibody layers of interest were deemed successful.

3.2.2 Experimental

All samples of uncoated and coated particles and bacteria were washed using centrifugation on the day of the experiment, unless otherwise specified. Prior to the start of the experiment, a sample of the prepared bacteria would be placed on agar plates and incubated to confirm that, after preparation the bacteria were viable.

Viable bacteria were rendered non-viable using Virkon, Antec International. This resulted in cell death without damaging the structure. In all experiments, the bacteria were assumed to either all be viable or non-viable. This assumption could lead to variability in the results, however, it was not possible stain samples as this would interfere with their dielectric properties. Bacteria required for experimentation was

reproduced in nutrient broth one day before experiments. This helped to ensure that only a minority of the population would be non-viable, since competition for nutrients and build of by-products would be minimal at this stage.

All other chemicals were obtained from Sigma, unless otherwise specified. In all experiments the suspending medium conductivity was measured using a Whatman CDM 4010 meter. For the Latex Particles and Macromolecules chapters the desired suspending medium was phosphate buffered saline (pH 7.4, 10 mM phosphate buffer, 27 mM potassium chloride and 137 mM sodium chloride). The conductivity of the solution was typically adjusted to a value of 500 μSm^{-1}, unless otherwise specified. This equated to a concentration of approximately 20 μM.

The desired suspending medium for the bacteria and bead complexes, in the *E. coli* chapter, was Mannitol solution, of concentration 170mM, made up with PBS solution, to equate to a conductivity of approximately 500 μSm^{-1}. The concentration of the Mannitol was determined from examination of literature[17] and a consideration of the osmotic potential exerted on the bacteria from the growth medium. The beads were suspended at a working concentration of 18 ± 4 $*10^9$ l^{-1}. A photograph of a sample during an experiment is shown in figure 3.17.

Electrorotation results were collected for the samples described in section 3.2.1.3 across a frequency range 0f 100 Hz to 5 MHz. Twenty-eight equidistant data points were collected between this frequency range.

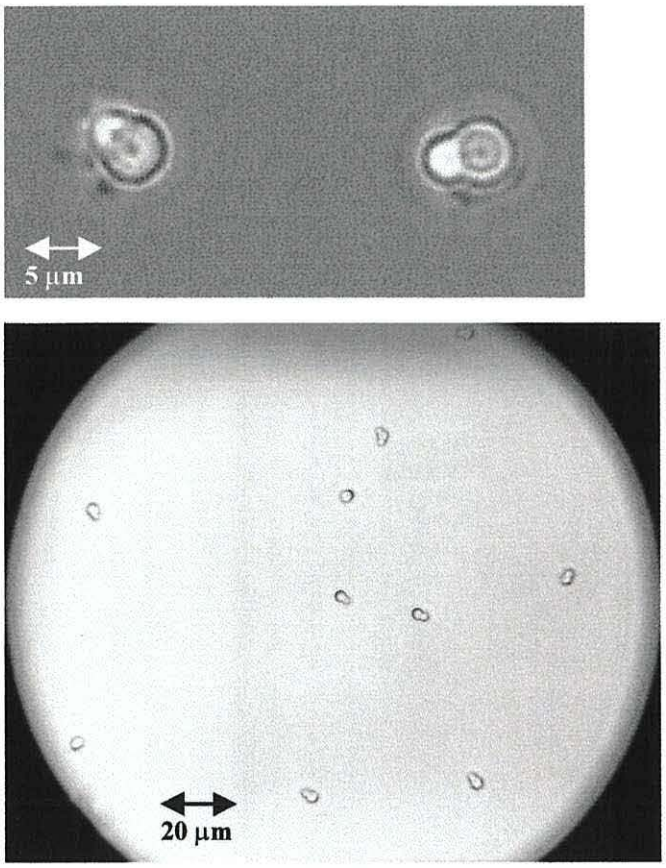

Figure 3.17. Photographs of (a) antibody coated latex beads with *E. coli* attached, and (b) overview of uncoated latex particles experiment.

The electrodes used were the 400 μm diameter 'bone' type[18, 19]. The 'bone' electrodes are optimised for electrorotation by making the chamber enclosed by the electrode edges circular in shape. The electrode's shape is described by the fourth order polynomial[20]:

$$y(x) = x^4 - 0.75x^2 + 1$$

See figure 3.18 for an illustration of the electrode shape. The electrode design provides a near uniform electric field in the central region and reduces unwanted dielectrophoretic forces that the particle may experience[20]. The microelectrodes were fabricated on glass microscope slides using gold photolithography, and the working space between the electrodes was 400 μm. The electrodes were cleaned using ultra-pure water and dried using a stream of nitrogen gas.

Rotation was monitored using a microscope and video recorder, see figure 3.18 for an illustration of the experimental setup[21]. Results were recorded on to a video tape and analysed at a later date. Commentary regarding the experiment was also recorded on to the video tape and provided information such as the date and time, details of the voltage.

The electrorotation experiments were performed in a semi-clean room maintained at a temperature of around 18°C. Experiments were completed on the same day that they started on, unless specified. Voltage across the electrodes was measured throughout the experiments using an oscilloscope.

20 μl of sample was pipetted on to the electrodes, which ensured a complete coverage. The rotation rates of the particles contained within the central third of the electrodes were monitored. Any particles that were considered to be too close to others, within three particle lengths, were not monitored. The rotation rate was recorded for a minimum of 10 seconds or at least one whole rotation. Electric field frequencies were started at 5 MHz and continued down to 100 Hz without removing the field.

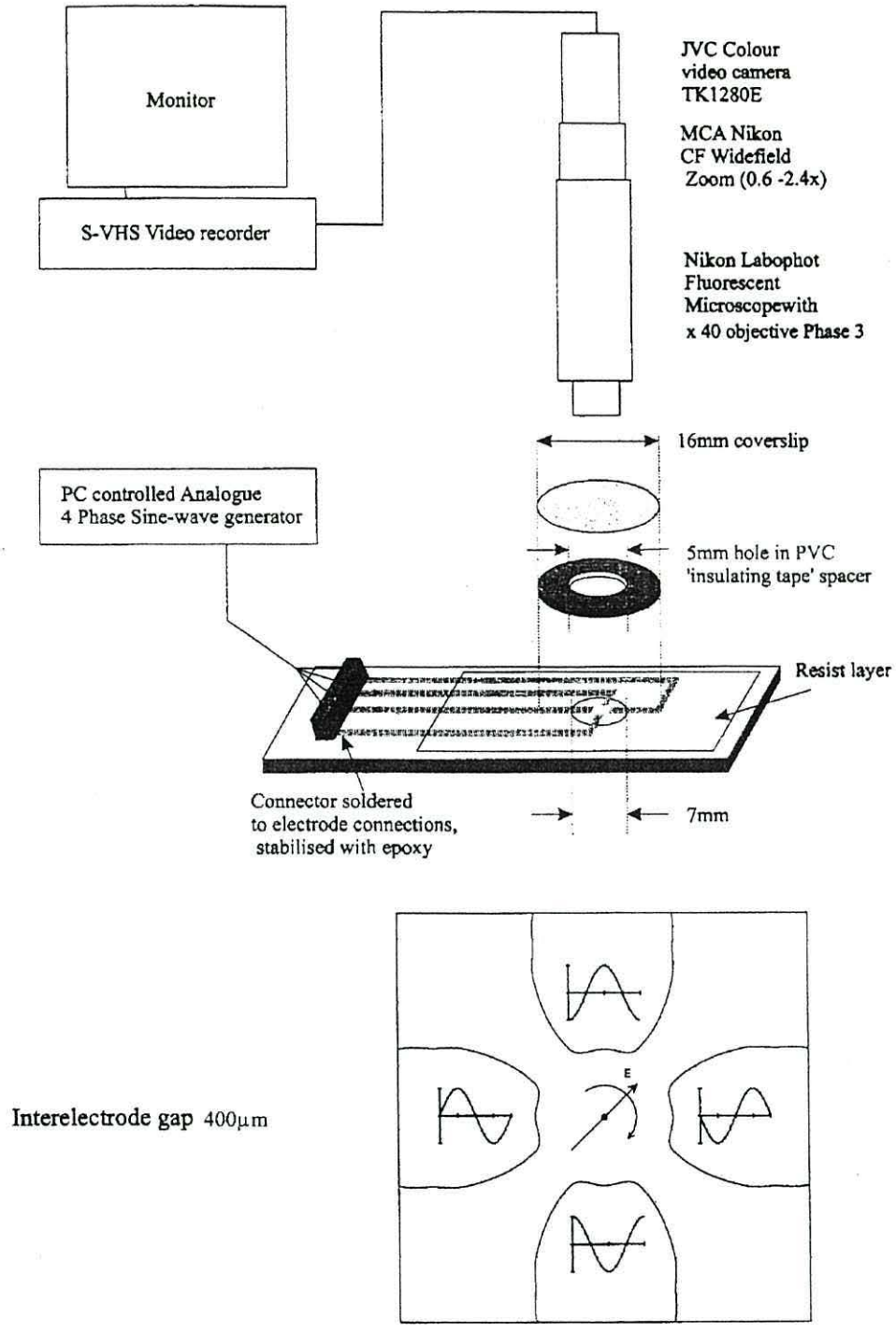

Figure 3.18. Electrorotation experiment setup, with a view of the 'bone' electrodes.

3.2.3 Results Analysis

Results were plotted on a log frequency scale and the curve fitted using polynomial equations provided by SigmaPlot, Jandel Scientific. A limited amount of error analysis was performed on some of the results presented in this study, when thought to be of interest or of significance. The analysis was not statistically significant due to the limited number of samples the experimental results were based on, since results from different experiments were not mixed.

The analysis performed was the 95% confidence of the standard deviation. First, the standard deviation of the sample is found. The standard deviation is a measure of how widely values are dispersed from the average value (the mean). The standard deviation was calculated using the "nonbiased" or "n-1" method, using the following formula:

$$\sigma = \sqrt{\frac{\sum_i (x_i - \bar{x})^2}{n}}$$

Where x is the set of numbers of population size n.

The 95 % confidence was then found on the standard deviation. The 'confidence' is the degree of confidence that a parameter lies in the given interval. If $\bar{x}$ is the mean of a random sample of size n from a normal population with variance σ^2 a central 95 % confidence interval for the population mean is given by:

$$\bar{x} \pm \frac{1.96\sigma}{\sqrt{n}}$$

3.3 References

[1] Smith WV and Ewart RH. J. Chem. Phys. 1948. 16(6): 592-599.

[2] Bangs LB. Uniform latex particles. 1984. Seradyn, Indianapolis, IN.

[3] Steward MW. Antibodies: Their structure and function. 1984. Chapman and Hall.

[4] Neidhardt FC. *Escherichia coli* and *Salmonella typhimurium*: Cellular and Molecular Biology. 1996.

[5] Editors: Sonenshein AL, Hoch JA and Losick R. *Bacillus subtillis* and other gram-positive bacteria: Biochemistry, physiology and molecular genetics. 1993.

[6] Oginsky and Umbreit. An introduction to bacterial physiology. 1959.

[7] Cooke M. *E. coli* and Man. 1974.

[8] Ingraham JL, Maaløe O and Neidhardt. Growth of the bacterial cell. 1983.

[9] J.D. Watson and F.H.C. Crick, 1953. *Nature* 171:737-738.

[10] J.D. Watson and F.H.C. Crick, 1953. *Nature* 171:964-967.

[11] Bangs LB. Particle Handling. 1983. The Latex Course. Bangs Laboratories, Inc.

[12] Bangs Laboratories, Inc. Covalent Coupling Protocols. Technical Note 13C. Bangs Laboratories, Inc.

[13] Quash G., Roch A.M., Niveleau A., Grange J., Keolouangkhot T. and Hupert J., The Preparation of Latex Particles with Covalently Bound Polyamines, IgG and Measles Agglutinins and Their Use in Visual Agglutination Tests. J. Immun. Meth. 1978; 22: 165-174.

[14] Rosenstein, Robert, "Immuno-aggulutination Particle Suspensions," US Patent # 4,582,810, April 15, 1986.

[15] Ghosh SS and Musso GF. Covalent attachment of oligonucleotides to solid supports. Nucleic Acids Res. 1987; 15: 5333-5372.

[16] Douglas AS and Monteith CA. Improvements to immunoassays by use of covalent binding assay plates. 1994. Clin. Chem. 40: 1833-1837.

[17] Stock JB, Rauch B and Roseman S. Periplasmic space in *Salmonella typimurium* and *Escherichia coli*. J. Biol. Chem. 1977; 252; 7850-7861.

[18] Dalton C, Goater AD, Pethig R and Smith HV. Viability of *Giardia intestinalis* Cysts and Viability and Sporulation State of *Cyclospora cayetanensis* Oocysts Determined by Electrorotation. Appl. Environ. Microbiol. 2001. 67(2): 586-590.

[19] Hughes MP. Computer-aided analysis of conditions for optimizing practical electrorotation. 1998. 43: 3639-3648.

[20] Dalton C, Goater AD, Drysdale J and Pethig R. Parasite Viability by Electrorotation. Col. Surf. A: Physicochem. Eng. Aspects. 2001. In Press.

[21] Goater AD. AC Electrokinetic Bioassays. Development of Electrorotation Assay for Analytes in Water. Ph.D. University of Wales, Bangor. 1999.

Chapter 4

Latex Particles

4.1 Introduction

The electrical properties of latex particle suspensions are characterized largely by their surface charge, for further details see Materials and Methods Chapter. Electrorotation measurements are particularly sensitive to the changes in the surface conductivity and suspending medium conductivity, see Theory chapter, and can be used as a responsive method of analysis to monitor changes in these. Of particular interest are changes in the surface conductivity of the particles, this can be utilized to monitor the efficiency of surface modifications, such as the addition of antibodies and bacteria, as covered in the *E. coli* chapter, and DNA binding, as covered in the Macromolecules chapter.

In later chapters electrorotation measurements will be shown to be sensitive enough to detect the presence or absence of viable or non-viable bacteria in antibody systems on beads and sensitive enough to detect the presence of macromolecules attached to the surface, both in a qualitative and quantitative way. This chapter provides a basic investigation of the underlying system, the latex particle, upon which all of these systems are based. It is necessary to understand this basic system to be able to provide sound judgements on any results arising from the latex particles systems.

This chapter will present results to show that unmodified latex particles provide distinct coherent electrorotation characteristics. A change in their environment or to their surface charge results in marked changes of their electrorotation characteristics. It will be observed that the electrorotation characteristics changed over time when it is anticipated that an 'aging' process occurs with the beads. It has been possible to detect these and other physico-chemical changes occurring in the latex particle suspension using the electrorotation assay.

4.2 Results

In this chapter several types of latex beads were used, the main particles of interest were those used in the following chapters, elliptical shaped beads with carboxylate surface groups. Two other particles were investigated, they were elliptical and peanut shaped beads with no additional surface functional groups. The latex particles were suspended in phosphate buffered saline (PBS) solution of varying concentrations. For details on the methods, experimental procedures and reagents see the Materials and Methods chapter.

4.2.1 Carboxylated elliptical latex beads in 430 μSm^{-1} PBS solution

Elliptical shaped beads with carboxylate surface functional groups were suspended in PBS solution of 430 μSm^{-1}. This suspending medium conductivity was the most commonly used throughout this study and in the following chapters. The electrorotation properties of these latex particles was studied, throughout the frequency range employed (100 Hz to 5 MHz).

The latex beads were observed to rotate in the same sense as the applied rotating field. This is termed co-field rotation, see the Theory chapter for further details. Two co-field rotation peaks characterize the spectrum - a low-frequency peak centered around 200 Hz and a high-frequency peak centered around 600 kHz.

It can be seen that latex beads exhibit a distinct electrorotation spectrum. Error bars have been included on this particular graph, for further details on how these are calculated see the Materials and Methods Chapter. They are included so that the reader understands that although the latex beads exhibit a distinct electrorotation spectrum the results are not perfect. In the low frequency region, typically below 1kHz, the variability becomes more significant than in the higher frequency region. This was typically observed throughout most of the following experiments and systems. The variability observed in figure 4.1 is of a typical magnitude and distribution that was observed for the rest of the uncoated latex results, whereas for modified particles they were less significant.

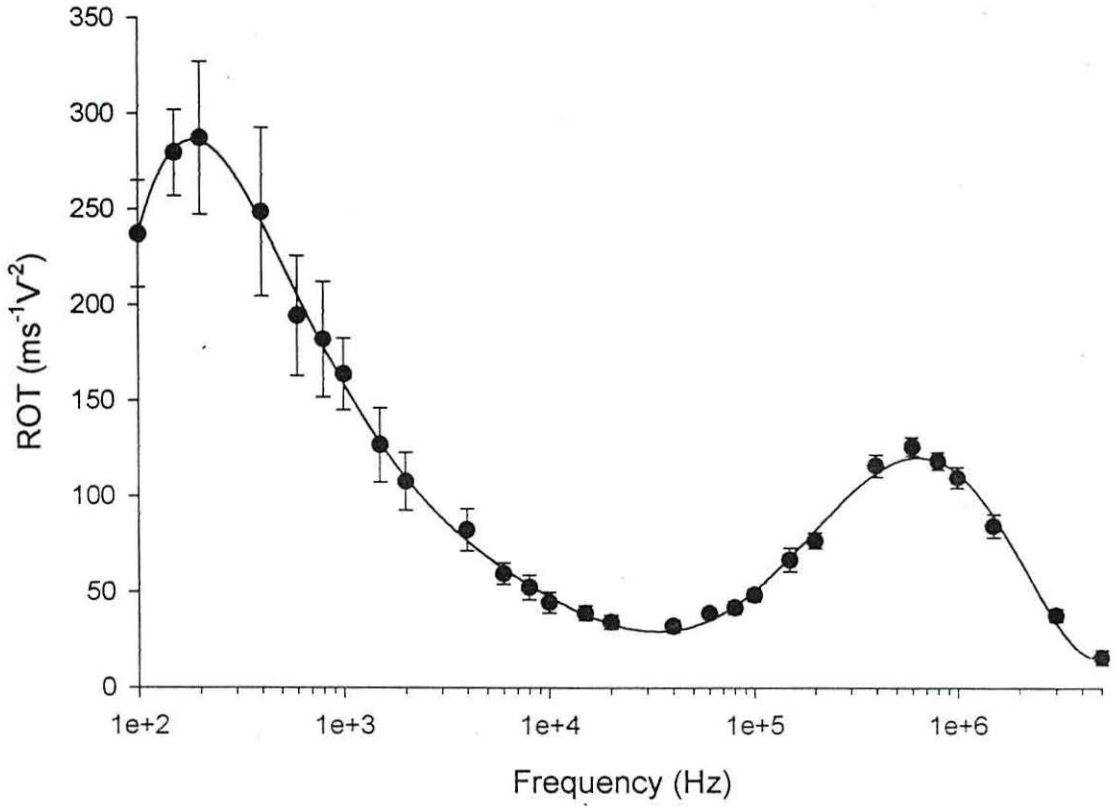

Figure 4.1. Electrorotation spectra of elliptical latex particles with carboxylate surface groups suspended in 430 μSm^{-1} PBS solution (where n = 7 beads). Error bars represent the 95% confidence of the standard deviation.

4.2.2 Changes in the spectra of elliptical carboxylated latex particles

It had been noted that the elliptical shaped beads with carboxylate surface functional groups suspended in 430 μSm^{-1} PBS solution seemed to exhibit an 'aging' effect, that is, the spectra would coherently change over time. The electrorotation properties of the particles were studied when freshly prepared and after 24 hours storage at 4°C, the results are displayed in figure 4.2. It should be noted that although the results displayed in figure 1 are for the same system they were performed as different experiments, and were not using the same prepared sample.

The latex beads spectra were characterized by two co-field rotation peaks. For the freshly prepared beads, the low-frequency peak was centered on 200 Hz and the high-frequency peak centered on 500 kHz. After the same sample of beads had been stored at 4°C for 24 hours the spectra had changed in shape. It was now no longer possible to observe the low-frequency peak, since it did not peak at over 100 Hz, however, its magnitude could become much more significant than the high-frequency peak. The high-frequency peak of the beads became centered on 1.2 MHz and was reduced in magnitude.

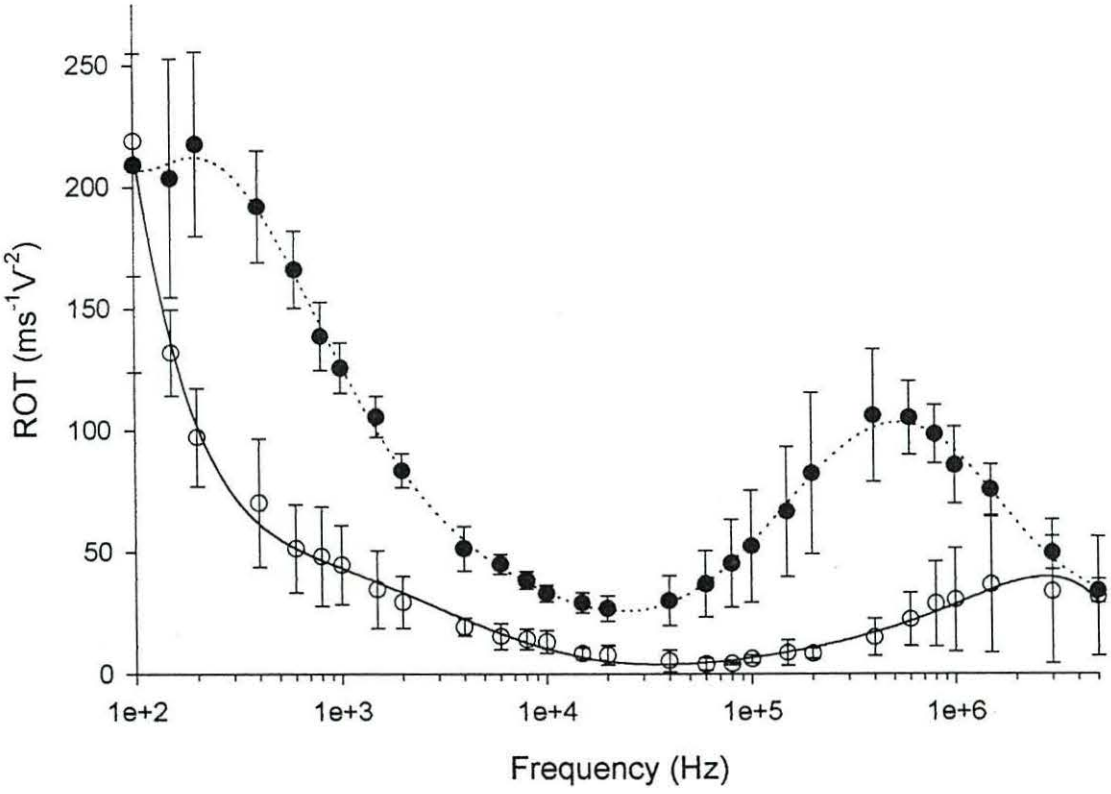

Figure 4.2. Electrorotation spectra of carboxylated elliptical latex particles suspended in 430 μSm^{-1} PBS solution after preparation (●) and after 24 hours storage at 4°C (○) (for a sample of 13 particles). Error bars represent the 95% confidence of the standard deviation.

4.2.3 Artificial 'aging' of carboxylated elliptical latex's by acidification

It was thought that the 'aging' affect may be due to protonation of the surface groups, hence the particles were treated with strong acid. In this experiment, filtering with ultra pure water cleaned the beads, this saved time during the preparation which would hopefully minimize any aging effects that might occur in the sample during the preparation. The beads were then suspended in ultra pure water, with a conductivity of 100 μSm^{-1}, and their electrorotation properties monitored over a period of 23 hours. Storage was at 4°C. The results are displayed in figure 4.3.

A portion of beads were pre-treated with 0.1M hydrochloric acid (pH 4.0) for 90 minutes then suspended, as above, in ultra-pure water and the electrorotation properties of the particles were studied. After the acid treatment, the beads exhibited no electrorotation response. After 24 hours suspension in ultra-pure water very slow co-field rotation started to appear again around the high frequency peak and the low frequency peak region.

For the beads that had only been cleaned in water the results were similar to those observed in figure 4.1, with both a high and a low frequency co-field electrorotation peak. The position of the high frequency peak appears to be subjected to a slight increase in frequency but decreases in magnitude after 23 hours storage. Similar to the beads in figure 4.2, the low frequency peak has decreased significantly in magnitude after 23 hours storage.

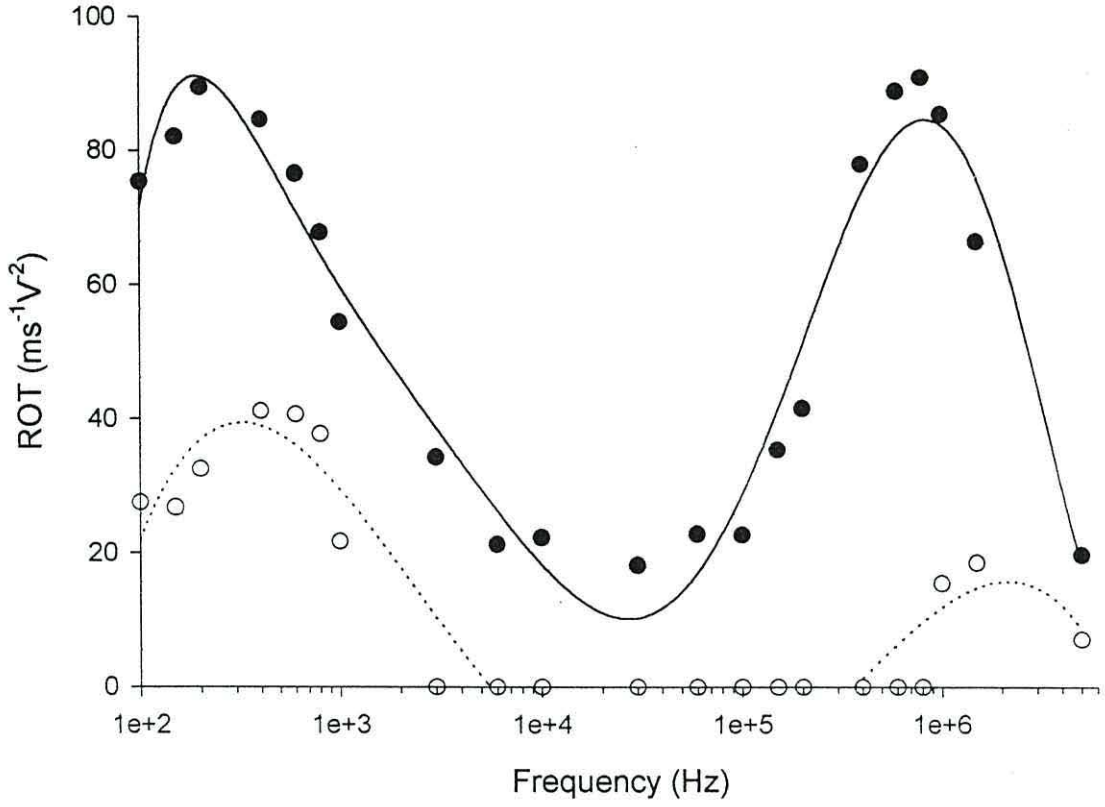

Figure 4.3. Electrorotation spectra of carboxylated elliptical latex particles suspended in ultra-pure water. Freshly prepared (●) and after 23 hours storage at 4°C (○).

Although fairly sensitive methods for measuring solution conductivity were available these required large volumes sizes (18ml) compared to the sample prepared (1ml). An indication of the conduction changes occurring within the sample was obtained by measuring the voltage across a 1 ohm resistor connected to an electrode, to which 6 $V_{p\text{-}p}$ was applied, throughout the experiment. Since the magnitude of the current passing through a solution is related to the ion concentration. The voltage was measured for the beads suspended in ultra-pure water over the experimentation period. The results are displayed in figure 4.4.

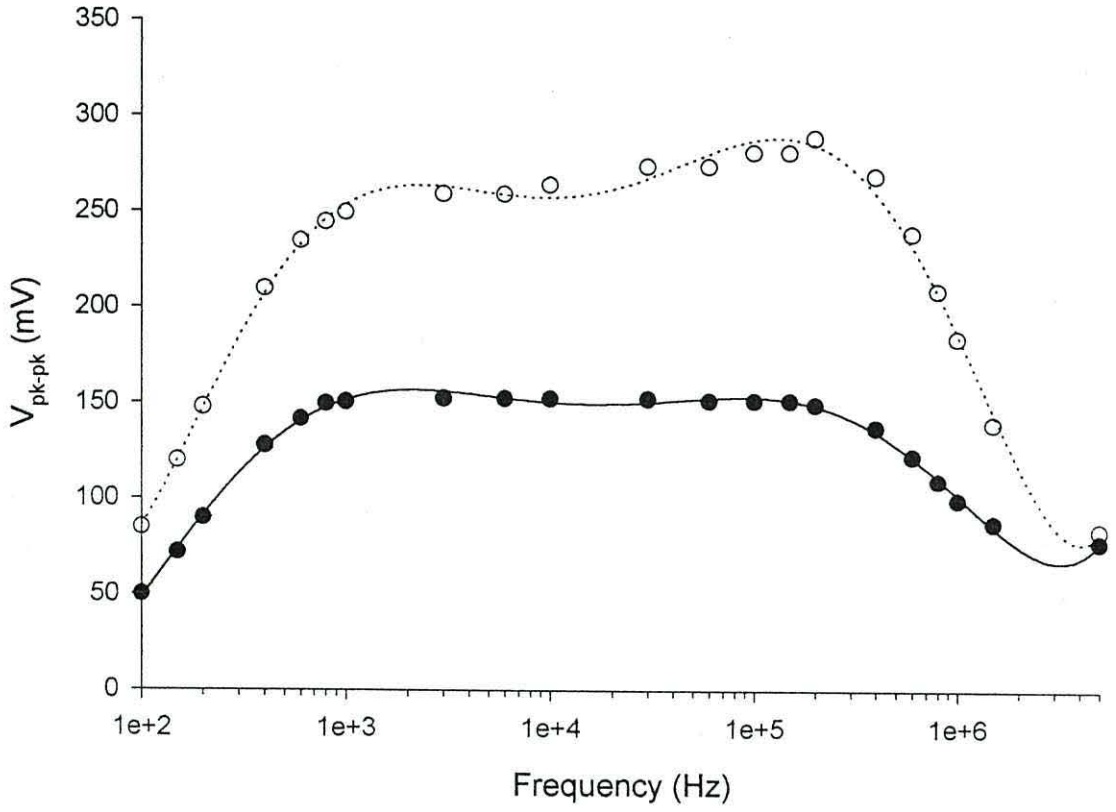

Figure 4.4. Graph indicating the change in medium conductance (voltage) of samples of elliptical latex beads with carboxylate surface functional groups in ultra-pure water after preparation (●) and after 23 hours storage at 4°C(○).

It can be seen that the change in electrorotation spectrum with time is accompanied by an apparent change in medium conductance. The characteristics in figures 4.2 and 4.3, corresponding to a decrease in the electrorotation peak magnitude, appear to be accompanied by a rise in the medium conductance.

4.2.4 Affect of relatively high conductivity PBS solutions

Elliptical shaped beads with carboxylate surface functional groups were suspended in a range of concentrations of normal PBS. The latex particles were cleaned by ultra-filtration and were suspended in PBS solutions whose conductivities were adjusted to the following: 10 mSm^{-1}, 25 mSm^{-1}, 50 mSm^{-1} and 75 mSm^{-1}. The electrorotation

properties of these latex particles were studied, throughout the frequency range monitored, see figure 4.5 for details.

All of the beads spectra were characterized by two co-field rotation peaks, a low-frequency peak and a high-frequency peak. As the conductivity of the suspending medium increased the magnitude of the high frequency peak decreased and the peak frequency increased. The low frequency peak decreased in magnitude.

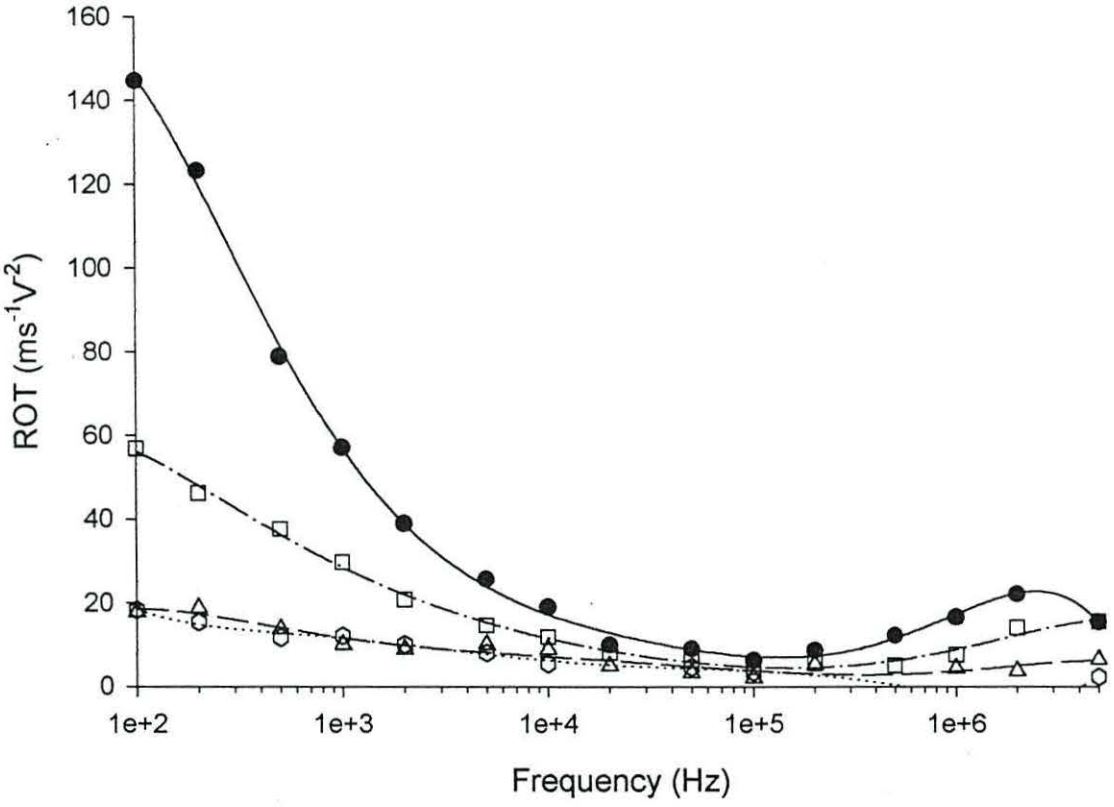

Figure 4.5. Electrorotation spectra of elliptical latex particles with carboxylate surface functional groups suspended in a range of relatively high conductivity normal PBS solution. The conductivities were: 10 mSm^{-1} (●), 25 mSm^{-1} (□), 50 mSm^{-1} (△) and 75 mSm^{-1} (○).

4.2.5 Affect of relatively low conductivity PBS solutions

Elliptical shaped beads with carboxylate surface functional groups were suspended in a range of concentrations of PBS. The latex particles were suspended in solutions of ultra pure water, at 150 μSm^{-1}, and PBS solutions, at 430 μSm^{-1}, 620 μSm^{-1} and 2100 μSm^{-1} respectively. The electrorotation properties of these latex particles were studied, throughout the frequency range employed, see figure 4.6 for details.

The position of the high frequency peak appears to increase in frequency but decreases in magnitude for an increase in suspending medium conductance. By contrast, the low frequency peak decreases in frequency but increases in magnitude, for an increase in suspending medium conductance. The notable exception to these observations are the results for the particles suspended in 620 μSm^{-1} PBS solution which shows a high frequency peak magnitude much larger than would be expected. It would have been expected to lie between those obtained for the 430 μSm^{-1} and the 2100 μSm^{-1} PBS solutions, however, it lies between the results for the ultra-pure water (at 150 μSm^{-1}) and the 430 μSm^{-1} PBS solution.

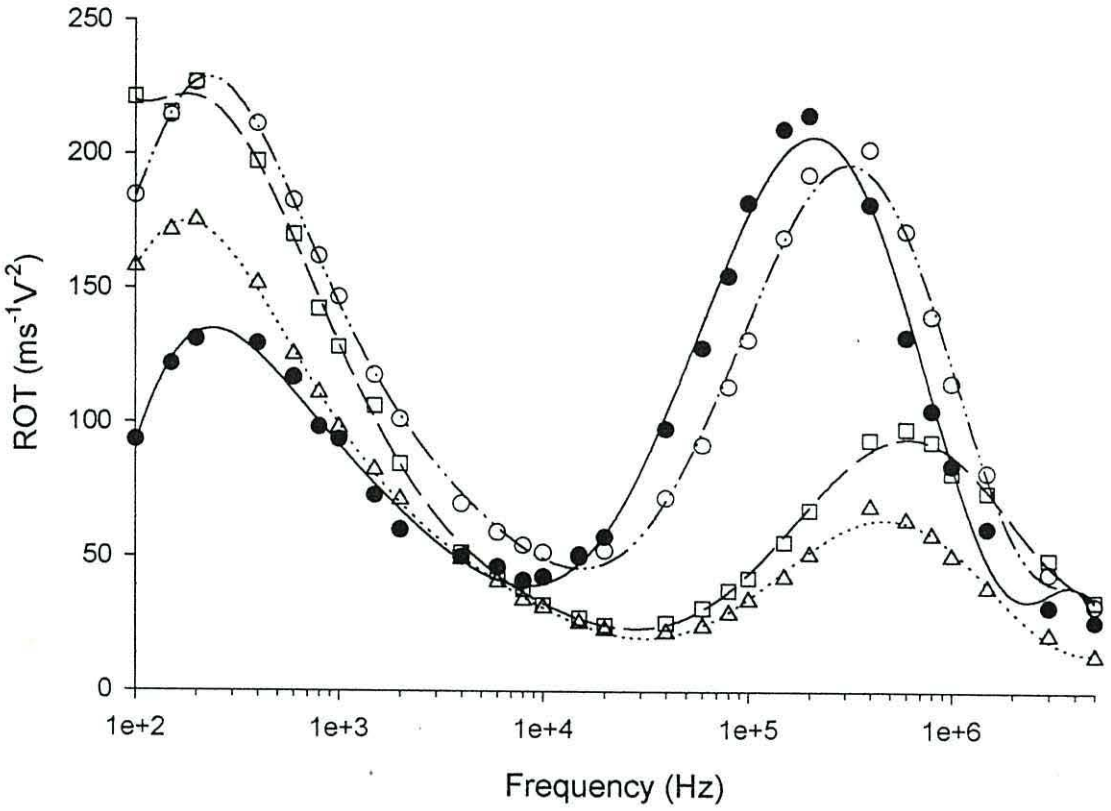

Figure 4.6. Electrorotation spectra of elliptical latex particles with carboxylate surface functional groups suspended in a range of relatively low conductivity normal PBS solution. The conductivities were: ultra-pure water (at 150 μSm^{-1}) (●), 430 μSm^{-1} (□), 620 μSm^{-1} (○) and 2100 μSm^{-1} (△).

4.2.6 Summary of the affects of suspending media conductivity

The results of the previous two experiments have been collated to observe general trends across the concentration from 470 μSm^{-1} to 75 mSm^{-1}, see figure 4.7.

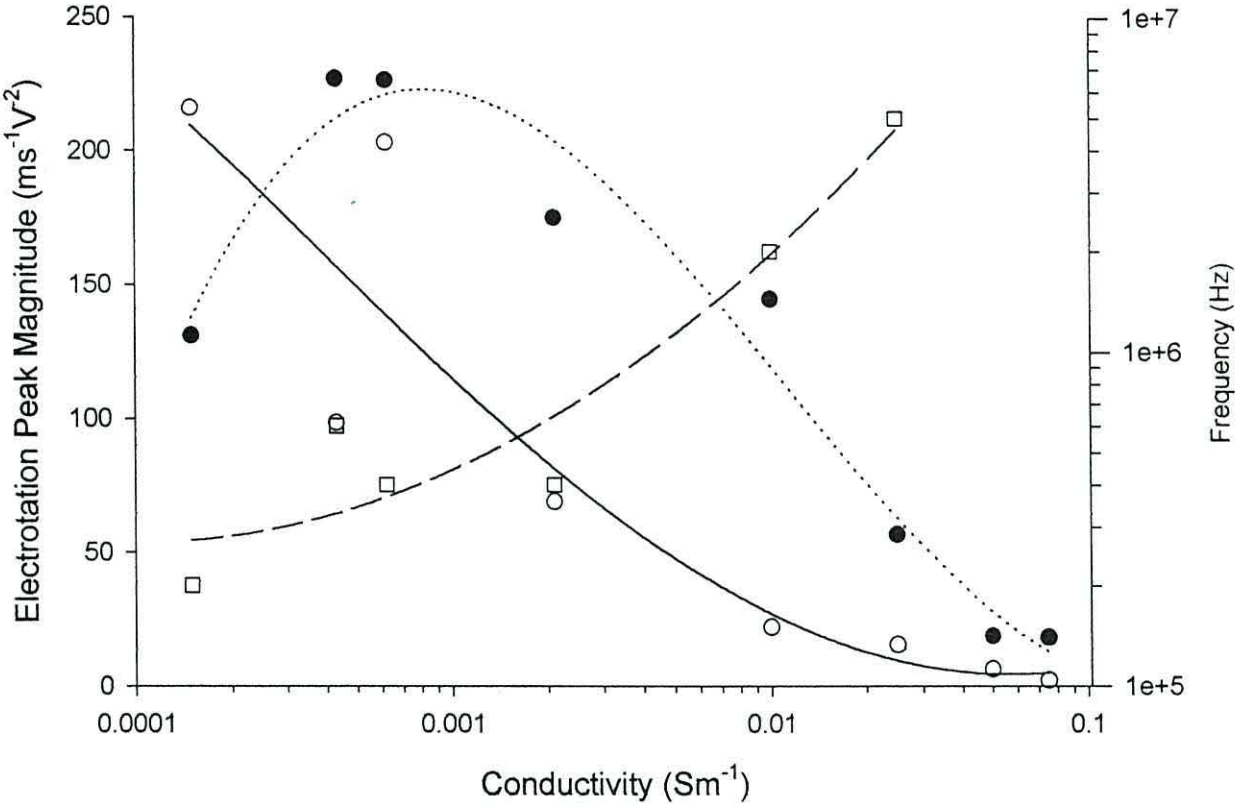

Figure 4.7. Summary of the changes in the high frequency peak magnitude (○) and frequency (□) and the low frequency peak magnitude (●) for carboxylated elliptical particles suspended in increasingly conductive PBS solutions.

For increasing suspending media conductivity it can be seen that the high frequency peak magnitude decrease exponentially. It decreases dramatically up to 10 mSm^{-1} when it appears to reach a minimal value, where increasing conductivity appears not to have any further affects. In contrast, the high frequency peak frequency increases exponentially. For increasing suspending medium conductivity, the low frequency peak initially increases, up to 630 μSm^{-1}, then decreases exponentially.

The zeta potential for carboxylated elliptical latex particles was measured across a range of suspending media conductivities using a Coulter Delsa Analyser, the results are presented in figure 4.8. The results show that for increasing suspending media conductivity the Zeta potential decreases, that is, becomes less negative. It should be noted that at 538 μSm^{-1} the zeta potential appeared to increase, that is, become more negative. This anomalous result occurs at around the same conductivity as the anomalous increase in the electrorotation high frequency peak magnitude of the particles in section 4.2.5 (and summarized in this section).

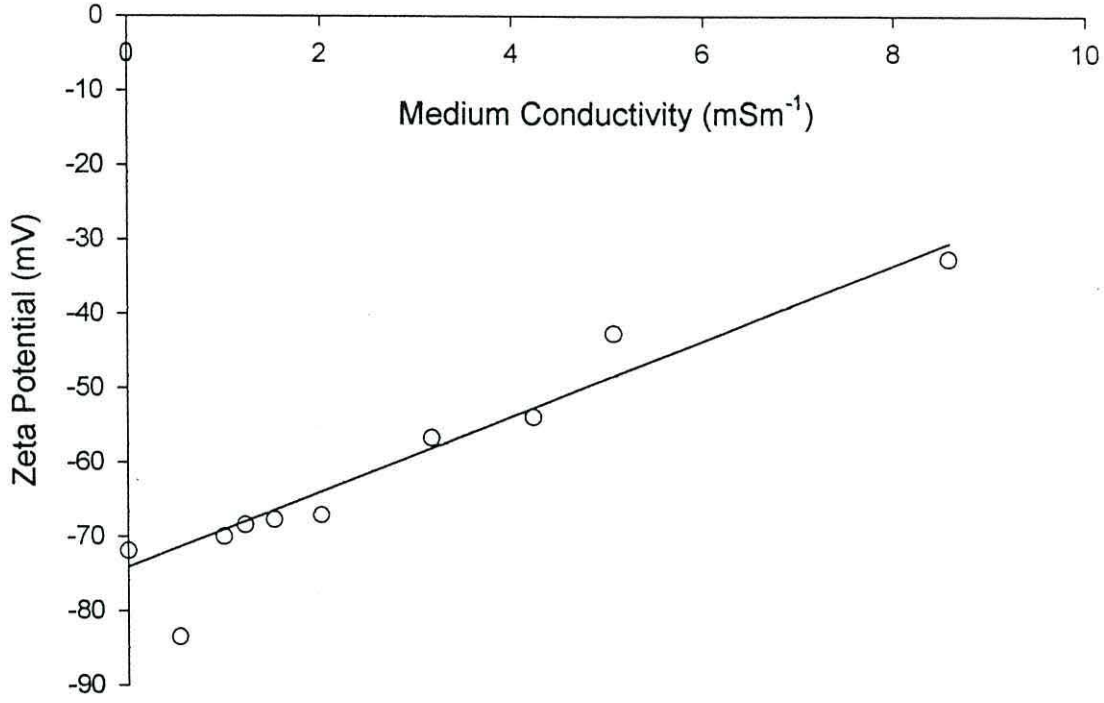

Figure 4.8. Variation in the Zeta potential, of carboxylated elliptical latex particles, with increasing suspending medium conductivity.

4.2.7 Elliptical latex beads without surface functional groups

Samples of elliptical shaped beads with carboxylate surface functional and elliptical shaped beads with no additional surface functional groups were prepared and suspended in 430 μSm^{-1} PBS solution. The electrorotation properties of these latex particles was studied, throughout the frequency range monitored (100 Hz to 5 MHz), see figure 4.9.

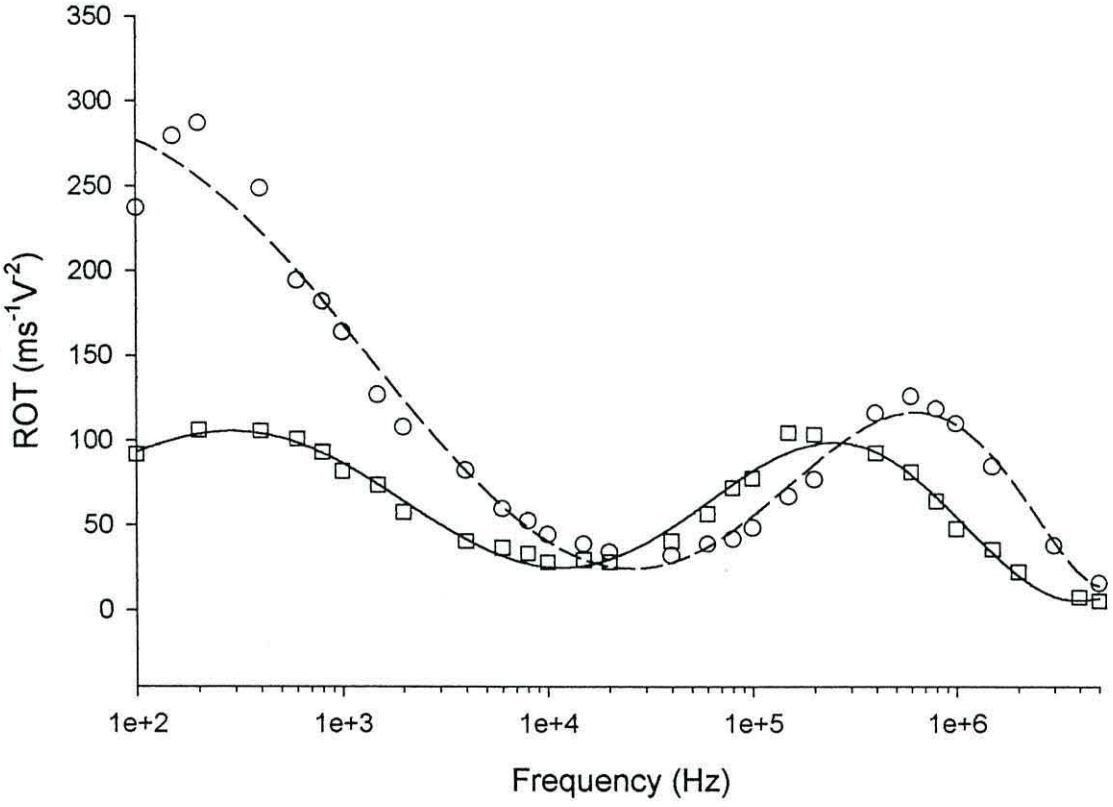

Figure 4.9. Electrorotation spectra of elliptical latex particles with additional carboxylate surface functional groups (○) and no additional surface functional groups (□) suspended in 430 μSm^{-1} PBS solution.

Comparing the particles with the additional carboxylate surface groups and those with no additional surface groups, both the high and low frequency peaks are reduced in magnitude, with the low frequency peak becoming approximately equal in magnitude to the high frequency peak. The low frequency peak is centered on a higher frequency, a shift from around 100 Hz to 300 Hz for the particles without additional surface groups.

The high frequency peak is centered on a lower frequency, a shift from 600 kHz to 200 kHz. It should be noted that although the results displayed in figures 4.1 and 4.9 are for the same system they were performed as different experiments, and were not using the same prepared sample.

4.2.8 Beads without surface functional groups in PBS solution

Samples of elliptical shaped beads and peanut shaped beads with no additional surface functional groups were prepared and suspended in 430 μSm^{-1} PBS solution. The electrorotation properties of these latex particles were studied, throughout the frequency range monitored (100 Hz to 5 MHz), see figure 4.10.

The spectra appear to be very similar with the latex beads rotating field at similar rates and displaying two co-field peaks. The low frequency peak is centered on 300 Hz. The high frequency peak is centered on 250 kHz for the peanut shaped beads compared to 150 kHz for elliptical shaped beads. The magnitude of the high frequency peak is slightly reduced for the elliptically shaped sample.

The zeta potential of both particles was measured using a Coulter Delsa Analyser. When suspended in PBS solution of conductivity 516 μSm^{-1} the zeta potential was measured to be 67.9 ±3.7 mV for the elliptical shaped beads and 63.8 ±4.9 mV for the peanut shaped beads.

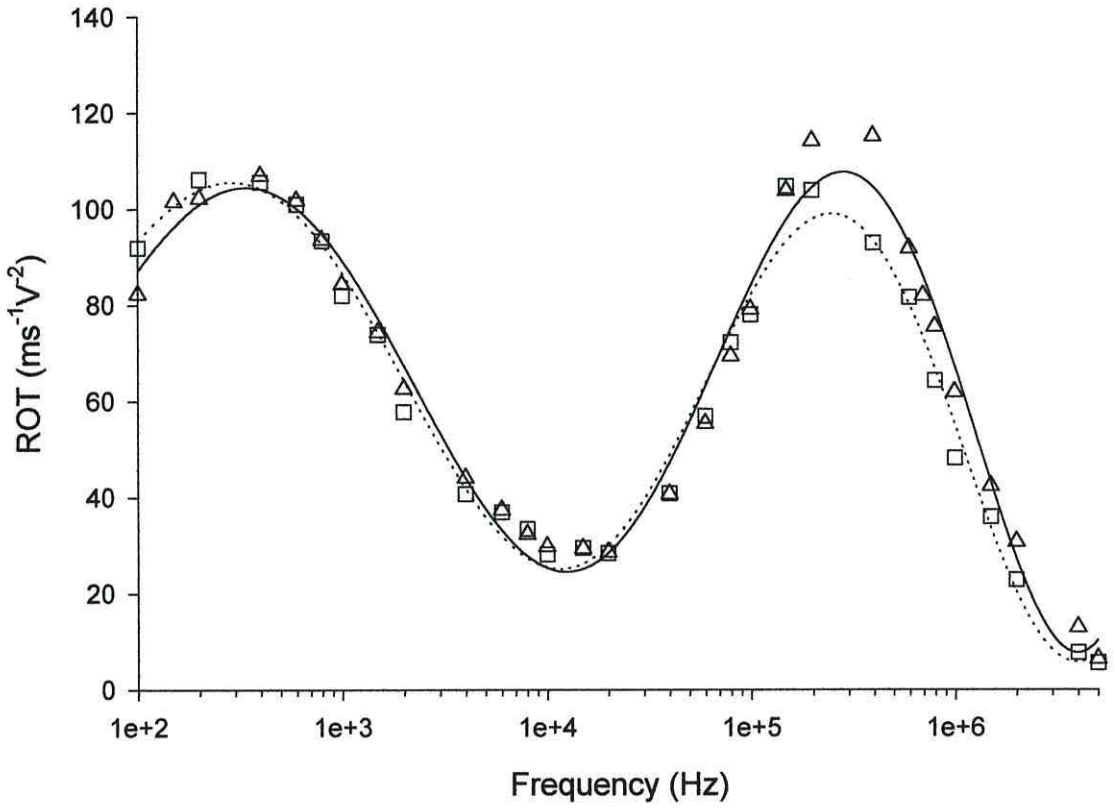

Figure 4.10. Electrorotation spectra of elliptical latex particles (□) and peanut shaped latex particles (△) with no additional surface functional groups suspended in 430 μSm^{-1} PBS solution.

4.2.9 MatLab Modelling

The single shell MatLab model was used to analyse all of the data reported in this chapter. The result are summarized below in Table 4.1. The results were obtained by maintaining the following parameters: $a1 = 3\ \mu m$, $A = 0.09$ and $Kb = 20\ nSm^{-1}$.

The values for *Kc2* and *Ks* were used to adjust the result for the high frequency peak. An increase in *Kc2*, suspending medium conductivity, results in an increase in the peak frequency and a decrease in the magnitude. Increasing *Ks*, the surface conductivity, results in an increase in the magnitude, but does not affect its peak frequency.

The values for *t* and *b* were used to model the low frequency peak. Increasing *a* results in reduction in the peak frequency. Increasing *t* increases the steepness of the peak.

The emboldened data is that modeled for the results from the elliptical carboxylated latex particles suspended in 430 μSm^{-1} PBS solution. The results show a good agreement with each other, however, it does show some spurious calculated results, namely that for the suspending medium conductivity. Comparing the calculated results for sections 4.2.4 and 4.2.5, in order to model the high frequency peak the suspending medium needs to be set to a value nearly six times that measured. Once the value for the measured suspending medium conductivity reached 2.2 mSm^{-1} the calculated MatLab values were in closer agreement. Also, the modeled results for the ultra-pure water conductivity, from section 4.2.3, are very high and are not in agreement with modeled results for other sections. In addition, the low frequency peaks were variable in their results.

Experimental Conditions				MatLab Modelling Results			
				High Frequency Peak		Low Frequency Peak	
Chapter Section	Bead Type	Conductivity of Suspending Medium (Sm^{-1})	Conditions	Suspending medium conductivity (Sm^{-1})	Particle Surface conductivity (Sm^{-1})	Low Frequency Dispersion (t)	Relaxation Distribution Factor
4.2.1	Elliptical carboxyl modified	**430 μ**	**Freshly prepared**	**2.35 m**	**440 p**	**5**	**0.61**
4.2.2		**430 μ**		**2.20 m**	**370 p**	**6**	**0.63**
4.2.2		430 μ	After 24hrs storage at 4°C	8.00 m	750 p	8	0.60
4.2.3		100 μ	Freshly prepared	3.10 m	460 p	85	0.65
4.2.3		100 μ	After 24hrs storage at 4°C	6.30 m	470 p	3	0.98
4.2.5		150 μ	Freshly prepared	0.80 m	230 p	550	0.62
4.2.5		**430 μ**		**2.35 m**	**370 p**	**65**	**0.62**
4.2.5		620 μ		1.30 m	360 p	230	0.58
4.2.5		2.2 m		1.90 m	240 p	400	0.56
4.2.4		10 m		8.00 m	620 p	250	0.50
4.2.4		25 m		16.00 m	1.17 n	600	0.46
4.2.4		50 m		30.00 m	1.9 n	2500	0.44
4.2.4		75 m		50.00 m	2.9 n	5000	0.38
4.2.7		**430 μ**		**2.55 m**	**460 p**	**65**	**0.58**
4.2.7	Elliptical un-modified	430 μ		0.95 m	160 p	520	0.62
4.2.8	Peanut un-modified	430 μ		1.15 m	200 p	650	0.59

Table 4.1 Summary of MatLab results obtained using the single-shell model and the results reported in this chapter.

4.2.10 Summary

As previous discussed a basic investigation of the underlying system, the latex particle, was required since all of the work in this study are based on this assay. This chapter has provided results in several key areas:

- **Carboxylated elliptical particles suspended in 430 μSm^{-1} PBS solution.**
  The main results of interest are presented in section 4.2.1. It was important to study this area since the work in this study is based on these particles in this suspending medium. Good coherent responses were obtained however, it was noticed that the spectra seemed to change with time, hence the following area of study.

- **Changes in the spectra of carboxylated elliptical particles with time.**
  Sections 4.2.2 and 4.2.3 demonstrated the problems with storage of the particles in low conductivity media. The particles experienced an apparent 'aging' effect. This affect appeared to be more pronounced at low conductivity suspending media and to be accelerated by treatment with acid. Since experiments in this study were performed in low conductivity media this area was investigated further by investigations into the affect that suspending media conductivity and particle surface conductivity had on the particles.

- **Affect of suspending medium conductivity on carboxylated elliptical particles.**
  Sections 4.2.4, 4.2.5 and 4.2.6 present results to show how the suspending media conductivity affects the electrorotation properties and the zeta potential of the particles. In general coherent tends were identified, however, some anomalous results were also observed

- **Comparison of latex particles of differing geometry and surface properties.**
  Sections 4.2.7 and 4.2.8 present results to show how a change in the particle's surface properties and geometry affects the electrorotation spectra.

4.3 Discussion

The four key areas of results, described in the previous section will be discussed in this section. Initially the following areas will be dealt with independently:

- Carboxylated elliptical particles suspended in 430 μSm^{-1} PBS solution.
- Affect of suspending medium conductivity on carboxylated elliptical particles.
- Affect of pH on carboxylated latex particles.
- Comparison of latex particles of differing geometry and surface properties.

Finally, the changes in the spectra of carboxylated elliptical particles with time, the 'aging' affect will be discussed, since this draws on results and discussions from all of the sections.

4.3.1 Carboxylated elliptical particles in 430 μSm^{-1} PBS solution

Dielectric measurements for suspensions of charged latex spheres indicate the existence of two dispersions[1, 2]. The two electrorotation peaks in figure 1 are dispersions. The high frequency dispersion is generally assigned to the Maxwell-Wagner interfacial polarization mechanism and the lower frequency dispersion has been interpreted as a relaxation of the electrical double layer associated with the surface charge of the particle[3].

For the high frequency dispersion the results obtained by Arnold et al[4], for carboxylated particles of 5.29 μm diameter, are in close agreement to those observed here. They found that for a solution with a conductivity of 600 μSm^{-1} the high frequency dispersion was centered on 175 kHz compared to around 600 kHz for the particles in this study. Other authors have made electrorotation measurements on larger latex spheres[5] and dielectrophoretic measurements on sub-micron latex spheres[3] that are also in agreement with these results.

For the low frequency dispersion the results obtained by Arnold et al[4], for carboxylated particles of 5.29 μm diameter, are also in close agreement to those observed here. They

found that, for a solution with a conductivity of 600 μSm^{-1}, in the low frequency region the rotation rate increased with decreasing frequency, however, they did not observe a peak for the dispersion. This observation was also sometimes to be made during future results of this study. Arnold noted that it was tempting to believe that a peak would be attained if a sufficiently low frequency could be reached. He noted that there was a lack of experimental reports on this area and that the magnitude of this dispersion was disputed. In this study, the magnitude of the dispersion varies between around 220 $ms^{-1}V^{-2}$ and 275 $ms^{-1}V^{-2}$. From the MatLab results, in section 4.2.9, it can be seen that the result calculated for the low frequency dispersion for the carboxylated elliptical particles suspended in 430 μSm^{-1} was not consistent. Arnold hypothesizes that in this region, the medium next to the particle will be modified by the ionic double layer. He goes on to say that within this double layer there will be an increased concentration of counter ions to the particle surface charge. The ratio between the local counter ion concentration and that in the bulk falls off exponentially with a characteristic length equal to the Debye length[6]. This length was calculated to be 120 nm in the 600 μSm^{-1} solutions that he used. The polarizability of the diffuse double layer has been put forward as the cause of the large permittivity of latex (and probably other particle) suspensions at low frequencies and this polarizability will change the effective permittivity next to the particle.

The diffuse double layer owes its existence to the particle surface properties of the particle. Arnold[4] calculates that the majority of the diffuse double layer is not rigidly coupled to the particle. He presumes that the low frequency rotations measures something entirely different from those observed by measurements on bulk suspensions, such as dielectric measurements. The low frequency dielectric measurements are of the electrical appearance of the double layer/particle assembly as seen from the outside, whereas electrorotation probes the field inside the diffuse shell. Maier's[5] electrorotation measurements in the low-frequency region, on larger latex spheres, are also in agreement with these results.

Error bars were included in figure 4.1, they show an increasing significance at low frequencies, less than 1 kHz. The origin of this variability could be due to the aging affect, which is discussed in more detail in later sections. However, since the spectra

show a coherent response, it is more likely to be due to slight differences in particle size, ±2% according to the manufacturers and differences in the electrophoretic mobility's of the particles. Arnold et al[4] measured ±6% deviation for the zeta potential's of 5.29μm diameter carboxylated latex particles. Maier[5] measured a standard deviation of 4.6% in electrophoretic mobility's for 9.67 μm diameter carboxylated latex particles.

It can be seen that latex beads exhibit a distinct electrorotation spectrum. The MatLab results showed good agreement between the results for the high frequency peak, giving a calculated surface conductivity of between 370 – 460 pSm^{-1}. However, the calculated results for the suspending medium are not accurate at this low conductivity. The low frequency peak proved to be less consistent and more significant variability was observed in this region. It is the high frequency peak that will be used to monitor changes in the surface properties in the future chapters, since this area appears to be more reliable. These particles will be used as the basis of the systems under investigation in this study. The particles will be modified, using antibodies, bacteria and DNA, and the electrorotation properties monitored.

4.3.2 Affect of pH on carboxylated latex particles

In section 4.2.3 it was noted that after treatment with hydrochloric acid the carboxylated particles did not rotate when subjected to a rotating electric field. This was considered to be significant since it was felt that this could help to explain the mechanism behind the aging affect. It is therefore considered to be of interest for the discussion.

Other authors have investigated the affect of pH on latex particles. Ho et al[7] made measurements of the reduction of electrophoretic mobility with increasing acidic conditions, to the point where at a pH 4 the mobility reversed. Maier[5] investigated the affect of pH on elliptical latex particles. He measured a reduction in the magnitude of the low frequency peak, by nearly one-third, as well as an increase in the significance of the errors, for a decrease in the solution pH from 8.3 to 4.1. For a decrease in the solution pH, from 8.3 to 4.1, he demonstrated that the high frequency peak showed a slow anti-field rotation. From his conductometric titration data he elucidated that the

acid groups contributing to the surface charge are mainly, if not entirely, carboxyl groups. He continues to explain that the strong acid group, that is sulfate groups, from the production, is present on nearly all types of such particles (this was confirmed by the manufacturers of the particles in this study[8]). Maier hypothesized that the absence of strong acid groups on his particles made it possible to suppress surface charges nearly completely at around pH 4, at the particle's equivalence point. This was attributed to the acid groups on the surface of the bead reaching an undissociated state leading to a reduction in the electrophoretic mobility.

Latex beads are a giant three-dimension polystyrene copolymer with the following arrangement, figure 4.11:

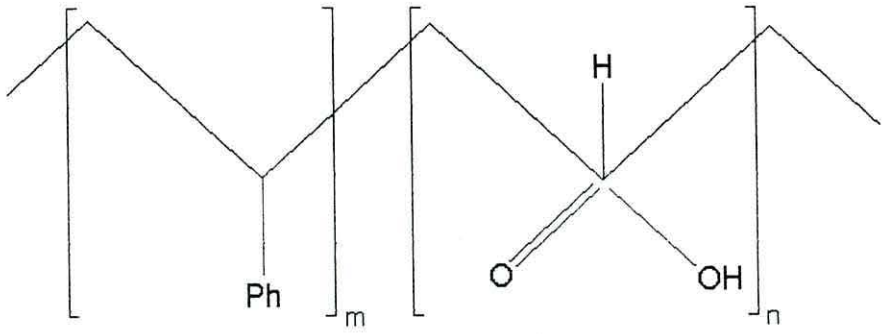

Figure 4.11. Chemical arrangement of the polystyrene latex beads. *Ph* represent the phenyl groups and *m* and *n* are the number of repeating units.

However, since the beads are stored in a salt solution, the carboxyl group is unlikely to be found in that form. It is most likely to have a metal cation, from the suspending medium, associated with the oxygen, figure 4.12:

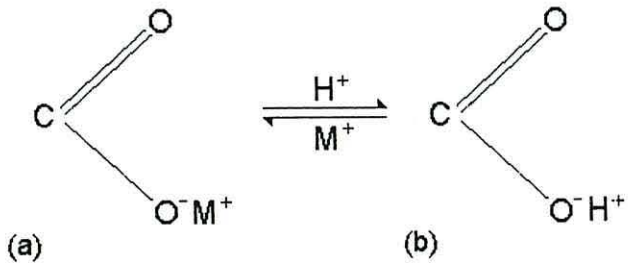

Figure 4.12. Carboxyl group (a) when stored in salt solution and (b) after protonation.

It is anticipated that with time the carboxyl group is gradually protonated by the low conductivity media. This would result in a reduction in the rotation rate since the particle now 'appears' to be less conductive, to the point where the particle conductivity appears to be equal to that of the suspending medium. If this happened, the dipole moment of a particle, which is dependent on the Clausius-Mosotti factor, see equations 31, would tend to zero, resulting in a reduction in the rate of rotation. If the particle surface conductivity were reduced to below the suspending medium conductivity anti-field electrorotation would be observed.

4.3.3 Affect of suspending medium conductivity

The affect on the electrorotation spectra and the zeta potential of carboxylated elliptical beads suspended in solutions PBS of varying conductivities was investigated. The results are presented in sections 4.2.4, 4.2.5 and 4.2.6. The aim was to find out more about the affects of increased suspending medium conductivity.

In general, from MatLab modelling, an increase in suspending medium conductivity alone would result in a decrease in magnitude and increase in frequency of the high frequency peak. Whereas the low frequency peak would be expected to decrease in frequency but increase in magnitude. In the experimental results the high frequency peak decreased in magnitude and increased in frequency and the low frequency peak, in general, showed a decrease in magnitude, not an increase. The increase in suspending medium was associated with a reduction in the zeta potential of the particle. However, there were some anomalous effects. The low frequency peak showed an increase in magnitude, in the low conductivity region, 150 to 2100 μSm^{-1}, conforming to the mode, however, in increasingly ionic solutions the magnitude decreased. Since there is significant variability associated with the sub 1kHz region this affect could possibly be discounted.

The increase in magnitude and frequency of the high frequency peak with increasing suspending medium conductivity was also observed by Maier[5] and Arnold[4]. Maier investigated the affects over the range 1.17 to 2.207 mSm^{-1} of solutions made from a mixture of sodium hydroxide and acetic acid. He attributed the changes in the

magnitude to changes in the dissociation state of the surface carboxyl groups resulting in an increase in the electrophoretic mobility. Arnold[4] links the decrease in magnitude to an increase (that is, becoming less negative) in the electrophoretic mobility with increasing ionic strength. An increase in electrophoretic mobility of the carboxylated elliptical beads was also observed in this study, accompanying a decrease in the magnitude of the high frequency peak. Ho et al[7] also studied the affect of increasing ionic concentration on rubber latex particles. They found that the electrophoretic mobility increases exponentially then plateaus off with increasing ionic strength to a maximum.

In theory, if there is no chemical absorption of ions in the latex particles, for an increasing electrolyte concentration, at a constant pH, a decrease in the electrophoretic mobility should be observed, due to a compression of the double layer. Although, this decrease in electrophoretic mobility has been observed by the authors above and by others[16]. Tuin et al[9] and Yates et al[10] have observed that as the electrolyte concentration increases, the electrophoretic mobility first increases in value and then decreases only when a certain electrolyte concentration is surpassed. This was also observed in this study. For the suspending medium conductivity of 538 μSm^{-1} the zeta potential of the particle reached a maximum value before decreasing exponentially.

Another anomalous experimental result was the electrorotation of the particles in the 620 μSm^{-1} suspension. They are very similar to those obtained for the ultra-pure water, when it would be expected that they would lie between those obtained for the 430 μSm^{-1} and the 2.1 mSm^{-1} PBS solutions. This coincides with the anomalous result observed for the zeta potential of the particles. Other authors have also observed this type of anomalous electrokinetic behavior in polystyrene latex particles electrophoretic and zeta potential measurements. Shirahama and Suzawa[11] also observed this affect for zeta potential measurements on carboxylated latexes. These affects have also been observed by many other authors[12, 13, 14]. Various authors have tried to explain these changes in mobility via the 'hairy layer' model[14, 15, 16], the 'co-ion adsorption' model[16, 17, 12], or by surface conductivity[18].

The 'hairy layer' model assumes that the latex particle is covered by a layer of protruding, flexible, polymer chains ("hairs") having terminal end groups, such as the sulfate groups, left from the manufacture, or carboxyl groups[16, 14, 9]. As the ionic strength decreases the repulsion between these charged groups increases and the hairy layer expands. This results in the slip plane moving outwardly, and the net charge transported electrokinetically decreases.

The co-ion adsorption model assumes, in the case of negatively charged particles, that anions, which are less hydrated than cations, are closer to the apolar surface[16, 17, 12]. These anions are not believed to be chemically absorbed on specific sites and the magnitude of the electrokinetic potential depends on the valency of the co-ions.

In the surface conductivity model, the presence of mobile Stern-layer anions causes the mobility to decrease and the conductivity to increase, in comparison with the case where surface conductivity is absent[18]. According to this model, not only does the diffuse double layer contribute to the surface conductance an affect between the slipping plane and particle interface is also operative.

There are currently not enough results in this study to discount or prove any one of these theories. However, the co-ion adsorption model agrees with conventional dielectric theory. The latex particles are fully polymerised during manufacture and it is assumed that the 'hairy layer' model is unlikely. It is expected that any protruding chains with terminal end groups would be so tightly packed so as not to be flexible. Ho et al[7] use this model to explain a decrease in the electrophoretic mobility in latex particles, however, they talk about the hairy layer being composed of long chain fatty acid soaps, polypeptides and proteins. Since the particles in this study were thoroughly cleaned and unmodified it is not expected that this would be a representative model for these results. The surface conductivity model also seems unlikely. This counter-ion migration affect is observed in other systems such as solutions of DNA. In these systems the DNA remain static and weakly attracted anions migrate along the negatively charged phosphate backbone. This typically occurs at high frequencies, in excess of 10MHz for DNA, where the particle is no longer able to respond to the alternating field. Since the

latex particle is able to respond at the frequencies used in this study this model is unlikely to represent the system.

It seems most likely that the co-ion adsorption model best describes the system here. Arnold et al[4] uses this model of the system to explain both the dispersion attributed to the Maxwell-Wagner affect and the low frequency dispersion. However, it doesn't explain the anomalous initial increase in the zeta potential observed in this studies results. Shirahama and Suzawa[11] hypothesize that the increase in zeta potential may be due to the adsorption of chloride ions from the bulk solution onto the particle surface resulting in the surface becoming more negative.

In the MatLab results, the surface conductivity was modeled to increase from 240 pSm^{-1} to 2.2 nSm^{-1} for an increase in suspending media conductivity, from 2.2 mSm^{-1} to 75 mSm^{-1}, supporting the results and discussion in this section. The value for the low frequency dispersion (t) was modeled as increasing from 230 s to 5000 s for an increase in suspending medium conductivity, from 620 μSm^{-1} to 75 mSm^{-1}. Below 2.2 mSm^{-1} the modeled surface conductivity were small and variable, not showing any discernable trend. In this region the calculated suspending medium conductivity was difficult to model and was not in agreement with the measured results.

These results provide additional information concerning the 'aging' effect of the beads. They exemplify how significantly the conductivity of the medium must increase to result in significant changes in the spectra.

4.3.4 Latex particles of differing geometry and surface properties

Comparing the elliptical carboxylate modified and un-modified particles spectra, the results were very similar, however, the MatLab results were very different. They showed a very significant decrease in the surface conductivity, from 460 pSm^{-1} to 160 pSm^{-1}. Although a decrease may have been expected a decrease in the suspending medium was also modeled, which would not be expected. For this reason, the modeled results are viewed with some skepticism. If the suspending medium was kept constant, although the peak frequency would not be accurately modeled, the magnitude could be a

modeled by only a slight reduction in the surface conductivity, to approximately 400 pSm^{-1}. So it is anticipated that the slight difference is most likely due to a differing of surface conductivity.

The polystyrene particles are made using sulfonate-type surfactant. The sulfonate surface groups are covalently bound to the surface and gives rise to an inherent negative surface charge. In addition, carboxylate modified latex also have active hydrophilic COOH groups on their surface. Bangs[8] has noted the presence of both sulfate and carboxyl groups on the carboxyl modified latexes. He measured, using conductometric measurements, that the sulfate density is approximately half that of the carboxyl. In theory, the unmodified latex particles should possess just the sulfate surface groups[8] giving rise to a much lower surface conductivity. If this was the case, the MatLab modeled results for the surface conductivity could be considered to be a reflection of the system. If the reduction in the suspending media conductivity is to be discounted, this may not be the case.

Bastos-González et al[19] works indicates the evidence of both carboxyl and sulfate surface groups on particles that would be expected to just have sulfate groups. In their study, they investigated the surface properties of latex particles with differing surface properties, including carboxylate modified latex particles and particles with sulfate surface groups. They used both conductimetric methods and by observed the affect of increasing suspending medium conductivity on the electrophoretic mobility. For carboxylate modified particles, they measured an electrophoretic mobility of 3.0 m^2/Vs compared to a value of 2.9 m^2/Vs for those with sulfate surface groups, when suspended in a solution of sodium chloride of approximately 20 μM concentration.

From the conductimetric titration's on the sulfate particles he ascertained that both strong acid (sulfate) and weak acid (carboxyl) groups were present on the surface of the particles, when it might have been expected to only observe strong acids on the surface. A number of other authors[20, 21, 22] have reported both groups in this kind of latex. There are two ways that this could happen. First, the transformation of sulfate groups into hydroxyl groups through Kolthoff reaction[23] and finally to carboxyl groups due to the oxidation of these groups. Second, although not likely to be applicable in the system

studied in this work, the sulfate groups can be oxidized directly into carboxyl groups[13], with long reaction times and at high temperatures.

Since Bangs[8] observes both strong and weak acid groups on the carboxylate modified latex particles and Bastos-González et al[19] also observe them on particles with sulfate surface groups it is anticipated that the surfaces of the two particles used in this study, carboxylate modified and un-modified latex particles, are very similar. This would explain the similar results for their electrorotation spectra and account for only slight differences in their surface conductivity.

Comparing the results for the elliptical and peanut shaped latex particles, with no additional surface groups, the results show no appreciable differences. Any differences are mostly likely due to the differing surface areas.

4.3.5 The 'aging' affect

An 'aging' affect was noted in the latex particle systems, that is, a change in the spectra, generally a decrease in magnitude and an increase in peak frequency of the high frequency peak, for further details see sections 4.2.2 and 4.2.3. This 'aging' effect was seen in all of the investigated systems, although in the 'multi-shelled' systems it appeared to be less pronounced, see *E. coli* and Macromolecules chapters. Maier[5] also noted a reduction in the electrorotation spectra of approximately one-third over time.

The MatLab modelling results for the aging affect on elliptical carboxylated particles suspended in ultra-pure water were not entirely in agreement with those obtained for 430 μSm^{-1} PBS solution. To obtain the increase in the high frequency dispersion peak frequency the suspending medium conductivity is predicted to increase. For the 430 μSm^{-1} PBS suspension the suspending medium conductivity was calculated to have increased almost four-fold and the calculated surface conductivity more than doubled. The MatLab results obtained for the aged samples are similar to those obtained for the particles suspended in 10 mSm^{-1} PBS solution. This increase in calculated surface conductivity, with increased suspending medium conductivity, was obtained for suspensions of PBS of increasing ionic strength in section 4.2.4.

For the ultra-pure water suspension the suspending medium conductivity was calculated to have more than doubled, from a value of 3.1 mSm^{-1} to 6.3 mSm^{-1}, this is in close agreement to those results obtained in section 4.2.3. The modeled suspending media value was much higher than the modeled results for section 4.2.5. No significant change was calculated for the surface conductivity. This was also observed for the results modeled for section 4.2.4, for the 430 μSm^{-1} and the 620 μSm^{-1} suspensions. In general, at low suspending media conductivities, the results calculated were variable and showed no discernable trend. It is likely that the 'aging' affect is due to a combination of both increases in the suspending medium conductivity and changes in the surface properties of the particle.

A possible motivation for the rise in ionic concentration could have been bacterial contamination, however, no bacterial contamination was ever detected using standard agar plating techniques. Samples were stored at 4°C and only sterile techniques were employed for the sample preparation. In addition, it seems highly unlikely that bacteria would survive these harsh environmental conditions and if they did would be more likely to be actively saving ions.

It is expected that the ultra-pure water soaked beads, in section 4.2.3, would eventually exhibit little or no electrorotation behavior if left for a sufficient length of time. It seems reasonable to hypothesize that, since this is a time dependent process, that ions could be 'leaching' out of the beads, resulting in a rise in conductance. Arnold et al[4] reports that despite extensive washing a slow increase in suspending medium conductivity was observed. The results from the MatLab modelling, in section 4.2.9, and the monitoring of the voltage across a 1 ohm resistor, in section 4.2.3, agree with this increase. In addition, the electrorotation results in sections 4.2.4 and 4.2.5, confirm the affect of increasing ionic strength on the latex particles. However, the origins of this rise cannot yet be determined. In an attempt to confirm this hypothesis a recognised chemical technique, which measures the concentration of ions in solution, Inductive Coupled Plasma (ICP), was employed. Unfortunately, these tests proved to be inconclusive.

Other authors that have observed the aging effect in latex spheres have concentrated on monitoring this affect through the particle's surface conductivity or its electrophoretic mobility[8, 19]. Bangs has monitored this affect by measuring the parking area of sulfate groups on polystyrene latexes[8]. This work shows that the parking area increases over time, by approximately one-third after 6 months. He attributes the rise to the hydrolysis of sulfate groups to hydroxide groups over time[24, 10]. Although the beads used in the present work are carboxylated latexes the surfaces contain these sulphate groups and could therefore experience this aging effect described by Bangs. Heating can apparently accelerate this aging effect[19, 13]. However, this would most likely lead to a reduction in the particle's surface conductivity. If the MatLab results in section 4.3.4 were accurate the hydroxide groups, which Bangs attributes to the aging affects, would need to be transformed to carboxyl groups. The work done by Bastos-González et al[19] could confirm this. Using conductimetric titration's on carboxylated latexes he found that both strong and weak acids were present on the particle. After heat treatment no strong acids were present but the amount of weak acids had increased. This would be expected to increased the surface conductivity of the particles. Conductimetric and potentiometric results confirmed this while measurements of the electrophoretic mobility are inconclusive.

4.4 Conclusions

Coherent repeatable results were obtained for carboxylated elliptical particles suspended in 430 μSm^{-1} PBS solution and can therefore be used as a reliable basis for the work following this chapter. The origin of the high frequency dispersion appears to be well understood in the literature, unlike the low frequency dispersion.

The electrorotation assay is a sensitive technique and is able to detect changes to the latex particle's environment. For instance, it is sensitive to changes in the suspending medium. Discernable trends were observed for increasing ionic strength that were sometimes in agreement with the model of the system. Some anomalous results were obtained which may be attributed to the adsorption of anions. Measurable differences were obtained for latexes with differing surface properties, unmodified and carboxylate modified.

Problems with an 'aging' affect in the particles was attributed to a rise in the suspending medium conductivity and a change in the surface properties. The change in the surface properties is probably an increase in surface conductivity, due to an increase in the number of carboxyl groups present. However, there is not enough data and the model is not refined enough to prove this conclusively. To reduce the effect of the 'aging' of the prepared beads, experiments in this study were always prepared and completed on the same day, unless otherwise specified.

The MatLab modelling results were useful in helping to draw conclusions or substantiate theories. One draw back was the lack of accuracy in modelling the suspending medium conductivity for the low values, under 2.2 mSm^{-1}.

4.5 References

[1] Schwan HP, Schwarz G, Maczuk J and Pauly H. *J. Phys. Chem.* 1962; 66:2626.

[2] Sasaki S, Ishikawa A and Hanai T. Dielectric Properties of Spherical Macroion Suspensions. 1. Study on Monodisperse Polystyrene Latex. *Biophys. Chem.* 1981; 14:45-53.

[3] Green NG and Morgan H. Dielectrophoretic investigations of sub-micrometer latex spheres. *J. Phys. D: Appl. Phys.* 1997; 30:2626-2633.

[4] Arnold WM, Schwan HP and Zimmerman U. Surface conductance and other properties of latex particles measured by electrorotation. *J. Phys. Chem.* 1987; 91: 5093-5098.

[5] Maier H. Electrorotation of colloid particles and cells depends on surface charge. *Biophysical J.* 1997; 73:1617-1626.

[6] McLaughlin S. *Curr. Top Membr. Transp.* 1977; 9:71.

[7] Ho CC, Kondo T, Muramatsu N and Ohshima. Surface structure of natural rubber latex particles from electrophoretic mobility data. *J. Col. And Intf. Sci.* 1996; 178:442-445.

[8] Bangs LB. Uniform latex particles. 1984. Seradyn, Indianapolis, IN.

[9] Tuin G, Senders JHJE and Stein HN. Electrophoretic properties of monodisperse polystyrene particles. *J. Col. And Intf. Sci.* 1996; 179:522-531.

[10] Yates DE, Otterwill RH and Goodwin JW. *J. Col. And Interface Sci.* 1977; 62:356-8.

[11] Shirahama H and Suzawa T. Surface characterization of soap-free carboxylated polymer latices. *Polymer Journal.* 1984; 16:795-803.

[12] Elimelech M and O'Melia C. *Col. Surf.* 1990; 44:165.

[13] Kamel AA, El-Aasser MS and Vanderhoff JW. The Preparation And Surface Characterization Of An Ideal Model Colloid. J. Dispersion Sci. and Tech. 1981. 2: 183-214.

[14] Midmore BR, Diggins D and Hunter RJ. The Effect Of Temperature And Ion Type On The Effective Charge In Polystyrene Lattices. *J. Col. Intf. Sci.* 1989; 129:153-161.

[15] Chow RS and Takamura K. Effects Of Surface-Roughness (Hairiness) Of Latex-Particles On Their Electrokinetic Potentials. *J. Col. Intf. Sci.* 1998; 125:226-236.

[16] Verdegan BM and Anderson MA. Influence Of Solvent On The Electrophoretic Mobility Of Polystyrene Latex. *J. Col. Intf. Sci.* 1998; 158:372-381.

[17] Voetgtli LP and Zukoski CF. Adsorption Of Ionic Species To The Surface Of Polystyrene Latexes. *J. Col. Intf. Sci.* 1991; 141:92-108.

[18] Van der Linde AJ and Bijsterbosch BH. Does The Maximum In The Zeta Potential Of Monodisperse Polystyrene Particles Really Exist - An Electrokinetic Study. *Croat. Chem. Acta.* 1990; 63(3):455-465.

[19] Bastos-González D, Hidalgo-Álvarez R and De Las Nieves FJ. Electrokinetic behavior of polystyrene latexes with different surface groups: effect of heat treatment. *J. Col. and Intf. Sci.* 1996; 177:372-379.

[20] Goodwin JW, Hearn J, Ho CC and Otterwill RO. *Brit Polym J.* 1973; 5:347.

[21] Goodall AR, Hearn J and Wilkinson HC. *Polym. Sci. Chem. Ed.* 1977; 15: 2193.

[22] Bijsterbosch BH. *Colloid Polym. Sci.* 1978; 256:343.

[23] Kolthoff IM and Miller IK. *J. Am. Chem. Soc.* 1951; 73: 3055.

[24] van den Hul HJ and Vanderhoff JW. *Brit. Polym. J.* 1970; 2:121-7.

Chapter 5

Escherichia coli and *Bacillus subtilis*

5.1 Introduction

The electrical properties of cell suspensions are determined to a large extent by their structural heterogeneity and surface charge, see Materials and Methods chapter for further details. During their life cycle, cells undergo numerous physico-chemical changes including structure and surface charge. Electrorotation measurements can be particularly sensitive to these changes and can be used as a responsive method of analysis, as was seen in the Latex Particles chapter.

The main cells of interest in this study were *Escherichia coli* (K12) and, to a lesser extent, *Bascillus subtilis*, for further details see the Methods and Materials chapter. The bacteria were first attached to a larger particle, an antibody-labelled latex bead of 5.2μm in length. Although the antibody-labelled particles provide distinct and coherent electrorotation characteristics of their own, the addition of a single bacteria to their surface results in marked changes to their electrorotation characteristics, even to the extent that the sense of the rotation is reversed. These characteristics are clearly changed with the addition of further bacteria to the surface of the microbead. The electrorotation assay can also differentiate between viable and non-viable bacteria.

There is the potential for applying this technique as a rapid and precise assay for the detection of viable and non-viable bacteria, which is particularly applicable to the food, water and healthcare industries.

5.2 Results

The results presented in this chapter are for the attachment of viable and non-viable *E. coli* to antibody coated beads. In addition, results for the attachment of *B. subtilis* are also presented. The Latex Particles chapter presents evidence for an 'aging' effect in the beads. This effect appeared to be less prevalent in the antibody coated beads, however, to minimise any of these affects, experiments were performed and completed on the same day as their preparation, unless specified. The suspending medium used throughout this chapter was 170 mM mannitol made with a phosphate buffered saline solution to equate to a conductivity of 500 μSm^{-1}.

5.2.1 Optimisation of *E. coli* Suspending Media

The experiments need to be performed in very low conductivity PBS solution. This requirement provides a very harsh environment for the bacteria, whose solutes are typically at a concentration of 100 to 150 mM. Initial electrorotation experiments on the *E. coli*, were inconsistent and obtaining binding to the antibody coated beads was difficult. As a result of this the affect of the suspending medium on the viability of the *E. coli* was investigated.

The viability of the *E. coli* was assessed by suspending them in the different mediums then, at given times, plate the bacteria on to agar plates. The plates were then incubated for 24 hours at 37°C after which time their relative growths rates were considered.

When suspended in ultra-pure water the *E. coli* showed only one small colony of growth on the agar plates. Staining to test the viability of this sample showed that the majority, >95 %, were non-viable. In addition, it was very difficult to obtain binding of the *E. coli* to the antibody coated bead when suspended in ultra-pure water.

Several other suspending mediums were tested: 170 mM glycerol, 170 mM mannitol, 280 mM mannitol, and dialysed nutrient broth. The relative growth rates for the latter three suspending mediums displayed in figure 5.1.

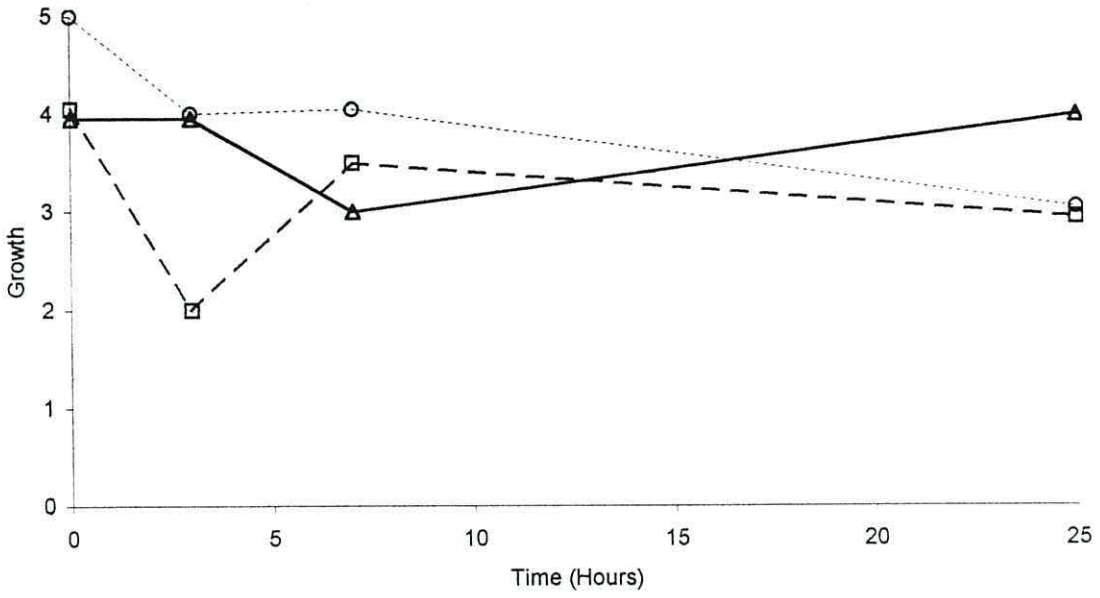

Figure 5.1. Comparative growth rates of *E. coli* in different growth media, nutrient broth (···○···), 280mM mannitol (-□-) and 170mM mannitol (—△—).

When suspended in nutrient broth the viability of the *E. coli* showed a decline over 24 hours. For the mannitol solutions an initial loss in activity was observed, however, after this the 170 mM solution appeared to show a relative increase in viability. The results for the glycerol suspending medium showed that little, if any viability was lost over the observed 24 hours, however, using this medium it was not possible to obtain a binding between the *E. coli* and the antibody coated beads.

Although these results are subjective, the 170 mM mannitol solution was chosen as the desired suspending medium on the basis that the viability was maintained for a sufficient length of time and would not affect the conductivity of the suspending medium and after consideration of the osmotic potential within the cell[1]. In addition,

the morphology of a sample of *E. coli* was observed over time, since the changes in shape are an indicator to the 'stress' placed on a sample[2].

The results presented in figure 5.2 indicate the stress that the *E. coli* are placed under when suspended in 170mM mannitol after being grown up in nutrient broth. The initially high percentages of cocoid shaped *E. coli* suggests that the sample is suffering from stress[2]. However, there are similar proportions of *E. coli* that are not showing signs of stress, which are displaying healthy activity and are elongated or are multiplying. As time increases, to around fifteen hours the number of healthy *E. coli* has increased, exponentially, and the number of *E. coli* showing stress has decreased, exponentially. After this time the relative ratios of healthy to stressed *E. coli* starts to level off. Fuller discussions of these results are presented in the Results section 5.3.3.

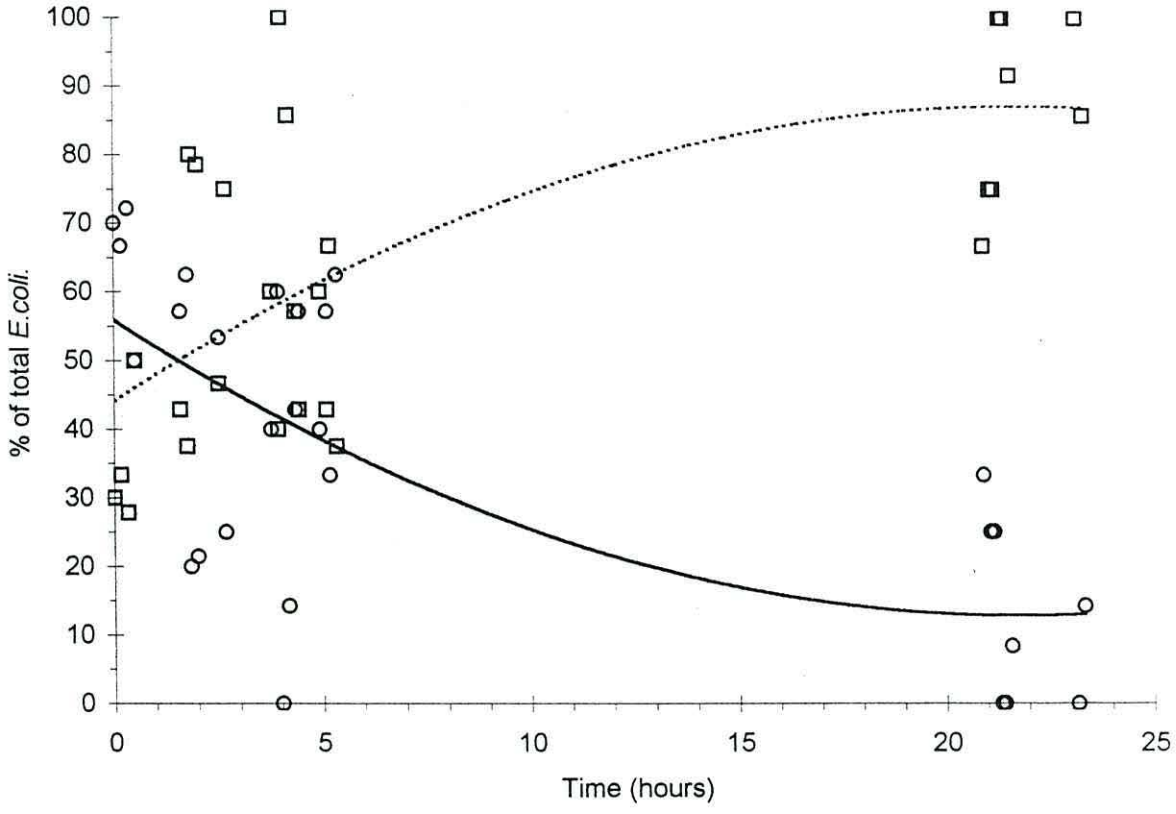

Figure 5.2. Graph showing how the number of cocoid shaped of *E. coli* (○) and those that are elongated or multiplying (□) changes with time. The solid line shows the trend for the cocoid shaped *E. coli* and the dotted line is that for the elongated or multiplying *E. coli*.

5.2.2 Optimum Antibody Concentration Required for the Bead Preparation

Electrorotation experiments on *E. coli* antibody coated beads were performed to determine the optimum amount of antibody required during the preparation. The following figures in this section describe the effect of including differing amounts of antibody in the preparation. The amounts of antibody are stated as the amount used in the preparation and are not the actual amount on the bead surface.

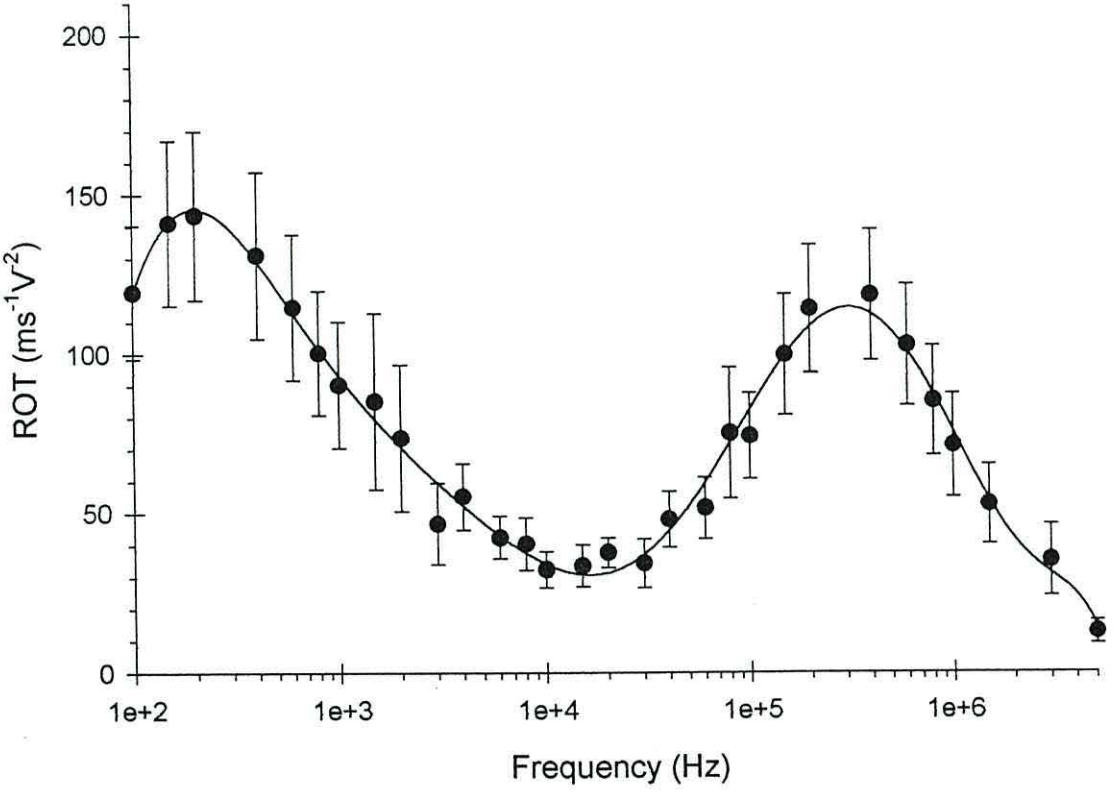

Figure 5.3. Electrorotation spectrum of latex beads coated with 5µl of *E. coli* antibody in 500 μSm^{-1} PBS solution, sample of 12 particles.

Antibody coated beads were observed to have two co-field peaks, a low frequency peak centred on frequencies below 1 KHz and a high frequency peak centred on frequencies around 300 KHz. The effect of increasing antibody concentration is summarised in

table 5.1. Figure 5.3 displays very significant variability, this could be due to there being insufficient antibody to form a complete coverage over all the beads. Studying the data, for this sample, revealed that there was a significant time related effect. During the course of the experiment, lasting two hours, the spectra was observed to decrease in magnitude, in a similar manor to that observed in section 5.3.6, which resulted in significant errors.

Using 10 and 15μl of antibody, in the preparation, the results are shown in figures 5.4 and 5.5, the errors in the spectra are significantly reduced. When this amount of antibody was used in the preparation of the beads was found to support sufficient adhesion of *E. coli*, up to ten.

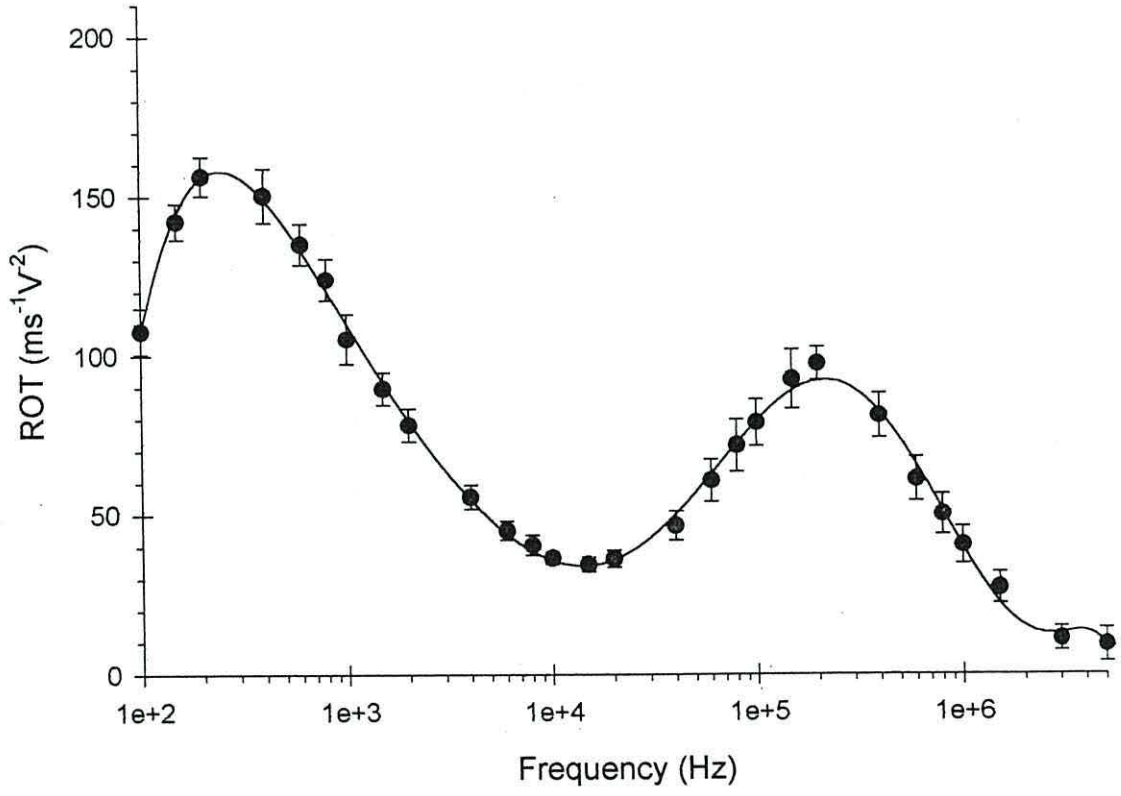

Figure 5.4. Electrorotation spectrum of latex beads coated with 10μl of *E. coli* antibody in 500 μSm^{-1} PBS solution, sample of 13 particles.

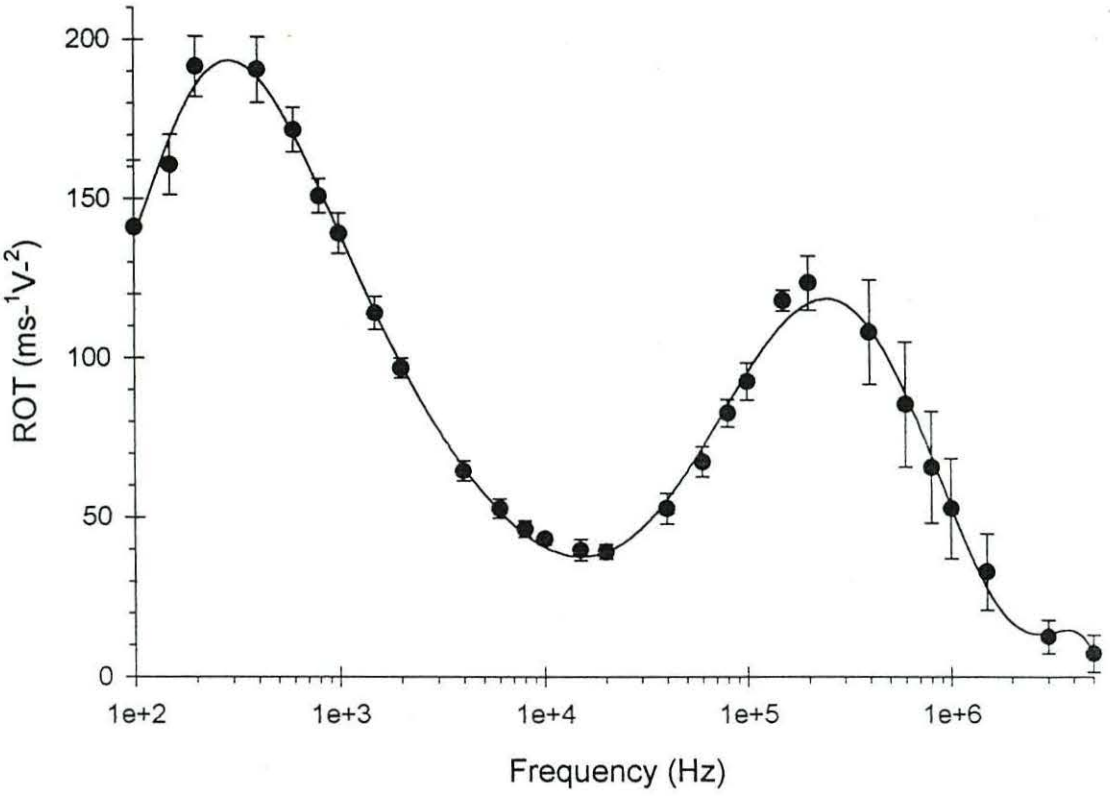

Figure 5.5. Electrorotation spectrum of latex beads coated with 15μl of *E. coli* antibody in 500 μSm^{-1} PBS solution, sample of 11 particles.

For further increases in the amount of antibody used in the preparation, increases in the variability are observed, see figures 5.6, 5.7 and 5.8, and the peak magnitudes decrease. These results coincided with the observation that for further increases in antibody (20μl or more) particles were observed to 'stick' to the glass in increasing numbers. Below a antibody aliquot of 20 μl, sticking to the glass slide was rarely observed. This effect increased with increasing amount of antibody, to the extent that for the preparation that used 30μl of antibody large numbers of beads, up to 50%, were considered to be stuck to the glass surface.

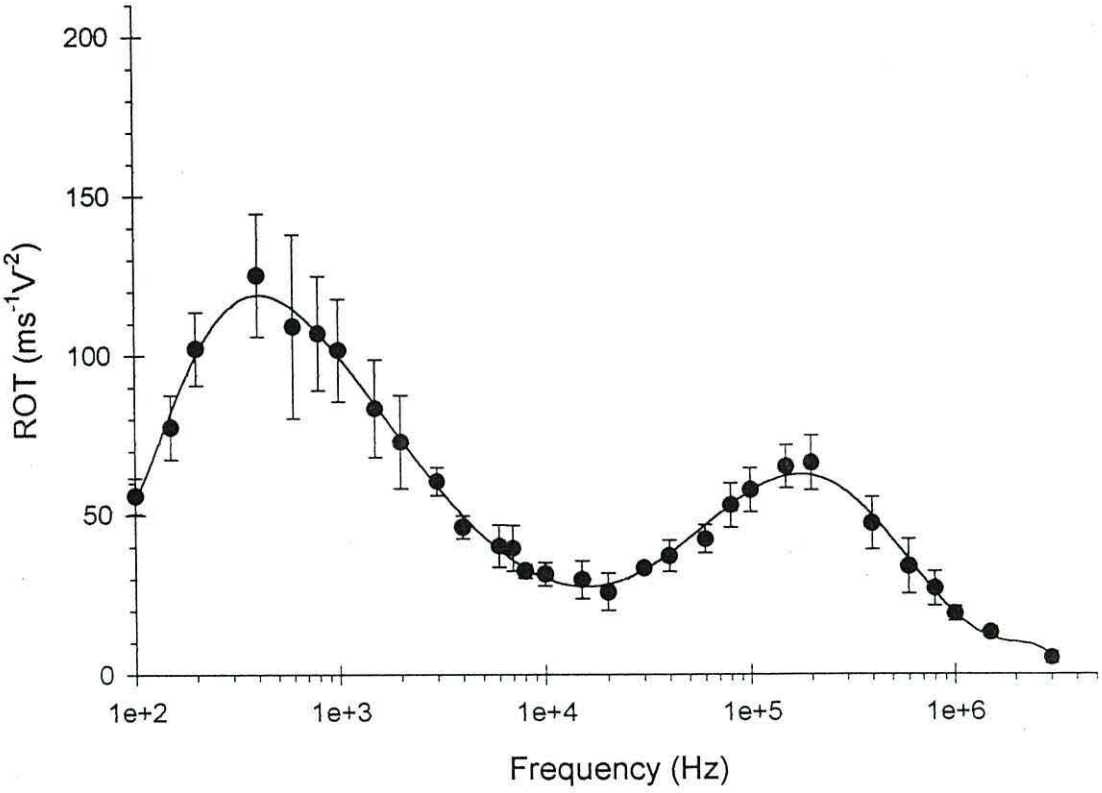

Figure 5.6. Electrorotation spectrum of latex beads coated with 20μl of *E. coli* antibody in 500 μSm^{-1} PBS solution, sample of 6 particles.

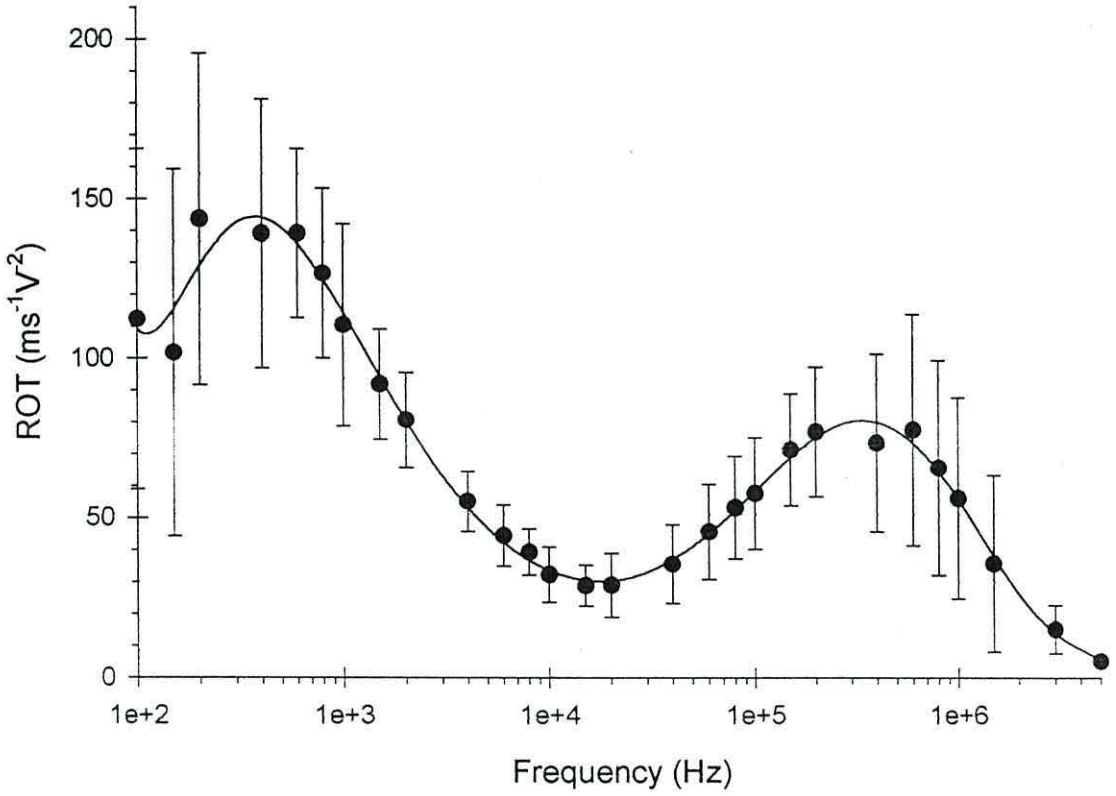

Figure 5.7. Electrorotation spectrum of latex beads coated with 25μl of *E. coli* antibody in 500 μSm^{-1} PBS solution, sample of 9 particles.

All spectra followed the typical pattern, having both a high and low frequency peak. As antibody coverage increases the low frequency peak shows a slight increase in frequency and generally decreases in magnitude. The high frequency peak shows a tendency to decrease in frequency and in magnitude.

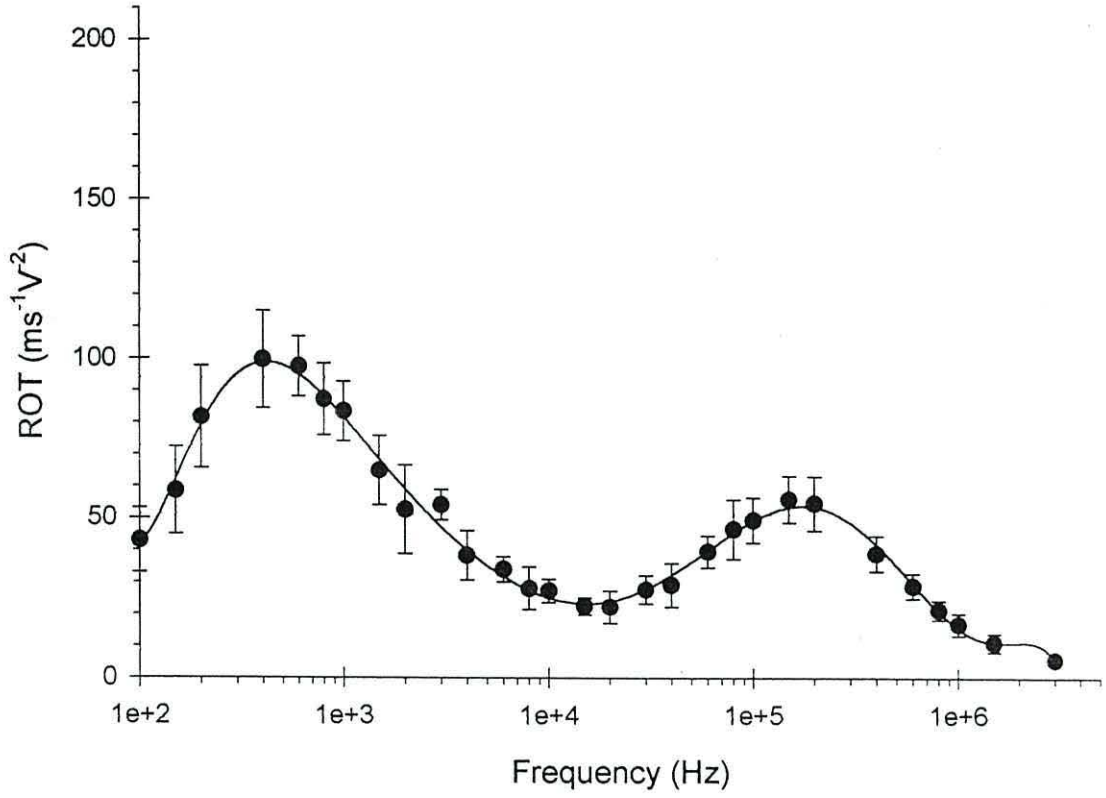

Figure 5.8. Electrorotation spectrum of latex beads coated with 30µl of *E. coli* antibody in 500 µSm^{-1} PBS solution, sample of 12 particles.

Quantity of antibody used in the preparation (µl)	**Low Frequency Peak**		**High Frequency Peak**	
	Magnitude ($ms^{-1}V^{-2}$)	% Variation	Magnitude ($ms^{-1}V^{-2}$)	% Variation
5	143.6	18.5	118.6	17.4
10	156.4	3.9	97.5	5.5
15	191.5	5.0	123.9	6.9
20	125.2	9.2	66.4	12.8
25	143.7	36.2	77.2	36.1
30	99.8	15.3	56.1	13.0

Table 5.1 Table summarising the results from figures 5.3 to 5.8. It shows how the magnitudes and the variance changes with increasing amounts of antibody.

5.2.3 Change of antibody coated bead spectra with time

The electrorotation characteristics of *E. coli* antibody coated beads, using 15 μl of antibody in the preparation , were investigated, with respect to time, since any errors in this system could be amplified in the *E. coli* system, the results are shown in figure 5.9.

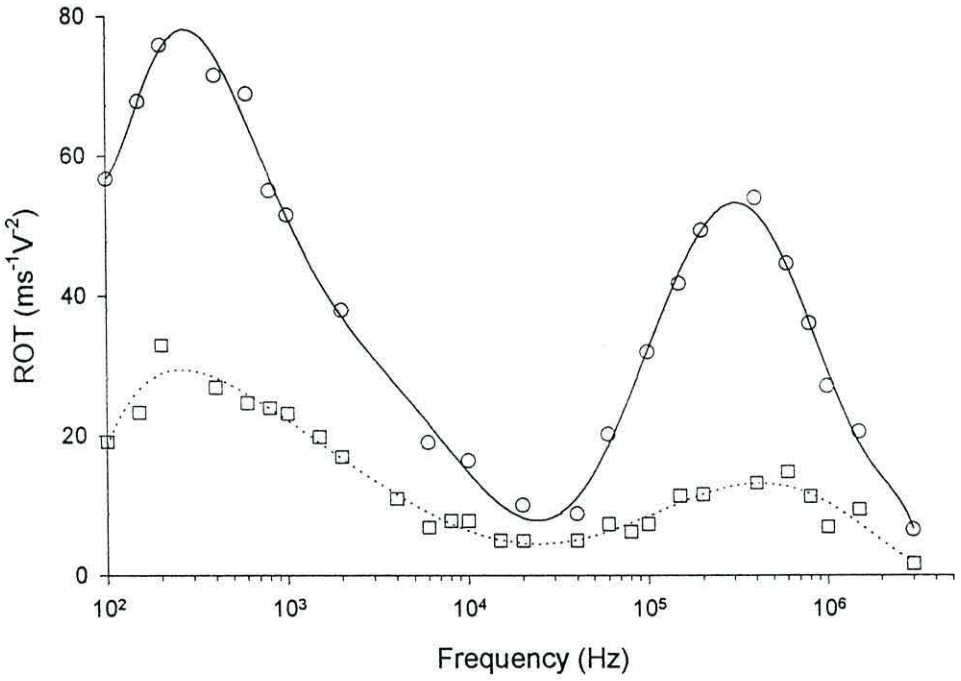

Figure 5.9. Electrorotation response of *E. coli* antibody coated latex beads, freshly prepared (○) and after one month of refrigerated storage (□), suspended in 500 μSm^{-1} PBS solution.

As has already been observed, in section 5.2.2, the antibody coated beads provide distinct coherent characteristics, with two co-field peaks. The freshly prepared antibody coated beads, two co-field peaks are centered around 200Hz and 400kHz with magnitudes of approximately 79.5ms^{-1}V^{-2} and 55 ms^{-1}V^{-2} respectively. However, it was noticed that after approximately one month in storage a significant loss in activity had occurred, to the extent that it was difficult to observe an *E. coli* bound to the surface of

these beads. It was also noted that the beads did not fluoresce as brightly as when they were freshly prepared.

5.2.4 MatLab Modelling of Antibody Coated Beads

The single shell MatLab model was used to analyse the antibody data reported in the previous sections, 5.2.2 and 5.2.3. The result are summarised below in table 5.2. The results were obtained by maintaining the following parameters: $a1 = 3\ \mu m$, $A = 0.09$ and $Kb = 20\ nSm^{-1}$.

The values for *Kc2* and *Ks* were used to adjust the result for the high frequency peak. An increase in *Kc2*, suspending medium conductivity, results in an increase in the peak frequency and a decrease in the magnitude. Increasing *Ks*, the surface conductivity, results in an increase in the magnitude, but does not affect its peak frequency. The values for *t* and *b* were used to model the low frequency peak. Increasing *t* increases the steepness of the peak.

The results show a good agreement with each other for the calculated suspending medium conductivity, however, the calculated results are more than twice that measured. The particle surface conductivity, in general, showed a decrease for increasing amounts of antibody used in the preparation. The most significant differences between the freshly prepared sample and the one month old sample is that the surface conductivity has decreased and the suspending medium conductivity has increased.

Experimental Section	Volume of antibody used for preparation (µl)	MatLab Modelling Results			
		High Frequency Peak		Low Frequency Peak	
		Suspending medium conductivity (Sm^{-1})	Particle Surface conductivity (Sm^{-1})	Low Frequency Dispersion (t)	Relaxation Distribution Factor
5.2.2	5	1.35 m	245 p	1800	0.52
5.2.2	10	1.00 m	150 p	1800	0.54
5.2.2	15	1.00 m	175 p	1500	0.52
5.2.2	20	1.00 m	115 p	1800	0.54
5.2.2	25	1.35 m	190 p	1000	0.54
5.2.2	30	0.90 m	100 p	3000	0.54
5.2.3	15	1.50 m	165 p	1800	0.56
5.2.3	15	2.00 m	140 p	2200	0.59

Table 5.2 Summary of MatLab results for antibody coated beads.

5.2.5 Detection of One Viable and One Non-Viable *E. coli*

As shown in figure 5.10, the antibody-coated beads were observed to rotate in the same sense as the applied rotating field. The spectrum is characterised by two co-field rotation peaks - a low-frequency peak centered around 200 Hz and a high-frequency peak centered around 400 kHz.

The results also show that the electrorotation spectrum of an antibody-coated bead is significantly altered when either a single viable or non-viable *E. coli* particle becomes attached to it. In particular, an anti-field rotation peak, centred around 40 kHz, emerges for a latex bead with one viable *E. coli* attached, and the high-frequency peak shifts from 400 kHz up to 1.5 MHz. In addition, both co-field rotation peaks are significantly reduced. On attachment of a single non-viable *E. coli*, an anti-field rotation peak does not appear, but both co-field rotation peaks are significantly reduced, with the high-frequency peak shifting from 400 kHz up to 800 kHz.

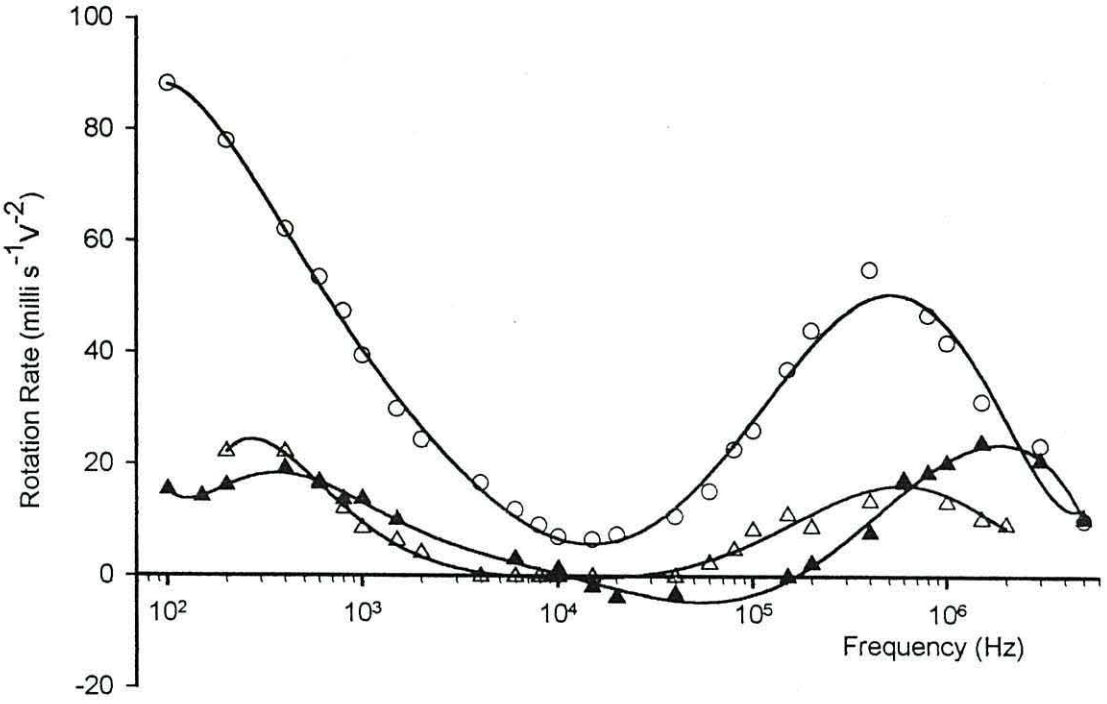

Figure 5.10. Electrorotation spectra obtained on addition of one viable (▲) and one non-viable (○) *E. coli* to the surface of separate antibody-coated beads (△).

It was possible to attach more than one *E. coli* to the surface of antibody coated beads, see section 5.2.7 for further details.

5.2.6 Change of *E. coli* Spectra With Time

Presented in figure 5.11 is an example of how the spectra of the beads with three attached *E. coli* could change with time during an experiment. It should be noted that the results presented here are examples of the most severe deviations observed they have been included for interest.

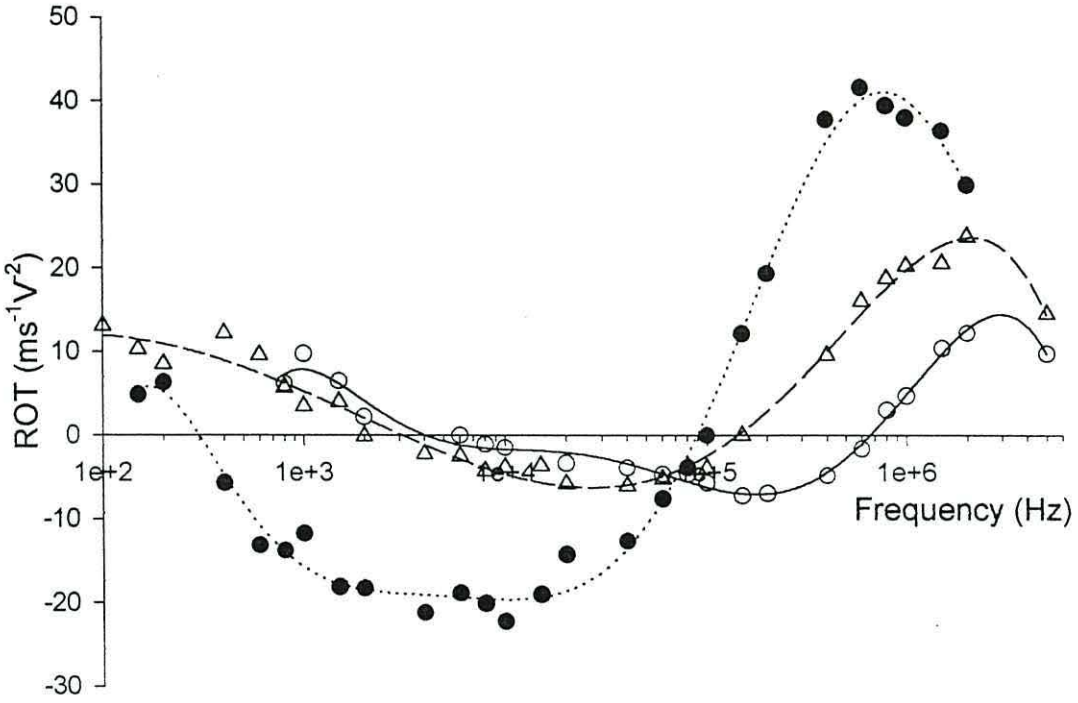

Figure 5.11. Change with time of electrorotation spectra of antibody coated beads with three *E. coli* bound to the surface. (—○—) are the results after 20 minutes, (···△···) after one hour and (···●···) after two hours from the start of the experiment.

All the spectra possess the same basic characteristics as described before except that those obtained in the earlier stages of the experiment generally have higher cross-over frequencies and the anti-field peak and high frequency co-field peak are smaller in magnitude than those obtained during the later stages of the experiment. It was noted that during all of the stages of the experiment the *E. coli* were of a healthy elongated or ellipsoidal shape and many were multiplying.

5.2.7 Further Addition of Viable *E. coli*

The electrorotation spectra of beads with more than a single attached *E. coli* were also investigated. With further addition of viable *E. coli* the anti-field peak grows in prominence see figure 5.12. The further accrual of *E. coli* on the bead surface also

affects the 'cross-over frequencies' at which the sense of rotation reverses. The lower 'cross-over frequency' decreases, whereas the higher one increases, and this trend has been observed for the attachment of up to 10 viable *E. coli* particles, see figures 5.13 and 5.14.

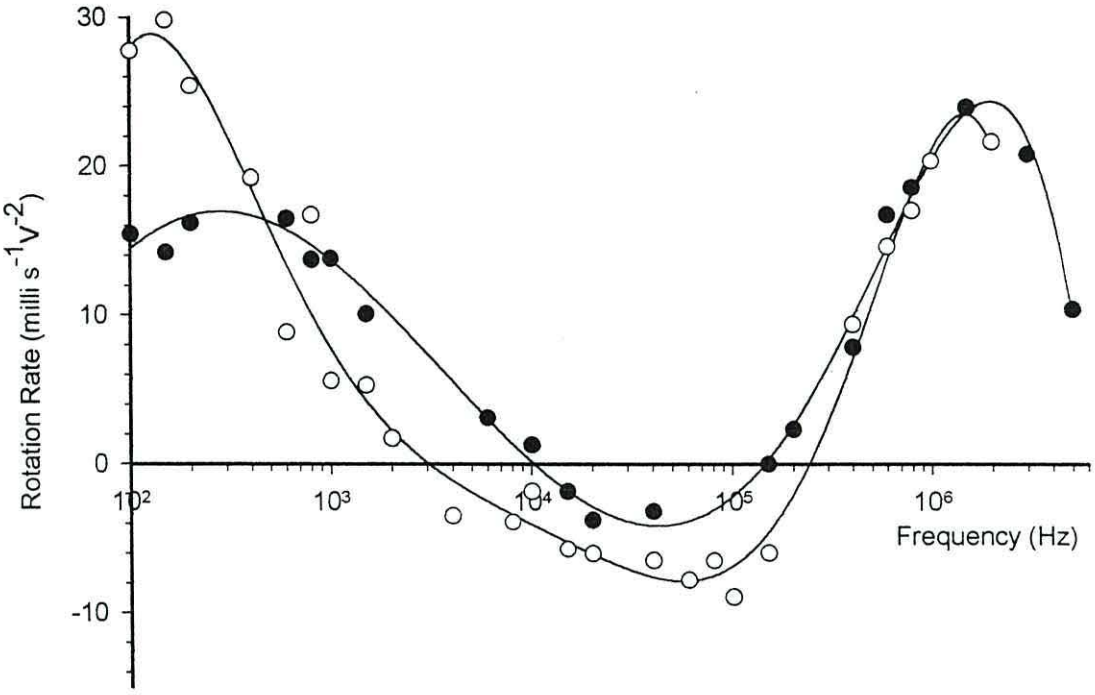

Figure 5.12. Electrorotation spectra obtained on addition of one viable (●) and two viable (○) *E. coli* to the surface of separate antibody-coated beads.

In another experiment the addition of up to nine *E. coli* was investigated, the results are displayed in figures 5.13 and 5.14. The same form was observed for the spectra as was previously observed. For the addition of further *E. coli* to the surface of the bead the high frequency cross-over increased slightly, whereas the low frequency cross-over decreases significantly. The magnitude of the high frequency peak and the anti-field peaks increased with increasing numbers of *E. coli* attached to the surface of the beads. These trends were observed for all experiments of viable *E. coli*. Figure 5.14 shows the low frequency peak decreasing with increasing numbers of *E. coli*. Although this trend

was observed on several occasions it was not always as coherent. The error bars on figures 5.13 and 5.14 depict the minimum and maximum deviations.

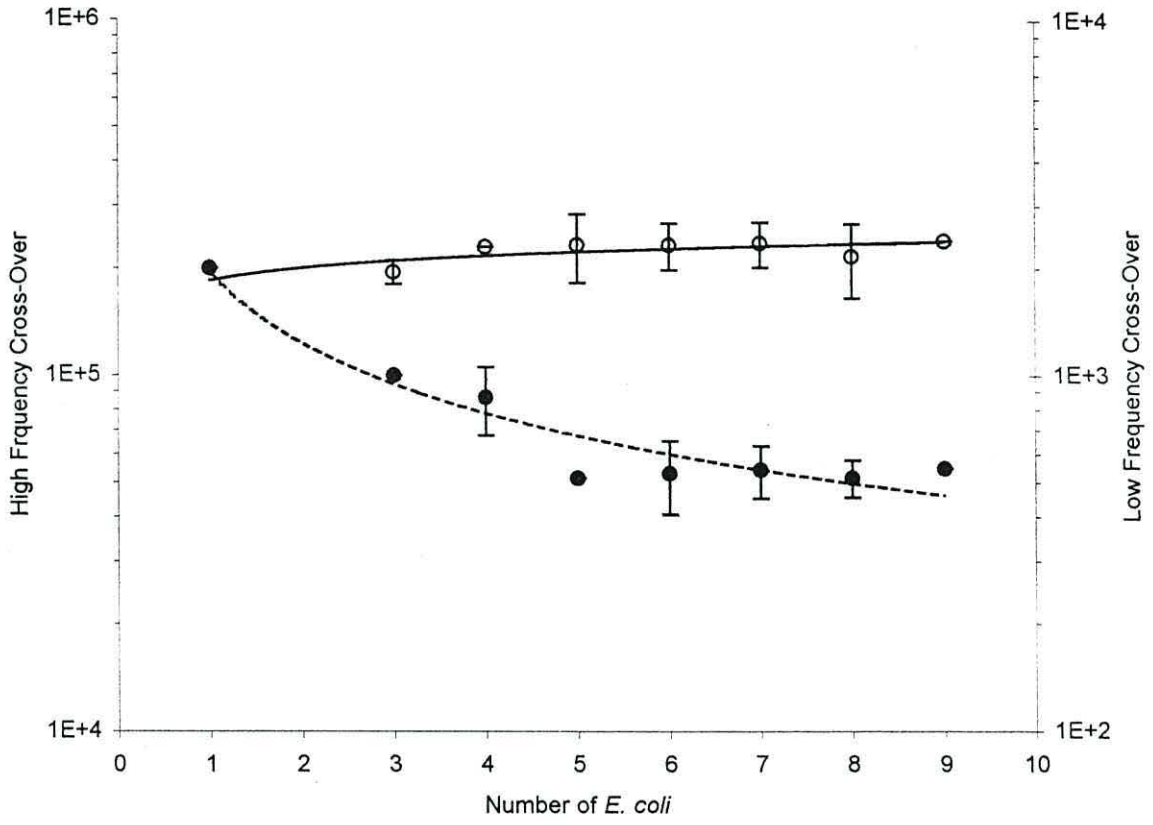

Figure 5.13. Change of the high frequency cross-over (○) and low frequency cross-over (●) for the addition of up to nine viable *E. coli* to the surface of separate antibody-coated beads. Error bars indicate the maximum and minimum deviations.

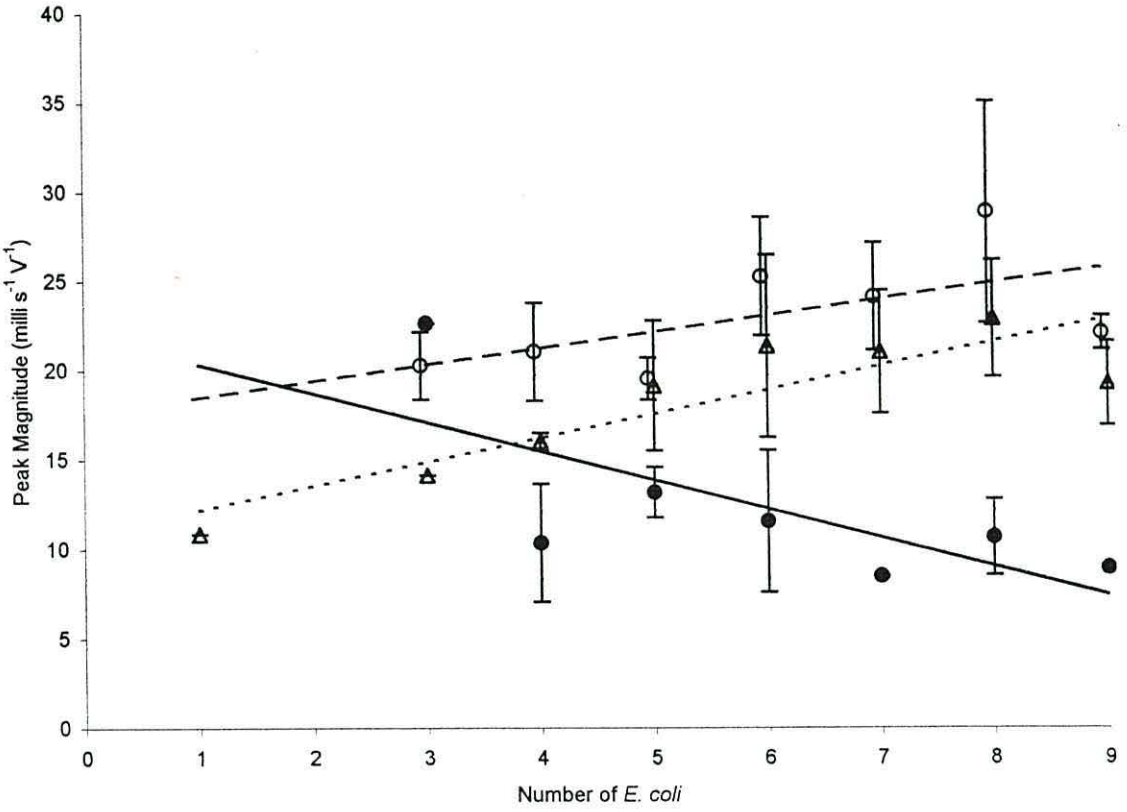

Figure 5.14. Change in magnitude of the high frequency peak (-⊖-), low frequency peak (–●–), and anti-field peak (···△···) for the addition of up to nine viable *E. coli* to the surface of separate antibody-coated beads. Error bars indicate the maximum and minimum deviations.

5.2.8 Further Addition of Non-Viable *E. coli*

The electrorotation spectra of beads with more than a single attached non-viable *E. coli* were also investigated. With further addition of non-viable *E. coli* an anti-field peak is introduced to the spectra see figure 5.15. The further accrual of *E. coli* on the bead surface leads to an increase in the high frequency cross-over frequency and a decrease in the low frequency cross-over frequency, see figure 5.16. In addition, the magnitude of the high-frequency peak and anti-field peak increases, see figure 5.17.

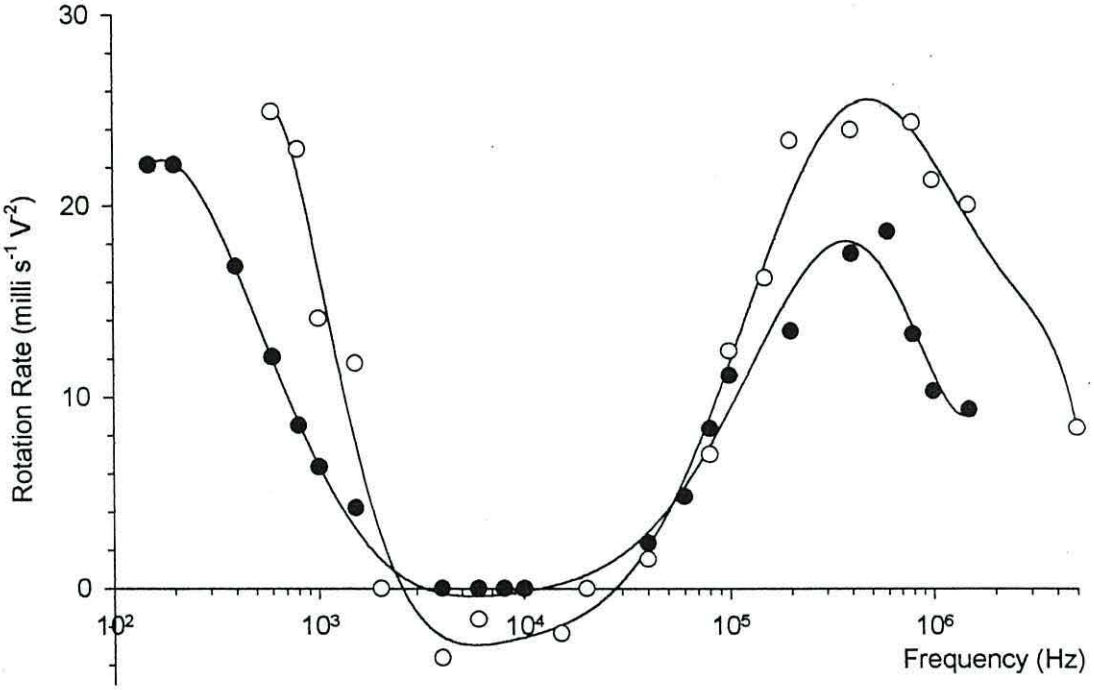

Figure 5. Electrorotation spectra obtained on addition of one non-viable (●) and two non-viable (○) *E. coli* to the surface of separate antibody-coated beads.

This trend was observed for the addition of up to eight non-viable *E. coli*, the results are displayed in figures 5.16 and 5.17. Although, with the addition of more than one non-viable *E. coli*, the trends were the same as those for viable *E. coli* the magnitude of the anti-field peak and the cross-over were significantly reduced. These trends were observed for all experiments of non-viable *E. coli*. No consistent trend was observed with respect to the low-frequency peak magnitude.

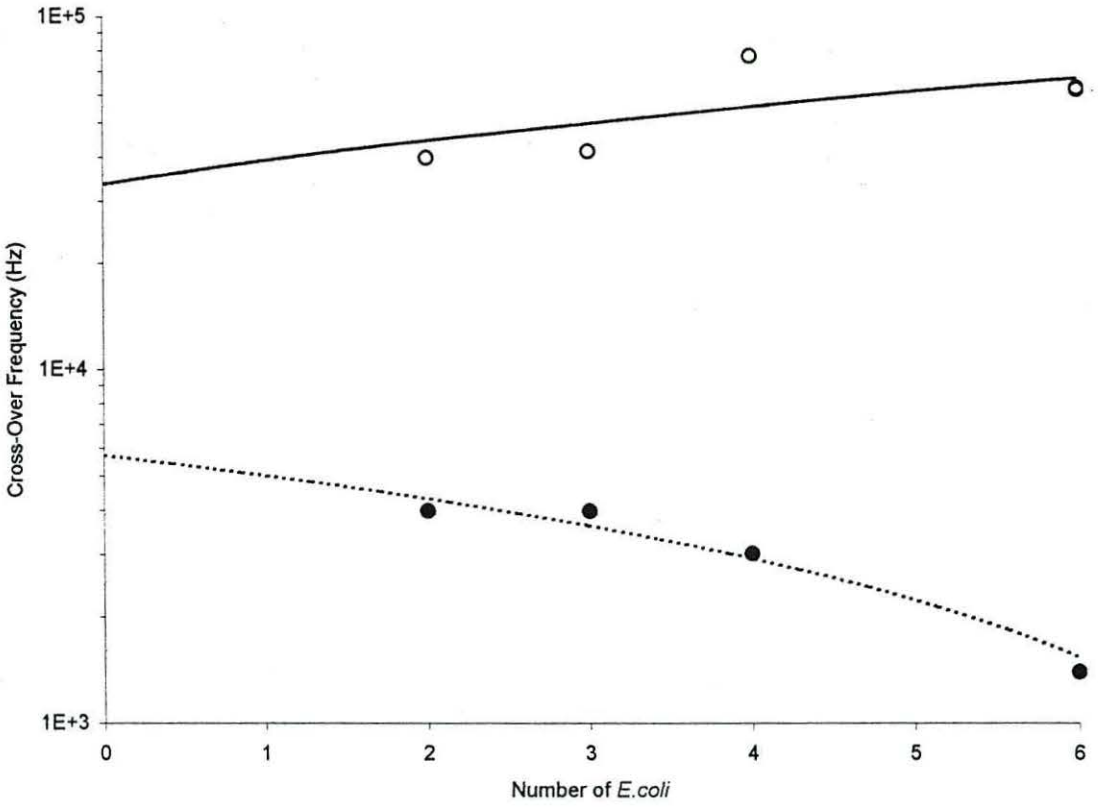

Figure 5.16. Change of the high frequency cross-over (○) and low frequency cross-over (●) for the addition of up to six non-viable *E. coli* to the surface of separate antibody-coated beads.

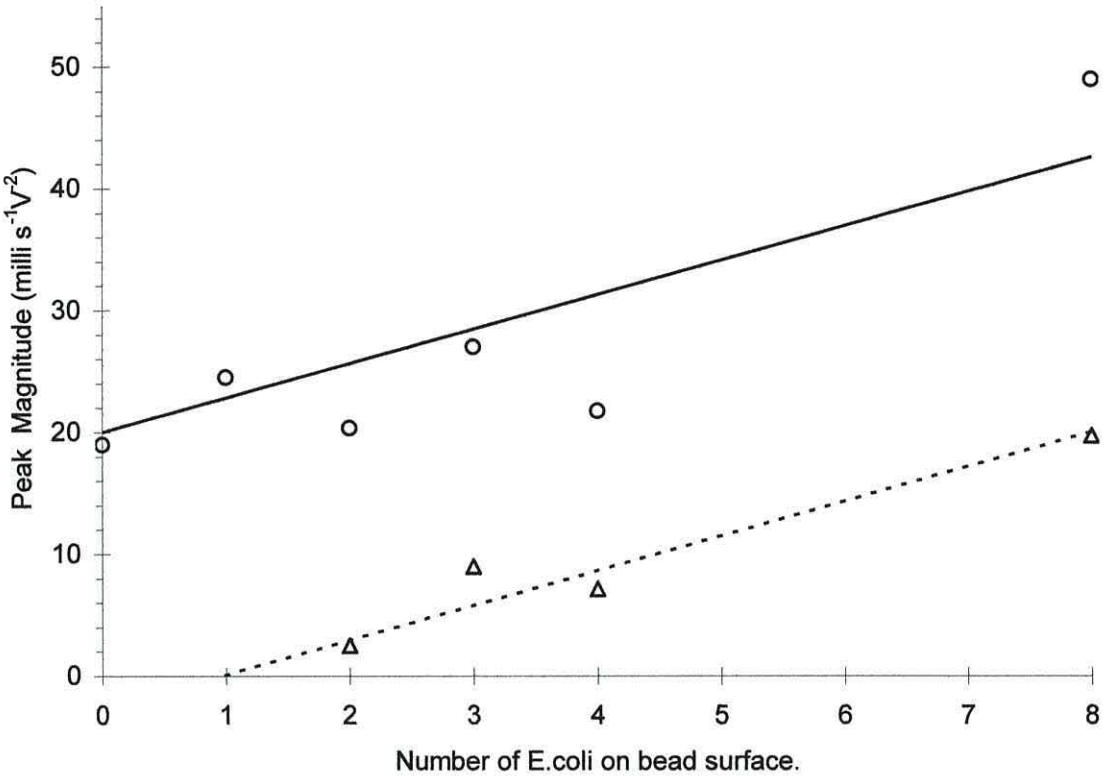

Figure 5.17. Change in magnitude of the high frequency peak (○) and anti-field peak (△) for the addition of non-viable *E. coli* to the surface of separate antibody-coated beads.

5.2.9 Analysis of four viable *E. coli*

The electrorotation spectra of antibody coated beads with four viable *E. coli* attached to the surface were analysed from several experiments, see figure 5.18. The error bars are the 95% confidence of the standard deviation, based on a sample of 21 beads.

Although the results show a repeatable coherent effect, variance is observed around the areas of interest:

- High frequency peak magnitude: 22.08 +/-3.57$ms^{-1}V^{-2}$
- Anti-field peak magnitude: 12.02 +/-5.42 $ms^{-1}V^{-2}$
- Low frequency cross-over: 1k +0.5k-0.2kHz
- High frequency cross-over 240k +65k-80kHz

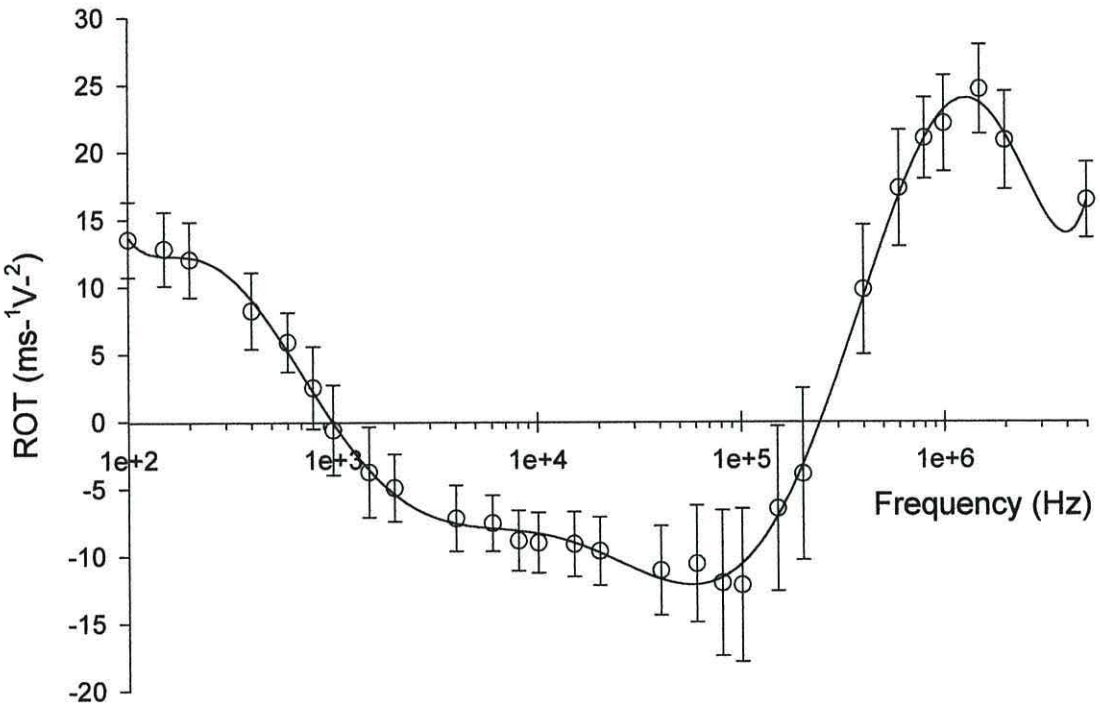

Figure 5.18. Electrorotation spectra of antibody coated beads with four viable *E. coli* attached to the surface. The error bars are the 95% confidence of the standard deviation, based on a sample of 21 beads.

5.2.10 MatLab Modelling of *E. coli* Coated Beads

The multi-shell MatLab model was used to analyse the attachment of up to three viable *E. coli* data reported in the previous sections, 5.2.5 and 5.2.7. The results are summarised below in table 5.3. The results were obtained by maintaining the latex particle diameter as *3 μm* and the suspending medium conductivity as *6.2* Sm^{-1}.

Latex Particle	Plus Antibody Coating	Plus One Viable *E. coli*	Plus Two Viable *E. coli*	Plus Three Viable *E. coli*

Latex Particle	**Plus Antibody Coating**	**Plus One Viable *E. coli***	**Plus Two Viable *E. coli***	**Plus Three Viable *E. coli***
Relaxation Distribution Factor	0.7	1.2 ± 0.2	6 ± 0.5	10 ± 1
Low Frequency Dispersion (t in secs)	0.0008	0.1 ± 0.02	3.5 ± 0.5	9.0 ± 1
Latex Particle Surface conductivity (nSm^{-1})	0.4	2.0 ± 0.2	0.8 ± 0.1	0.6 ± 0.1
Latex Particle Effective Relative Permittivity	4	2000 ± 200	2750 ± 200	4200 ± 200
Antibody layer Conductivity (μS)	10	200 ± 20	90 ± 10	60 ± 5
Antibody Layer Effective Permittivity	30	34 ± 4	26 ± 1	20.5 ± 1
Antibody Layer Effective Thickness (nm)	8	32 ± 2	27 ± 2	23 ± 1
E. coli Effective Conductivity (mSm^{-1})		7.6 ± 0.4	7.25 ± 0.25	9.0 ± 0.5
E. coli Effective Relative Permittivity		60 ± 1	60 ± 1	60 ± 1
E. coli Effective Thickness (μm)		1	1.2	1.2

Table 5.3 Summary of MatLab results for *E. coli* coated beads.

5.2.11 *Bascillus subtilis* Antibody Coated Beads

Some preliminary experiments were performed on the gram-positive bacteria *Bascillus subtilis* using the electrorotation assay. Since the electrorotation assay was able to detect differences between viable and non-viable *E. coli* it was thought that it may be possible to detect the difference between gram positive and gram negative bacteria. The differences in their dielectric properties resulting from the differences in the structure and properties of the cell envelope, see Materials and Methods chapter for further details.

The results in figure 5.19 are the electrorotation spectra for anti gram-positive antibody coated beads. The results are very similar to those found for *E. coli* antibody coated bead with two co-field peaks. The low frequency peak is centered around 200Hz and has a magnitude of approximately $95ms^{-1}V^{-2}$. The high frequency peak is centered around 250kHz and has a magnitude of around $40ms^{-1}V^{-2}$.

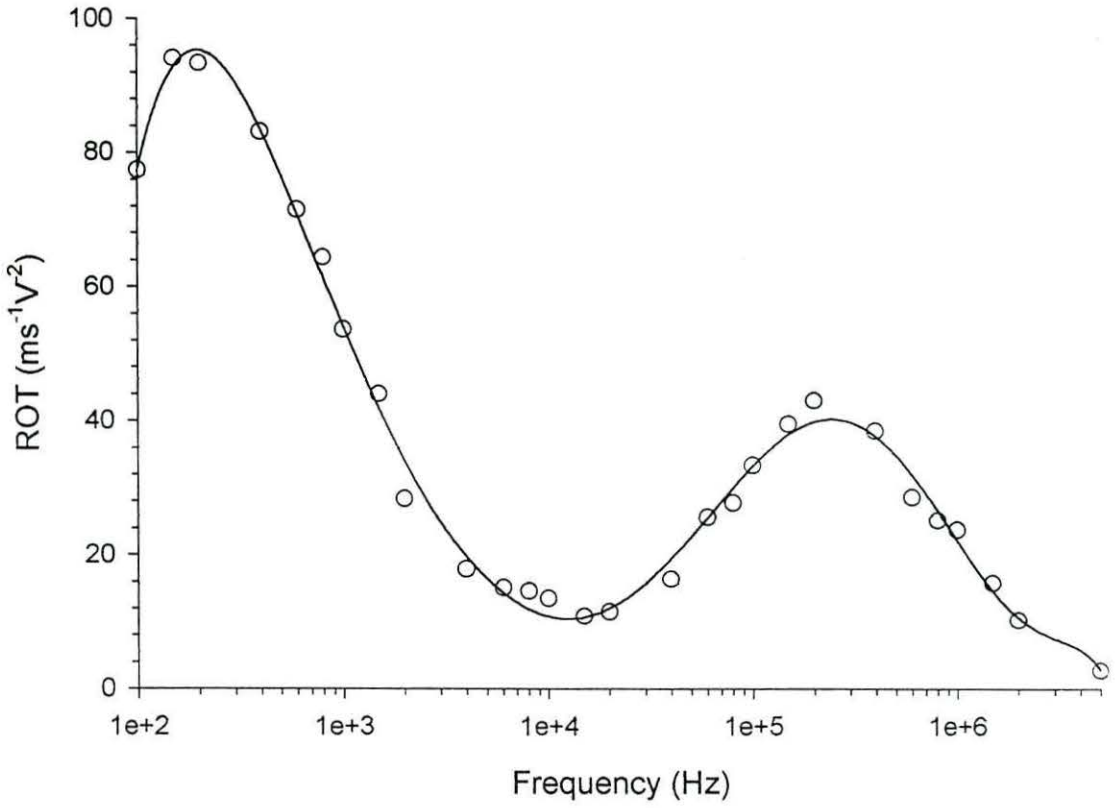

Figure 5.19. Electrorotation spectrum of latex beads coated with *Bascillus subtilis* antibody.

5.2.12 Attachment of Viable *Bascillus subtilis*

The results presented in figure 5.20 are for the attachment of one, two and three *B. subtilis* to the surface of the antibody coated beads. The results are similar to those found for *E. coli*, having two co-field peaks intersected by an anti-field peak. The main difference between the *E. coli* and the *B. subtilis* spectra is that the magnitudes of the high frequency co-field peak and the anti-field peak are significantly reduced. Also, the high-frequency cross-over is significantly reduced, by approximately one decade. It is now no-longer possible to observe the low-frequency peak.

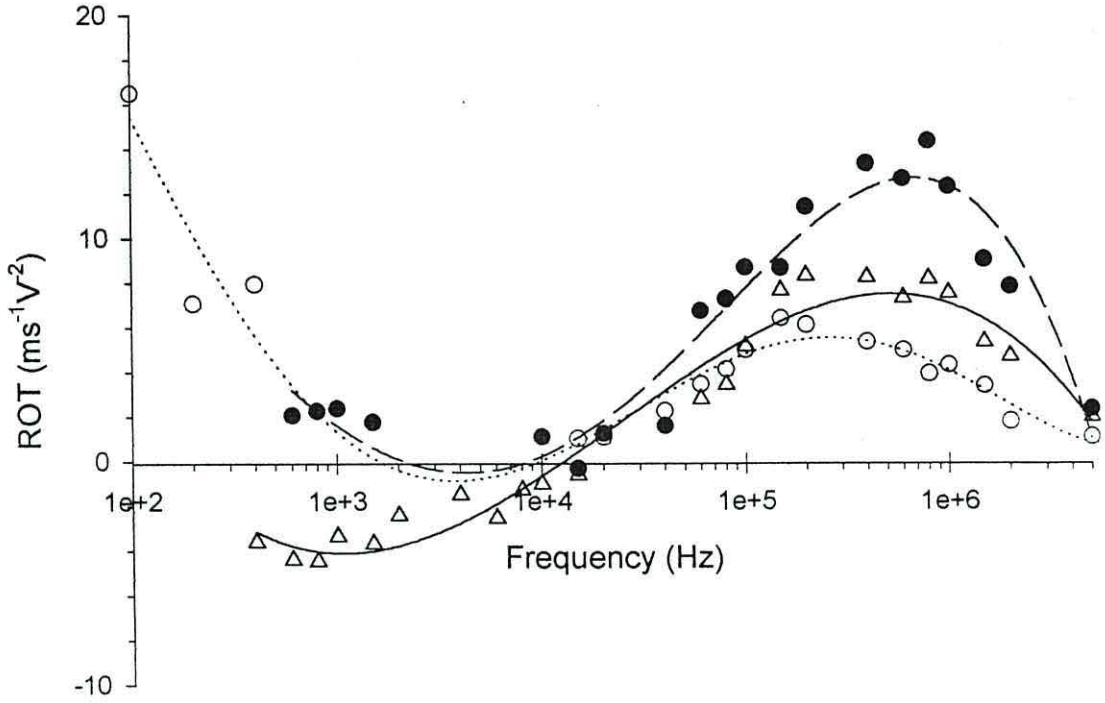

Figure 5.20. Electrorotation spectra obtained on addition of one (-●-), two (···○···) and three (—△—) viable *Bascillus subtilis* to the surface of separate antibody-coated beads.

5.2.13 Summary

As previous discussed a basic investigation of the underlying system, the latex particle, was provided in the Latex Particle chapter. The work in this chapter aims to build on this system by attaching antibodies to the latex particles and using these to 'capture' bacteria. This chapter has provided results in several key areas:

- **Optimisation of antibody coating on the latex particles.**

The main results of interest are presented in section 5.2.2. It was important to study this area since the work in this study is based on these antibody coated particles. Any

minimisation in the variability of the spectra at this stage would help to reduce any variability in the overall system. Good coherent responses were obtained however, it was noticed that the spectra seemed to change with time, hence the following area of study.

- **Changes in the spectra of antibody coated beads with time.**

Section 5.2.3 demonstrated the problems with storage of the particles. The particles experienced an apparent 'aging' effect. This 'aging' effect was in conjunction with a noticeable loss in activity of the antibody.

- **Affect of suspending medium on the *E. coli*.**

Section 5.2.1 presents results to show how the suspending media affects the viability of the *E. coli*.

- **Adhesion of *E. coli* to the latex particle.**

Sections 5.2.5, 5.2.7, 5.2.8 and 5.2.9 present results to show how the addition of *E. coli* to the surface of the particle affects the electrorotation spectra.

- **Changes in the spectra of *E. coli* coated beads with time.**

Section 5.2.6 demonstrated the how the *E. coli* spectra could change with time.

- **Adhesion of *B. subtilis* to the latex particle.**

Sections 5.2.11 and 5.2.12 present results to show how the addition of anti gram-positive antibody and subsequent adhesion of *B. subtilis* to the surface of the particle affects the electrorotation spectra.

5.3 Discussion

The aim of this chapter was to investigate the use of the electrorotation assay for the detection of bacteria. The key areas described in the previous section address this aim and will form the basis of the discussion.

5.3.1 Optimisation of antibody coating on the latex particles.

The origin of the two dispersions[3, 4] was discussed in the Latex Particles chapter. The high frequency dispersion is generally assigned to the Maxwell-Wagner interfacial polarisation mechanism and the lower frequency dispersion has been interpreted as a relaxation of the electrical double layer associated with the surface charge of the particle[5].

For the case where a clean bead is coated with an antibody, analysis of a single shell model[6] indicates that the change in the electrorotation spectrum arises as a result of a decrease in the effective conductivity of the bead's surface. This result is related to the fact that the uncoated latex particles have carboxyl surface functional groups, which results in their surface being able to support a relatively high surface conductivity associated with the percolation of counter-ions.

Ortega-Vinuesa et al[7] found that binding of the antibody results in a reduction of net negative surface charge. They covalently bound IgG antibody to carboxylated latex particles and studied the effect on the electrophoretic mobility. They found, for a pH 8.0, in a 30 mM potassium bromide solution the electrophoretic mobility of antibody coated beads was reduced from $-3.75*10^{8}$ m^2/Vs to $-1.75*10^{8}$ m^2/Vs on the addition of antibody. He also found that the electrophoretic mobility varied, with increasing ionic strength, in the same way as described for uncoated latexes, described in the Latex Particles chapter. That is, for increasing ionic strength the electrophoretic mobility decreased, that is, became less negative.

The MatLab modelling of the system confirmed this. In the Latex Particles chapter, uncoated carboxylated elliptical particles suspended in 530 μSm^{-1} PBS solution were calculated to have a surface conductivity of between 370 and 460 pSm^{-1}. This is compared to a value of 100 and 245 pSm^{-1} for antibody coated beads.

The aim of this section of work was to ascertain the amount of antibody that was required to be added during the preparation. Some practical limitations were observed, that is, when using 20 µl of antibody or greater during the preparation significant numbers of particles were observed to stick to the glass slide. To the extent that for the preparation that used 30µl of antibody large numbers of beads, up to 50%, were considered to be stuck to the glass surface. In addition significant variance was observed in the sample using only 5 µl of antibody. This was attributed to there being insufficient antibody to generate an evenly distributed antibody coating across the population of the particles. As a result of this, 15 µl was chosen as the volume of antibody to be used in the preparation of the beads. Using this quantity, the particles were observed to adhere up to ten *E. coli* to the surface of the bead.

5.3.2 Changes in the spectra of antibody coated beads with time.

In section 5.2.3 'aging' effect was demonstrated in the antibody coated beads. This 'aging' effect was in conjunction with a noticeable loss in activity of the antibody, that is, it was no longer observed to bind to *E. coli*.

The freshly prepared antibody coated beads co-field peaks are centered around 200Hz and 400kHz with magnitudes of approximately 79.5$ms^{-1}V^{-2}$ and 55 $ms^{-1}V^{-2}$ respectively. However, it was noticed that after approximately one month in storage a significant loss in activity had occurred, to the extent considerably fewer *E. coli* were found to be bound to the surface of the beads. It was also noted that the beads did not fluoresce as brightly as when they were freshly prepared.

It was anticipated that the FITC as degrading due to its light sensitivity, although the reason why was unknown. The MatLab results indicate a slight rise in the suspending medium conductivity and a decrease in the surface conductivity. It could be that the degradation of the FITC is somehow denaturing the antibody, hence its loss of activity hence only the slight change in the calculated surface conductivity. Or, it could be due to adsorbed antibody, from the preparation coming off the surface of the bead, however, this may not explain the loss in activity.

The most likely cause was attributed to the degradation of the FITC conjugate since unconjugated antibody did not display the loss in activity that had been observed with the FITC conjugated antibody.

5.3.3 Affect of suspending medium on the *E. coli*.

The aim of this work was to determine a suspending medium that would maintain the viability of the *E. coli*. The motivation for this were problems experienced maintaining the viability *E. coli* in weakly ionic solutions. The experiment needs to be performed in very low conductivity PBS solution, around 500 μSm^{-1}, which equates to a concentration of approximately 20 μM. This requirement provides a very harsh environment for the bacteria, whose solutes are typically at a concentration of 100 to 150mM.

Water-borne bacteria, such as *E. coli* have been shown to undergo 'stress' when suspended in non-ideal mediums[8]. When nutrients are scarce the bacteria become 'nutrient stressed'. This results in the bacteria becoming 'dwarfed' or spherical shaped[9, 10, 11, 12]. Amy and Morita[13] surmise that this miniaturisation results in a larger surface-to-volume ratio, a feature that may aid bacteria in obtaining substrates from nutrient poor environments. On provision of excess substrate the bacteria develop to 'normal' size[2]. Hence, the bacteria were observed for signs of 'stress' as an indicator of an 'ideal' suspending medium.

Initially advice was that the *E. coli* would 'survive' washing in ultra-pure water and suspended in low conductivity media, without nutrients. However, observations and plate tests from these experiments led to the determination that the majority of the bacteria were dead (>99%) and would not stick to the surface of the antibody coated beads. It was realised that this was exposing the *E. coli* to too much osmotic stress.

Mannitol, of concentration 280mM, is commonly used to counteract this problem. This technique proved fairly successful for attachment to the beads, which takes place in approximately one hour or less, but was not reliable for sustaining the viability of the *E. coli* over long periods of time, several hours.

Observations of the shape of the bacteria during the experiment lead to the conclusion that the *E. coli* were still being stressed. The concentration, 170mM, was determined from examination of literature and a consideration of the osmotic potential exerted on the bacteria from the growth medium. Stock et al determined that the osmotic strength of the periplasmic space was 170 mM[1]. Agar plate tests confirmed that the *E. coli* maintained their viability for an adequate length of time, in excess of several days, and that it was the most successful of all the solutions tested, however, using glycerol the bacteria would not stick to the surface of the beads.

5.3.4 Adhesion of *E. coli* to the latex particle

With the addition of more than one non-viable *E. coli*, the trends for increasing numbers of attached *E. coli* were the same as those for viable *E. coli* but the magnitude of the anti-field peak and the cross-over were significantly reduced.

To analyse the effects arising from the attachment of *E. coli* to the bead, a multi-shell model was required[6, 14] see Theory section for further details. Mathematical analysis implied that the results, in general, could also be explained by a reduction in the effective conductivity of the bead/antibody surface. For viable *E. coli* this is mainly associated with the highly resistive nature of its intact cytoplasmic membrane, see

Materials and Methods for further details. This effect is less significant when non-viable bacteria became attached, because one result of cell death is that the membrane looses its function as a selectively permeable membrane and becomes porous (conductive) to ions in general.

The rate of attachment of *E. coli* to the beads, and hence the rate of change of their electrorotation spectra, was found to depend on the concentration of the bacteria in the suspending fluid. Therefore, by monitoring the changes of electrorotation of a number of beads suspended in a solution containing *E. coli* it should in principle be possible to assay both the concentration and relative viability of the *E. coli*. This technique could also be used to determine the sensitivity of antimicrobial agents towards viable micro-organisms attached to the beads, in the same way as electrorotation measurements have been used to determine the toxicity of biocides towards biofilms grown on bead surfaces[14].

Current work is directed towards exploiting these observed changes in the electrokinetic behaviour of bead plus *E. coli* complexes in the selective dielectrophoretic manipulation and characterisation of bioparticles at low concentration levels[20].

The analysis of the electrorotation spectra of antibody coated beads with four viable *E. coli* attached to the surface showed a repeatable coherent spectra with some variability. The variability could be due to several factors:

- Difference in experimental conditions such as suspending media conductivity.
- Not all of the *E. coli* are viable. If not all of the attached bacteria were viable the magnitude of the anti-field peak and the high frequency peak would be reduced. In addition, the high frequency cross-over would be reduced and the low frequency cross-over would be increased. It is not possible to observe, under the microscope without the aid of dyes, differences in viability. For simplicity populations of bacteria are classed as all viable or non-viable. For the non-viable samples this is a fair assumption, since agar plate tests yielded no colonies. However, for viable

populations this is too simplistic. In reality a certain proportion of the population would be undergoing cell death. This percentage is dependent on the competition for nutrients and the toxicity level of the bacteria waste products. To minimise this percentage, bacteria were always removed from incubation during their growth stage and heavily diluted when suspended in mannitol, to try to minimise competition.

- The *E. coli* could be in different growth phases which results in them having different dielectric properties, thus affecting the electrorotation spectra. A change in the shape of the *E. coli* spectra with respect to time was observed and is discussed in section 5.3.5.
- The number of *E. coli* on the surface of the bead could have been incorrectly assessed. It should be noted that it can be difficult to accurately assess the number of *E. coli* attached to the surface of the bead.

5.3.5 Changes in the spectra of *E. coli* coated beads with time.

The electrorotation spectra for *E. coli* coated beads was observed to change with time, see section 5.2.6 for details. During the experiment the attached *E. coli* did not display the signs of stress described in the previous section, 5.3.3.

From some simple MatLab modelling of a micro-organism, no single change of the system can account for these changes described. However, a combination of a rise in cell wall conductivity and surrounding medium conductivity could account for the changes. This could be a realistic situation. Although the cell is osmotically balanced with its surroundings their still exists an ion gradient between the cell contents and cell surroundings. This would result in the cell wall appearing to become more conductive as the experiment progressed, since the ions would be diffusing out of the cell into the surrounding medium. However, no one part of a cell can change without it affecting the rest, thus making the system very difficult to model accurately.

A typical concentration of the dissolved solutes in a cell is 100-150mM, thus a similar concentration of suspending medium would be required to prevent significant ionic diffusion. Since the electrorotation assay cannot be performed at these high concentrations, this is a problem that is unlikely to be overcome.

The fact that the bacteria were at different growth stages might be responsible for the changes in the spectra with time. Authors, such as Diaper and Edwards[15] and Kashket[16, 17], have reported reductions in membrane potentials as bacteria enter the stationary phase, that is a phase of neither growth or replication. A reduction in membrane potential has also been reported during short-term starvation[18, 19], which the bacteria may have undergone, as they have been transferred from the nutrient broth where they were respiring aerobically to the mannitol solution which they have to anaerobicaly respire.

5.3.6 Adhesion of *B. subtilis* to the latex particle.

The results in figure 5.19 are the electrorotation spectra for *B. subtilis* antibody coated beads. The results are very similar to those found for *E. coli* antibody coated bead with two co-field peaks.

The results for the attachment of one, two and three *B. subtilis* to the surface of the antibody coated beads were also similar to those found for *E. coli*, having two co-field peaks intersected by an anti-field peak. The main difference between the *E. coli* and the *B. subtilis* spectra is that the magnitudes of the high frequency co-field peak and the anti-field peak are significantly reduced. Also, the high-frequency cross-over is significantly reduced, by approximately a decade. It appears that the low frequency peak could be at a much lower frequency than would have previously been observed.

To analyse the effects arising from the attachment of *B. subtilis* to the bead, a multi-shell model was required[6, 14] see Theory section for further details. Mathematical analysis implied that the results, in general, could also be explained by a reduction in

the effective conductivity of the bead/antibody surface as compared to the results for the *E. coli*.

This difference could be due to the differences in the structure of the cell envelope between gram-negative bacteria and gram-positive bacteria. In *B. subtilis*, the envelope is composed mainly of the thick peptidoglycan meshwork interwoven with other polymers. This is in contrast with *E. coli* that have a more complex cell wall structure with multiple layers in which an outer membrane layer lies on top of the thin peptidoglycan layer. This results in the *B. subtilis* appearing to have a more resistive membrane, see Materials and Methods for further details.

There were several problems with the experiment due to the long in comparison to the bead, up to three times in length. This resulted in the centre of the rotational axis not being the centre of the latex particle. Also, the *B. subtilis* were very motile and would not always remain stuck to the bead. These 'problems' made it difficult to compare the results directly with those for *E. coli*.

5.4 Conclusions

This work clearly demonstrates the sensitivity to be achieved using the electrorotation assay. The assay was able to indicate differing amounts of antibody present on the latex particles surface. The attachment of just one *E. coli* particle to the surface of a bead produces a significant response. Furthermore, the technique provides a rapid method for determining the viability of a single micro-organism.

Mathematical analysis implied that the results, in general, could also be explained by a reduction in the effective conductivity of the bead/antibody surface. For viable *E. coli* this is mainly associated with the highly resistive nature of its intact cytoplasmic membrane. This effect is less significant when non-viable bacteria became attached, because one result of cell death is that the membrane looses its function as a selectively permeable membrane and becomes porous (conductive) to ions in general.

The rate of attachment of *E. coli* to the beads, and hence the rate of change of their electrorotation spectra, was found to depend on the concentration of the bacteria in the suspending fluid. Therefore, by monitoring the changes of electrorotation of a number of beads suspended in a solution containing *E. coli* it should in principle be possible to assay both the concentration and the viability of the *E. coli*. However, it may be difficult, in a concentrated system to accurately assess the number attached and relative viability, since the spectra for viable and non-viable are similar in shape. For example, an electrorotation result for several attached bacteria could be due to three viable or a greater number of non-viable bacteria.

Current work is directed towards exploiting these observed changes in the electrokinetic behaviour of bead plus *E. coli* complexes in the selective dielectrophoretic manipulation and characterisation of bioparticles at low concentration levels[20].

This technique could also be used to determine the sensitivity of antimicrobial agents towards viable micro-organisms attached to the beads, in the same way as electrorotation measurements have been used to determine the toxicity of biocides towards biofilms grown on bead surfaces[20].

This work went on to demonstrate that gram positive bacteria, *B. subtilis*, can also be detected using the electrorotation assay. As with the *E. coli*, the attachment of just one bacterium to the surface of a bead produces a significant response but different to that obtained for *E. coli*. The technique provided a method for determining the difference between the two bacteria investigated here although direct comparisons of the two are difficult due to the differences in length.

5.5 References

[1] Stock JB, Rauch B and Roseman S. Periplasmic space in *Salmonella typhimurium* and *Escherichia coli*. *J. Biol. Chem.* 1977; 252(12): 7850-7861.

[2] Roszak DB and Colwell RR. Survival strategies of bacteria in the natural environment. *Microbiological Reviews* 1987; 51; 365-379.

[3] Schwan HP, Schwarz G, Maczuk J and Pauly H. *J. Phys. Chem.* 1962; 66:2626.

[4] Sasaki S, Ishikawa A and Hanai T. Dielectric Properties of Spherical Macroion Suspensions. 1. Study on Monodisperse Polystyrene Latex. *Biophys. Chem.* 1981; 14:45-53.

[5] Green NG and Morgan H. Dielectrophoretic investigations of sub-micrometer latex spheres. *J. Phys. D: Appl. Phys.* 1997; 30:2626-2633.

[6] Huang Y, Hölzel R, Pethig R and Wang X-B. Differences in the AC electrodynamics of viable and non-viable yeast cells determined through combined dielectrophoresis and electrorotation studies. *J. Phys. Med. Biol.* 1992; 37: 1499-1517.

[7] Ortega-Vinuesa J.L., Bastos-González D. and Hidalgo-Álvarez R. Comparative studies on physically adsorbed and chemically bound IgG to carboxylated latexes, II. *J. Col. Int. Sci.* 1995; 176: 240-247.

[8] Duncan S, Glover LA, Killham K and Prosser JI. Luminescence-based detection of activity starved and viable but nonculturable bacteria. *Appl. Environ. Microbiol.* 1994; 60; 1308-1316.

[9] Novitsky JA and Morita RY. Morphological characterisation of small cells resulting from nutrient starvation of a psychrophilic marine vibro. *Appl. Environ. Microbiol.* 1976; 32: 617-622.

[10] Novitsky JA and Morita RY. Survival of psychrophilic marine vibro under long-term nutrient starvation. *Appl. Environ. Microbiol.* 1977; 33: 635-641.

[11] Novitsky JA and Morita RY. Possible strategy for the survival of marine bacteria under starvation conditions. *Mar. Biol.* 1978; 48: 289-295.

[12] Dawson MP, Humphrey BA and Marshall KC. Adhesion: a tactic in the survival strategy of marine vibrio during starvation. *Curr. Microbiol.* 1981; 6:195-199.

[13] Amy PS and Morita RY. Starvation-survival patterns of sixteen freshly isolated open-ocean bacteria. *Appl. Environ. Microbiol.* 1983; 45: 1109-1115.

[14] Zhou X-F, Markx GH, Pethig R and Eastwood IM. Differentiation of viable and non-viable bacterial biofilms using electrorotation. *Biochim. Biophys. Acta* 1995; 1245: 85-93.

[15] Diaper JP and Edwards C. The use of fluorogenic esters to detect viable bacteria by flow cytometry. *J. App. Bacteriology* 1994; 77; 221-228.

[16] Kashket EV. Effects of aerobiosis and nitrogen source on the proton motive force in growing *Escherichia coli* and *Klebsiella pneumoniae* cells. *J. Bacteriology* 1981; 146; 377-384.

[17] Kashket EV. Proton motive force in growing *Streptococcus lactis* and *Staphylococcus aureus* cells under aerobic and anaerobic conditions. *J. Bacteriology* 1981; 146; 369-376.

Chapter 6

Macromolecules

6.1 Introduction

The electrical properties of DNA solutions are characterised to a large extent by their chemical composition, structure and internal interactions. Lengths of DNA are distinguished by the pattern of Adenine, Cytosine, Guanine and Thymine bases on the phosphate backbone. It is this unique combination of chemicals which gives us our genetic make-up.

Electrorotation measurements have been shown to be sensitive enough to detect the presence or absence of viable or non-viable bacteria, both in a qualitative and quantitative way. The previous chapter showed that it is possible to perform this analysis in a rapid assay, much faster than existing techniques. Since, it was possible to detect even the presence of the antibody on the surface of the bead, the assay has been extended to test a system which could be used for the detection of DNA.

As in the previous experiments, detection is still by physical observation using a light microscope therefor the antibodies were first attached to a larger particle a latex bead of 5.2μm in length. Although the antibody-labeled particles provide distinct and coherent electrorotation characteristics of their own, the addition more protein to their surface results in marked changes of their electrorotation characteristics. The electrorotation characteristics are further changed when the additional protein is conjugated with a more conductive object, such as a gold particle or FITC. It has been possible to clearly detect the presence of secondary and tertiary antibodies using the electrorotation assay. There is the potential for applying this technique as a rapid and precise assay for the detection of unique DNA sequences, which is particularly applicable to the healthcare industries.

6.2 Results

6.2.1 Detection of DNA primers

Electrorotation experiments were performed on both DNA-labeled latex beads and clean uncoated latex beads. 2mm diameter electrodes were used for these experiments.

Several experiments were performed on DNA-labeled latex beads and presented here are a sample of the best results. The results presented in figure 6.1 display the electrorotation characteristics for the 'Primer One', when attached to a latex particle. The spectra displays the usual high and low frequency co-field peaks centered around 500kHz and 100Hz and with average magnitudes of $5.7\pm1.1 ms^{-1}V^{-2}$ and $8.5\pm1.1 ms^{-1}V^{-2}$, respectively. It should be noted the that the speeds of rotation are very low, compared to those seen in previous chapters, and that the errors are very significant, up to ±17.5%.

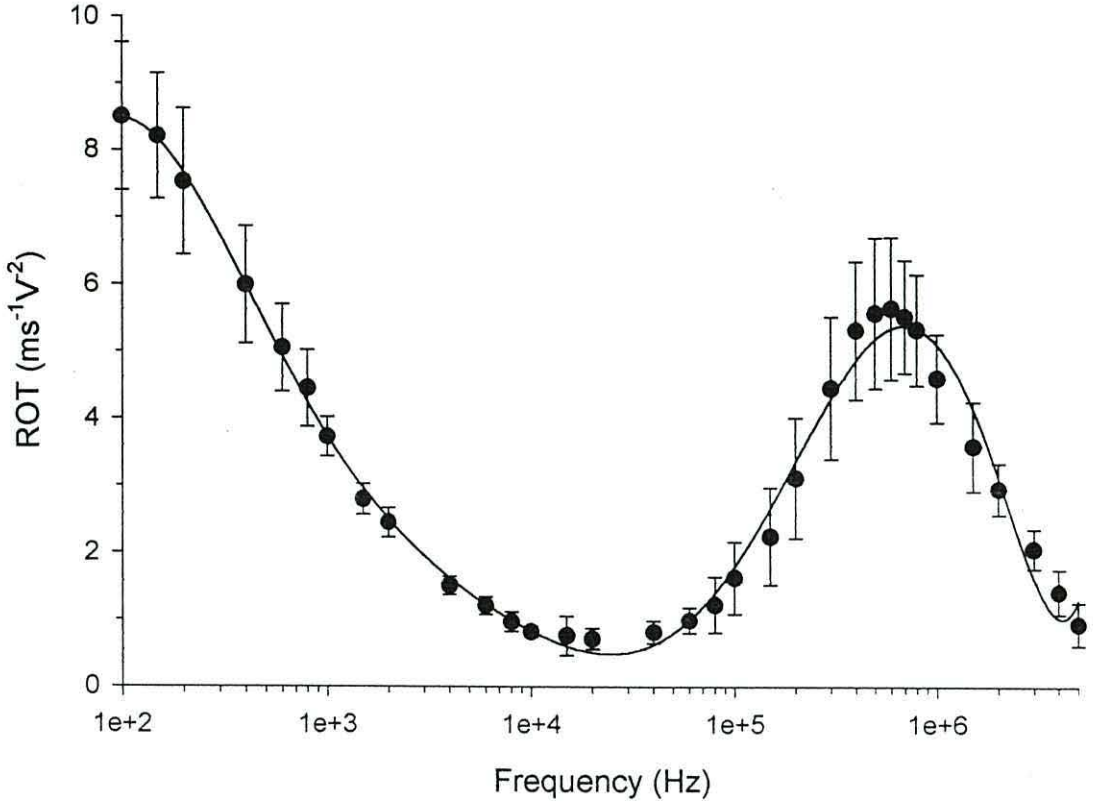

Figure 6.1. Electrorotation spectra of primer one.

Figure 6.2 displays the electrorotation results for 'Primer Two', when attached to a latex particle. The high and low frequency peaks are centered around 300kHz and 150Hz with average magnitudes of $8.6\pm0.3 ms^{-1}V^{-2}$ and $7.0\pm2.6 ms^{-1}V^{-2}$, respectively. Again, it should be noted the that the speeds of rotation are very low, compared to those seen in previous chapters, and that the errors are very significant, up to ±38%.

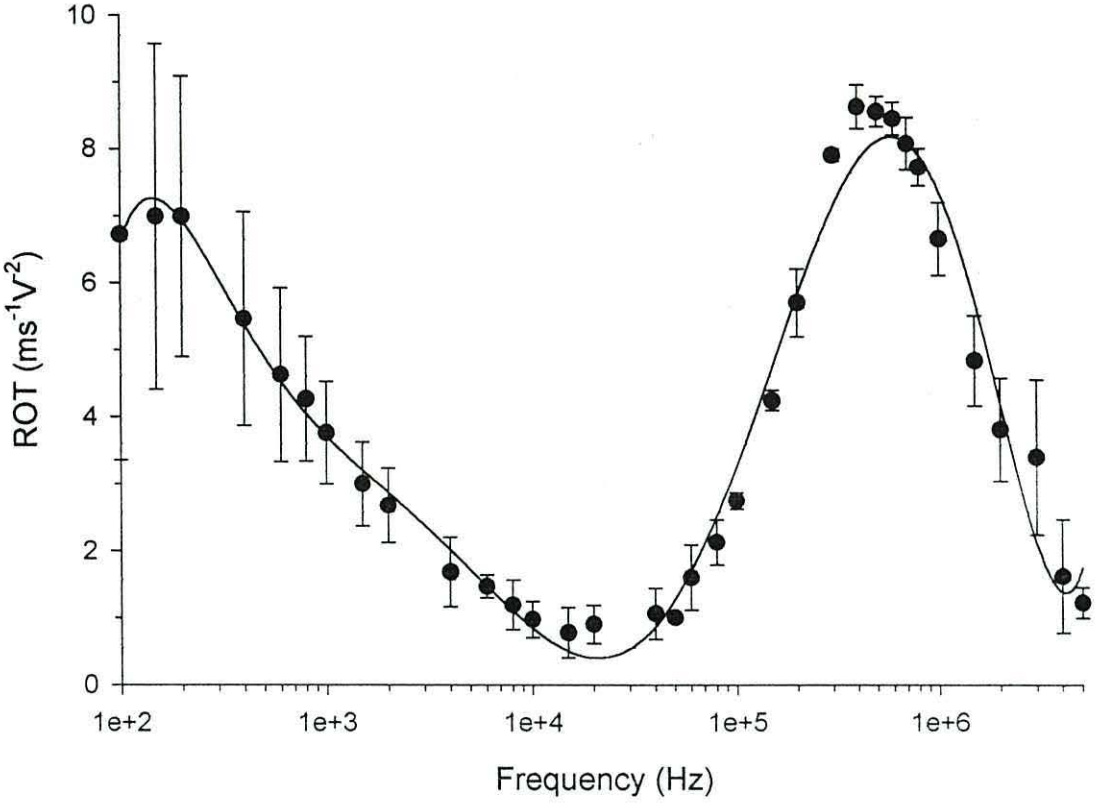

Figure 6.2. Electrorotation spectra of primer two. The error bars represent the minimum and maximum deviations only.

Further investigations of the primers yielded similar results. That is, two peaks of similar frequency and magnitude to those presented here, however, it was not always possible to distinguish between the two different primers' electrorotation characteristics and very significant errors were observed in all samples.

6.2.2 Primary antibody

In this experiment antibody, monoclonal anti-gram positive antigen antibody, developed in mice, was covalently attached to latex particles. The electrorotation spectra of antibody coated beads were analysed, see figure 6.3. As previously demonstrated in Chapter 5, throughout the frequency range monitored (100 Hz to 5 MHz) the antibody-coated beads were observed to rotate in the same sense as the applied rotating field. The

spectrums are characterised by two co-field rotation peaks - a low-frequency peak centred around 100 to 300Hz and a high-frequency peak centred around 200k to 400kHz. The error bars are the 95% confidence of the standard deviation. The results show a repeatable coherent effect especially around the areas of interest:

High frequency peak magnitude: 76.2 +/-4.9 $ms^{-1}V^{-2}$

Low frequency peak magnitude: 100.2 +/-6.7 $ms^{-1}V^{-2}$

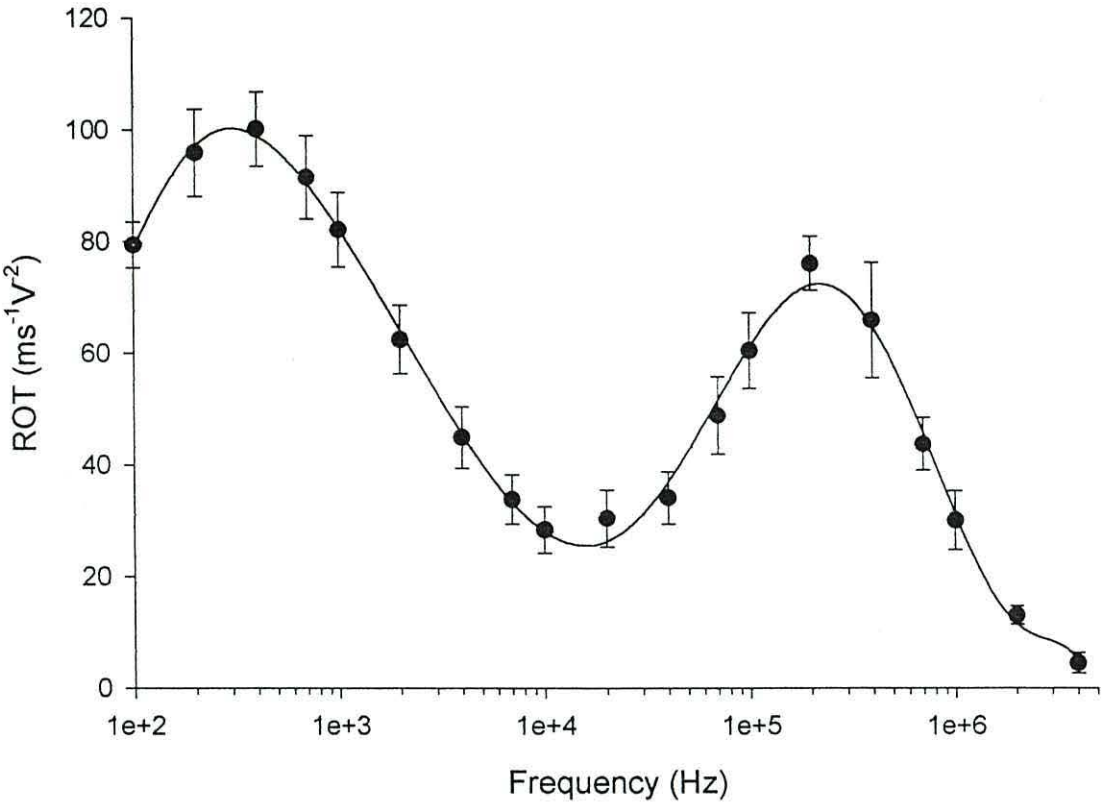

Figure 6.3. Electrorotation spectra of latex particles coated with primary antibody. Error bars are the 95% confidence of the standard deviation.

6.2.3 Secondary antibody

A sample of the beads used in the previous experiment were mixed with a secondary antibody, Anti-Mouse IgG, developed in a goats. The electrorotation spectra of the 'two layer' system was analysed, see figure 6.4. The error bars are the 95% confidence of

the standard deviation. The results show a repeatable but less coherent effect than was observed with just the single antibody system:

High frequency peak magnitude: 37.9 +/-7.5 $ms^{-1}V^{-2}$

Low frequency peak magnitude: 79.9 +/-20.1 $ms^{-1}V^{-2}$

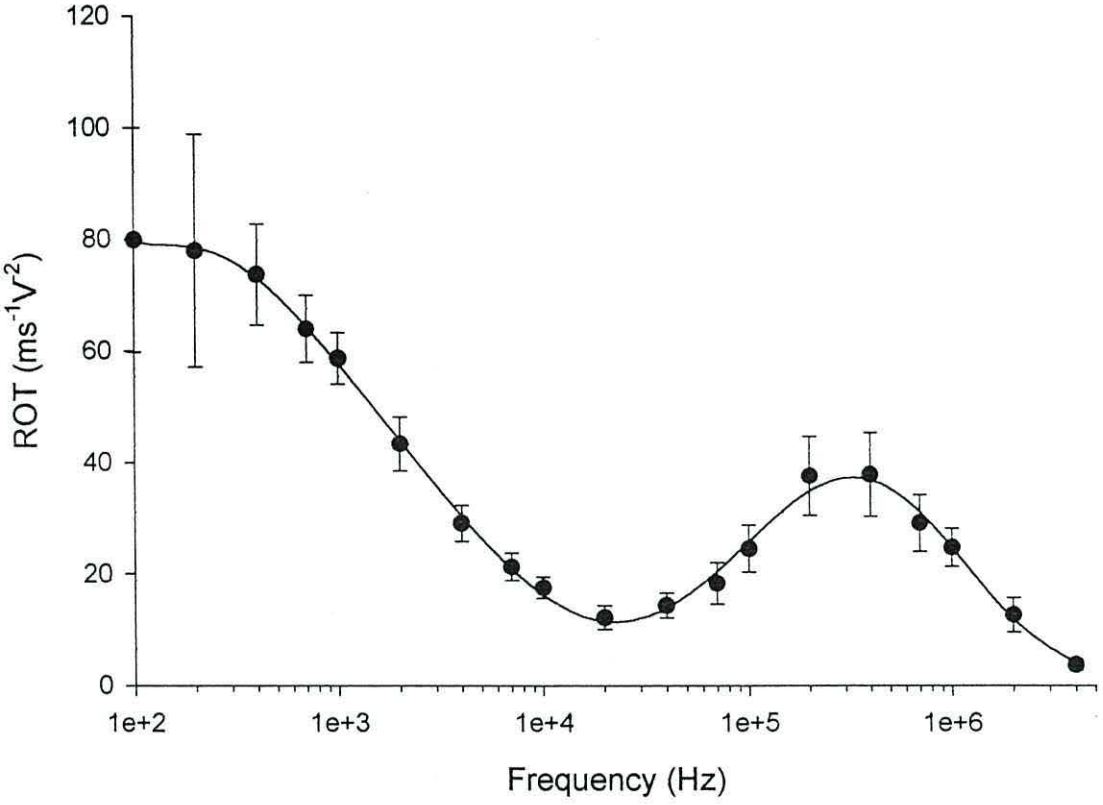

Figure 6.4. Electrorotation spectra of latex particles coated with primary antibodies and secondary antibodies. Error bars are the 95% confidence of the standard deviation.

6.2.4 Tertiary FITC conjugated antibody

Samples of the beads used in the previous experiment were mixed with a further antibody, FITC Conjugated Rabbit Anti-Goat. The presence of the tertiary antibody was detected using fluorescence microscopy. The electrorotation spectra of the 'three layer' system was analysed, see figure 6.5. The error bars are the 95% confidence of the

standard deviation. The results show a repeatable and more coherent effect than was observed with secondary antibody:

High frequency peak magnitude: 56.9 +/-10.9 $ms^{-1}V^{-2}$

Low frequency peak magnitude: 97.3 +/-6.6 $ms^{-1}V^{-2}$

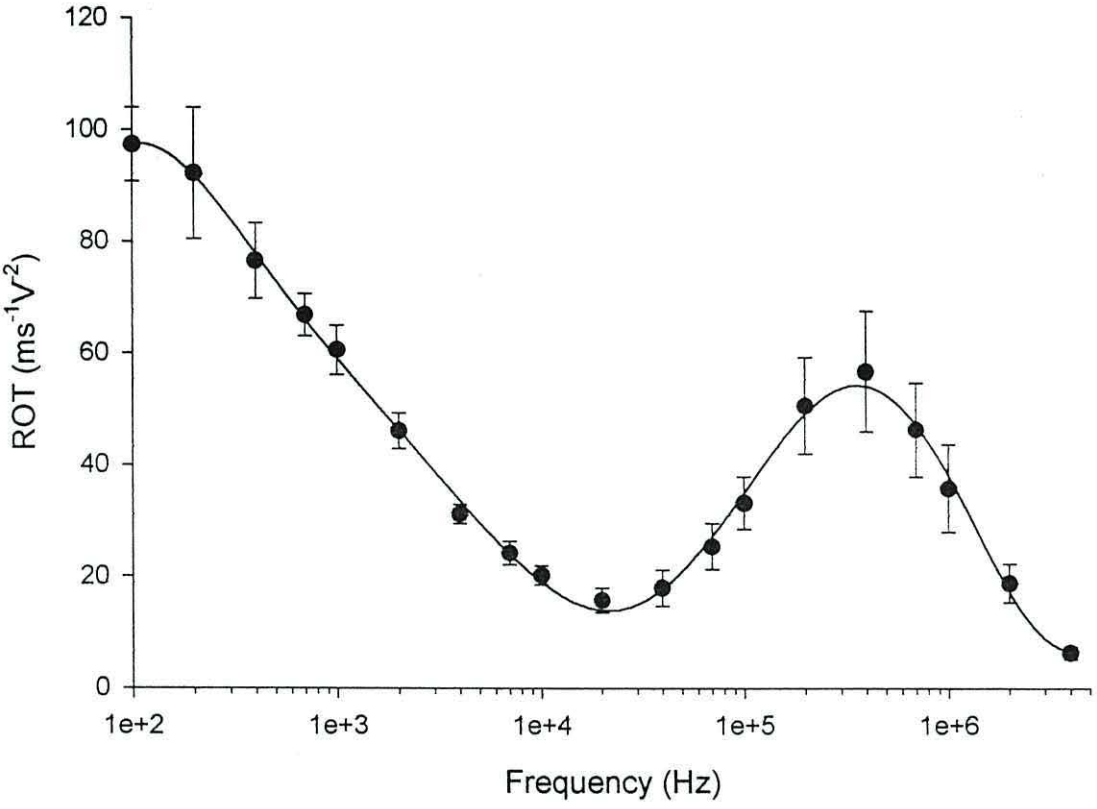

Figure 6.5. Electrorotation spectra of latex particles coated with primary antibodies, secondary antibodies and tertiary FITC-conjugated antibodies. Error bars are the 95% confidence of the standard deviation.

6.2.5 Summary of 'three layer' FITC antibody coated beads

Figure 6.6 compares the electrorotation results of the primary, secondary and the FITC-conjugated tertiary antibodies.

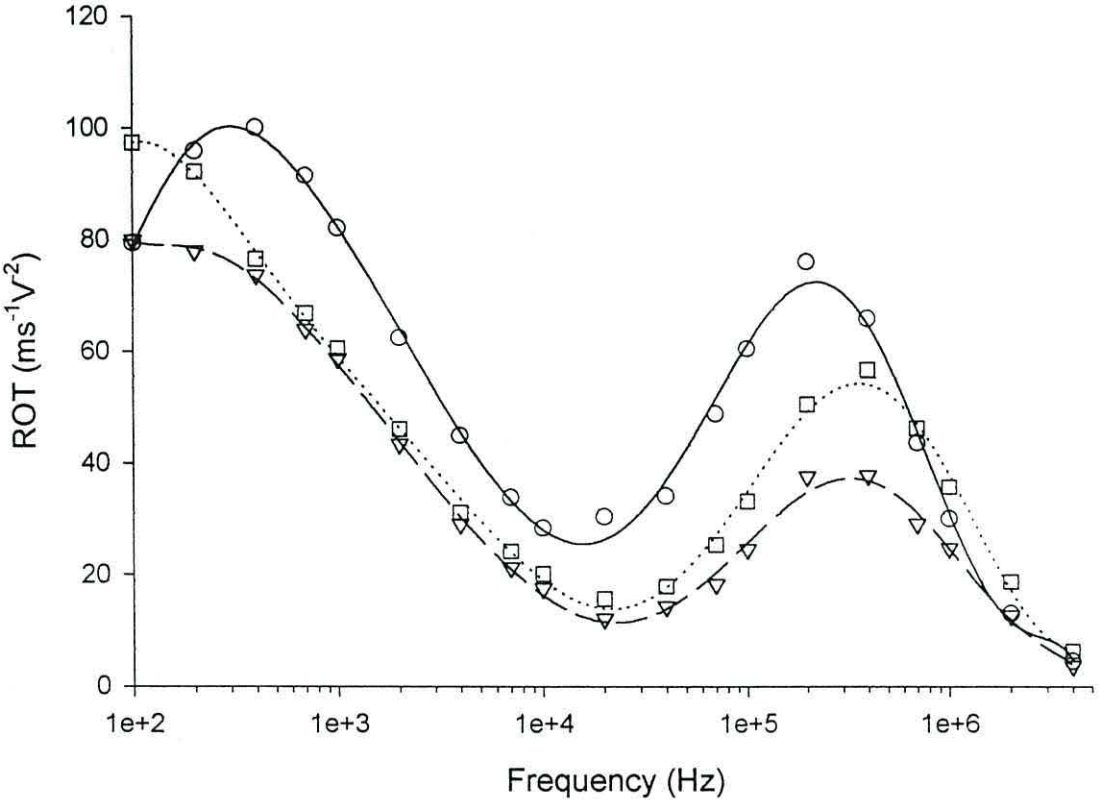

Figure 6.6. Electrorotation spectra of latex particles coated with only primary antibody(○), with additional secondary antibody (▽) and with a tertiary FITC-conjugated antibody added (□).

Addition of the secondary antibody results in a reduction in peak magnitudes, a halving of the high frequency peak magnitude, and the low frequency peak magnitude reduced by one fifth. In addition, the peak frequencies are increased slightly.

The tertiary antibody has a FITC conjugate and can be considered to be more conductive than an antibody without this conjugate. Addition of this tertiary FITC-conjugated antibody to the system results in an increase in the high frequency peak

magnitude, to lie between that for the primary antibody coated beads and the secondary antibody coated beads. The low frequency peak is increased in magnitude, to approximately the same as for the primary antibody coated beads.

6.2.6 Tertiary gold conjugated antibody

A sample of the beads used in the secondary antibody experiment, see section 6.2.3, were mixed with a further antibody, 10nm diameter gold conjugated rabbit anti-goat. The presence of this antibody was confirmed by the addition of a fourth antibody to the bead, FITC Conjugated Sheep Anti-Rabbit, and observation of the particle using fluorescence microscopy. The aim of this experiment was to drastically increase the surface conductivity of the beads so as to be able to easily differentiate between this set of beads and those with just secondary antibodies on the surface. The electrorotation spectra of the system was analysed, see figure 6.7. The error bars are the 95% confidence of the standard deviation. The results show a repeatable and more coherent effect than was observed with secondary antibody:

High frequency peak magnitude: 85.2 +/-5.9 $ms^{-1}V^{-2}$

Low frequency peak magnitude: 158.58 +/-12.8 $ms^{-1}V^{-2}$

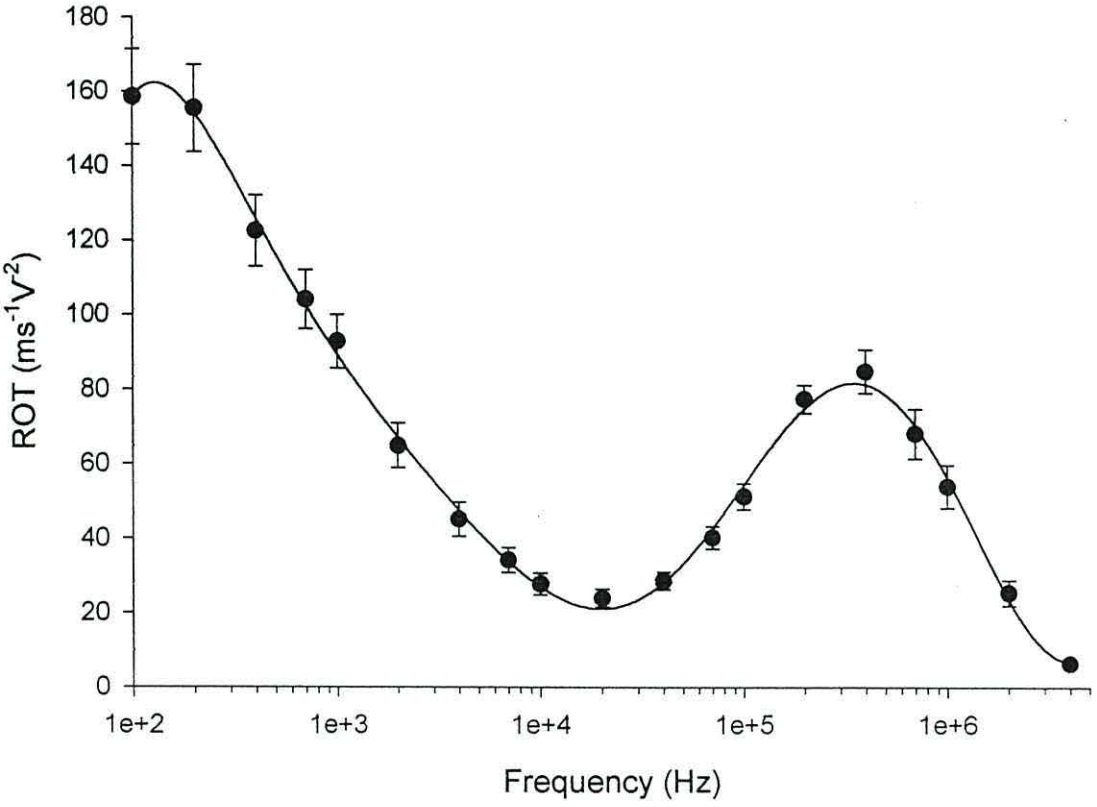

Figure 6.7. Electrorotation spectra of latex particles coated with primary antibodies, secondary antibodies and tertiary gold-conjugated antibodies. Error bars are the 95% confidence of the standard deviation.

6.2.7 Summary of 'three layer' gold antibody coated beads

Figure 6.8 compares the electrorotation results of the primary, secondary and the FITC-conjugated tertiary antibodies.

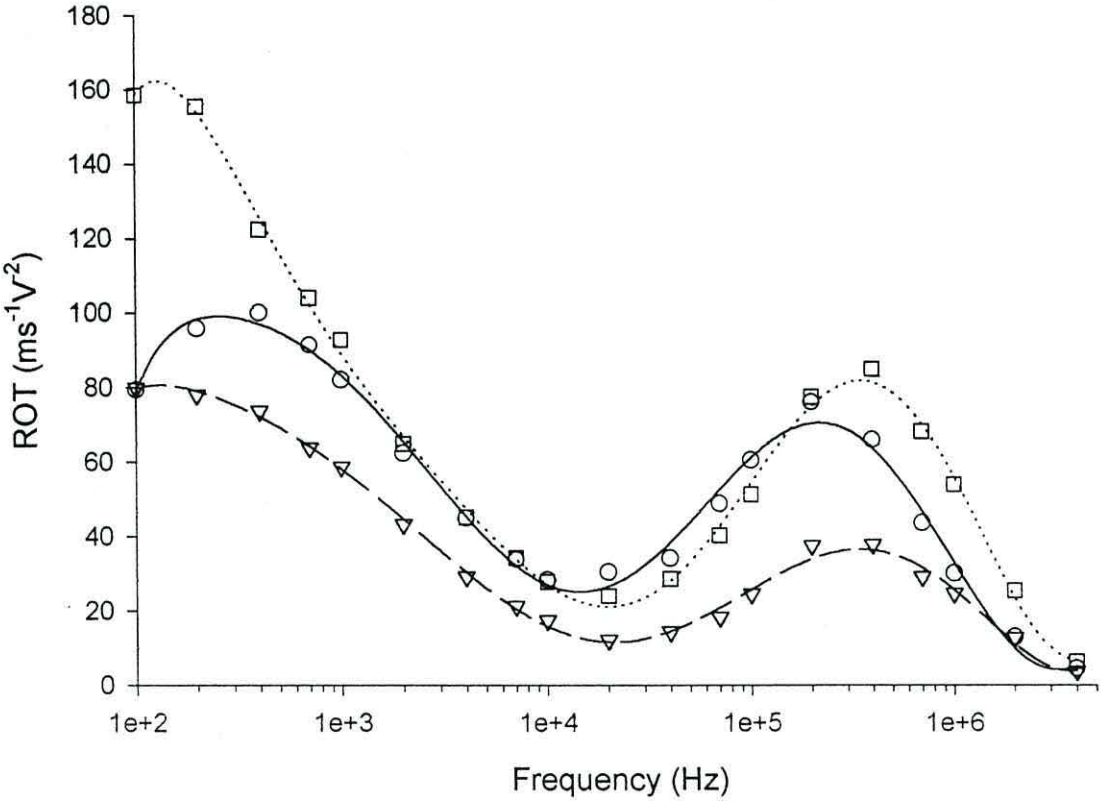

Figure 6.8. Electrorotation spectra of latex particles coated with only primary antibody (○), with additional secondary antibody (▽) and with a tertiary gold-conjugated antibody added (□).

Figure 6.8 shows that the electrortation spectrum of antibody-coated beads are significantly altered when additional antibodies are added to the system. Addition of the secondary antibody results in a reduction in peak magnitudes, a halving of the high frequency peak magnitude, and the low frequency peak magnitude reduced by one fifth. In addition, the peak frequencies are increased slightly.

Addition of the tertiary gold-conjugated antibody to the system has an acute affect. The tertiary antibody has a 10nm gold particle conjugated to it and can be considered to be more conductive than an antibody without this conjugate. Instead of reducing the

magnitudes further, the low frequency peak magnitude nearly doubles and the high frequency peak magnitude is more than doubled.

6.2.8 MatLab Modeling

The single shell MatLab model was used to analyse all of the data reported in this chapter. The result are summarised below in Table 6.1. The results were obtained by maintaining the following parameters: $a1 = 3\ \mu m$, $A = 0.09$ and $Kb = 20\ nSm^{-1}$.

The values for *Kc2* and *Ks* were used to adjust the result for the high frequency peak. An increase in *Kc2*, suspending medium conductivity, results in an increase in the peak frequency and a decrease in the magnitude. Increasing *Ks*, the surface conductivity, results in an increase in the magnitude, but does not affect its peak frequency.

The values for *t* and *b* were used to model the low frequency peak. Increasing *a* results in reduction in the peak frequency. Increasing *t* increases the steepness of the peak.

The results show a good agreement with each other, however, it does show some spurious calculated results, namely that for the suspending medium conductivity. The suspending medium was 430 μSm^{-1} PBS solution. In order to model the high frequency peak the suspending medium needs to be set to a value of between three and six times that measured.

Latex Particle Coating	MatLab Modeling Results			
	High Frequency Peak		Low Frequency Peak	
	Suspending medium conductivity (Sm^{-1})	Particle Surface conductivity (Sm^{-1})	Low Frequency Dispersion (t)	Relaxation Distribution Factor
Primer 1	2.6 m	220 p	20	0.73
Primer 2	2.2 m	220 p	60	0.66
Primer 2	2.6 m	260 p	60	0.66
Primary Antibody	1.2 m	138 p	11	0.77
Secondary Antibody	1.2 m	130 p	11	0.77
Tertiary FITC Antibody	1.2 m	133 p	1000	0.54
Tertiary Gold Antibody	1.2 m	143 p	180	0.50

Table 6.1 Summary of MatLab results obtained using the single-shell model and the results reported in this chapter.

6.3 Results and Discussion

6.3.1 Detection of DNA primers.

Section 6.2.1 presented results to show that DNA-labeled latex beads provide distinct electrorotation characteristics. Comparing primer one with primer two, the high frequency peak magnitude increased from 5.7 to 8.6 $ms^{-1}V^{-2}$ and the frequency decreased from 500 to 300 kHz. The low frequency peak magnitude decreased from 8.5 to 7.0 $ms^{-1}V^{-2}$. It should be noted that errors of up to 38% were observed in this system.

The origin of the two dispersions[1, 2] was discussed in the Latex Particles chapter. The high frequency dispersion is generally assigned to the Maxwell-Wagner interfacial polarisation mechanism and the lower frequency dispersion has been interpreted as a

relaxation of the electrical double layer associated with the surface charge of the particle[3].

For the case where a clean bead is coated with an antibody, analysis of a single shell model[4] indicates that the change in the electrorotation spectrum arises as a result of a decrease in the effective conductivity of the bead's surface. Typical results calculated in the Latex Particles Chapter show the surface conductivity to be calculated as approximately 370 pSm^{-1}, compared to a value of approximately 220 pSm^{-1} for the DNA coated particles. This result is related to the fact that the uncoated latex particles have carboxyl surface functional groups, which results in their surface being able to support a relatively high surface conductivity associated with the percolation of counter-ions.

Ortega-Vinuesa et al[5] found that binding of the antibody results in a reduction of net negative surface charge. They covalently bound IgG antibody to carboxylated latex particles and studied the effect on the electrophoretic mobility. They found, for a pH 8.0, in a 30 mM potassium bromide solution the electrophoretic mobility of antibody coated beads was reduced from $-3.75*10^{8}$ m^2/Vs to $-1.75*10^{8}$ m^2/Vs on the addition of antibody.

Looking at these two primers in isolation although both primers exhibit similar rotation magnitudes it could be said that there are significant enough differences between the two spectra to be able to identify different DNA primers. These results could be explained by an increase in the surface conductivity of the primer two system, or the differences could be due to a slight increase in the suspending medium conductivity.

The main source of errors was thought to be due to a variation in the amount of DNA on each bead. The beads were prepared using the single step coupling procedure which was thought to be the source of this problem. The carbodimer activated process works

by forming an intermediate product, an active ester, with any carboxylate groups. The active ester then attracts any nucleophiles around it, namely amine groups. This is how the bead-primer complex forms. If the primer was phosphorylated, attachment could occur through the 5'-end, however, the primers used did not have phosphorylated ends and all attachment was via the bases. The amine groups on the adenine, cytosine and thymine bases are attached to a double bonded carbon atom, this makes the nitrogen atom of this group an excellent nucleophile, and is also readily available for bonding. Any or all of these amine groups could be available for bonding to the carboxyl surface groups of the latex bead. This could lead to varying amounts of DNA on different beads giving rise to inconsistent results. Also, according to Bangs Laboratories[6], this method of coupling results in cross linking of DNA. Overall, this method would result in a reduced effectiveness of the primer for a hybridization procedure.

A two step coupling protocol[7] can be used to reduce the cross coupling, however, this significantly increases the amount of time required for preparation of samples. If the 5'-end had a suitably phosphorylated group, from work by Ghosh and Musso[12], it is known that only approximately 50% of the attachment is through the 5'-end. Even this would limit the effectiveness of the primer-labeled bead for any hybridization reactions.

There is a two-step covalent coupling reaction of a carboxylated latex particle with a protein[8]. The first step activates the carboxyl surface groups on the surface of the latex bead. Excess CDI is removed before the introduction of the protein, to prevent activation of any carboxylate groups on the protein. In this way the cross-coupling between proteins is minimised, resulting in a single layer on antibody or protein on the surface of the bead.

Since it is envisaged that the work could result in the monitoring of a PCR reaction or detection of blood analytes it is important to use a reliable method of end attachment. Thus, it is proposed that streptavadin coated beads should be used in conjunction with biotinylated primers, since these can be easily purchased and are relatively easy to detect using conventional methods. It is expected that this will provide a reliable system with primer-labeled beads available for hybridization reactions. The following system could be used:

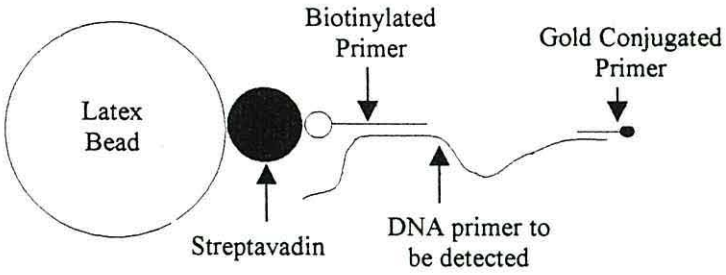

Figure 6.9. DNA-bead complex, using streptavadin coated latex beads, biotinylated primer polymerising with the primer of interest which, in turn, polymerises with a gold conjugated primer.

The proposed system, described in figure 6.9, would consist of streptavadin coated latex beads with biotinylated primers attached. The primers would be a complementary sequence to that which was required for detection. A primer with the complementary sequence would polymerize with the available primer, attached to the bead. It is anticipated that the differences in the electrorotation characteristics may not be significant enough to confirm the detection of the desired primer or may result in very slow rotation speeds. To aid the detection, a third primer would be added to the system, which would be gold conjugated, to increase the surface conductivity and significantly alter the electrorotation characteristics.

The main problem envisaged with this system is that as the number of 'layers' in the system increases the binding between them becomes less energetically favorable, thus preparation times would be significant in length. If the system showed significant enough differences between the 'layers' the system could be simplified. Instead of the initial base-line of streptavadin coated beads with biotinylated primers, the imprecise method of directly attaching the primer could be feasible.

Although all of the materials mentioned can be bought commercially they are expensive. Also, extensive knowledge of PCR reactions would be required. A new simplified system was proposed to test the initial value that this system could provide.

6.3.2 Detection of 'layers' of antibodies on beads

The system, described in figure 6.10, comprises of a primary antibody covalently attached to a latex bead. This is used to attract a secondary antibody. A third antibody is introduced to the system to either aid visible qualification of the system, using a FITC-conjugate, or to significantly alter the electrorotation characteristics of the system, using a gold-conjugate. It is this system that further investigation was based on.

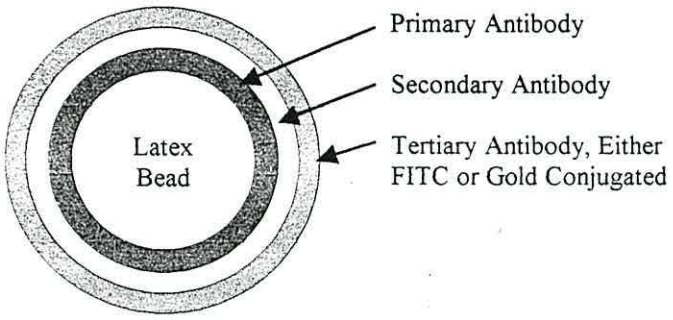

Figure 6.10. Trial system to prove the value of DNA detection using electrorotation.

It was demonstrated that the addition of the secondary antibody results in a reduction in peak magnitudes. This behavior can be modeled using the single–shell MatLab model of the system. The introduction of the second primer results in a decrease in the surface conductivity of the particle from 138 to 130 pS^{-1}.

Addition of the tertiary FITC conjugated has the effect on increasing the surface conductivity of the particle to 133 pSm^{-1}. In addition it has a significant effect on the low frequency peak, resulting in the relaxation distribution factor reducing from 0.77 to 0.50 and the relaxation time increasing from 11 to 1000 s.

Addition of the tertiary gold conjugated antibody to the system has an acute affect. The tertiary antibody has a 10nm gold particle conjugated to it and therefore is significantly more conductive than an antibody without this conjugate. Instead of reducing the magnitudes further, which would be the result of a non-conjugated antibody, the low

frequency peak magnitude nearly doubled and the high frequency peak magnitude is more than doubled, with an increase in its peak frequency too. MatLab modelling of the results shows an increase in the surface conductivity of the particle to 143 pSm^{-1}. In addition it has a significant effect on the low frequency peak, resulting in the relaxation distribution factor reducing from 0.77 to 0.54 and the relaxation time increasing from 11 to 180 s.

Some variability is observed in the results these could be due to several factors but are most probably due to the difference in the amount of antibody attached to the surface of the beads and any frictional effects between the antibody coated beads and the surface of the glass, as was observed in Chapter 5. Since the secondary antibody and tertiary antibodies are bound to the bead surface through the primary antibody any differences in the amount of primary antibody attached to the bead would increase any discrepancies in the amount of secondary antibody on a bead.

6.4 Conclusions

This work clearly demonstrates the sensitivity to be achieved using the electrorotation assay. The attachment of just a single layer of antibody to the surface of a bead produces a significant response. Further attachment of antibody modifies the electrorotation response to an extent where the technique provides a rapid method for determining the presence or absence of a secondary antibody.

To understand the various observed transformations in the electrorotation spectra, mathematical modelling was employed, using MatLab®. The particles were represented using the so-called single-shell model[8,9].

For the case where a clean bead is coated with an antibody, analysis of a single shell model indicates that the change in the electrorotation spectrum arises as a result of a decrease in the effective conductivity of the bead's surface. This result is related to the fact that the uncoated latex particles have carboxyl surface functional groups, which results in their surface being able to support a relatively high surface conductivity

associated with the percolation of counter-ions. Binding of the antibody results in a reduction of net negative surface charge[10].

Binding of additional antibody probably results in a further reduction of net surface charge. As seen in the previous chapter, it also has the affect of increasing the frictional effect between the glass slide and the bead. Addition of the more conductive tertiary antibodies to the system had a different affect. Analysis of the single shell model indicates that this is due to an effective increase in the bead's surface conductivity.

The rate of attachment of antibodies to the beads, and hence the rate of change of their electrorotation spectra, was found to depend on the 'layers' or amount of the antibody in the system and their conjugate. Therefore, by monitoring the changes of electrorotation of a number of beads suspended in a solution containing the antibodies it should in principle be possible to assay for both the presence of and concentration of the desired antibody. The analysis could be accomplished using a recently developed computer-aided technique for the automatic measurement of electrorotation[11].

The system could have been exploited to prove the presence or absence of the secondary antibody in a solution. If the secondary antibody had not been present, the gold-conjugated would not have been bound to the bead complex and the electrorotation characteristics would have remained unchanged. In the same way, this system could be extended to determine the presence or absence of a complementary primer using a system like the one proposed in figure 6.9. The gold conjugated antibody has been demonstrated to be a useful dielectric label.

6.5 References

[1] Schwan HP, Schwarz G, Maczuk J and Pauly H. *J. Phys. Chem.* 1962; 66:2626.

[2] Sasaki S, Ishikawa A and Hanai T. Dielectric Properties of Spherical Macroion Suspensions. 1. Study on Monodisperse Polystyrene Latex. *Biophys. Chem.* 1981; 14:45-53.

[3] Green NG and Morgan H. Dielectrophoretic investigations of sub-micrometer latex spheres. *J. Phys. D: Appl. Phys.* 1997; 30:2626-2633.

[4] Huang Y, Hölzel R, Pethig R and Wang X-B. Differences in the AC electrodynamics of viable and non-viable yeast cells determined through combined dielectrophoresis and electrorotation studies. *J. Phys. Med. Biol.* 1992; 37: 1499-1517.

[5] Ortega-Vinuesa J.L., Bastos-González D. and Hidalgo-Álvarez R. Comparative studies on physically adsorbed and chemically bound IgG to carboxylated latexes, II. *J. Col. Int. Sci.* 1995; 176: 240-247.

[6] Bangs LB. New developments in particle-based tests and immunoassays. 1993. The Latex Course. Bangs Laboratories, Inc.

[7] Bastos-González D., Ortega-Vinuesa J.L., Nieves F. J. De Las and Hidalgo-Álvarez R. Carboxylated latexes for covalent coupling antibodies, I. J. Col. Int. Sci. 1995; 176: 232-239.

[8] Huang Y, Hölzel R, Pethig R and Wang X-B. Differences in the AC electrodynamics of viable and non-viable yeast cells determined through combined dielectrophoresis and electrorotation studies. J. Phys. Med. Biol. 1992; 37: 1499-1517.

[9] Zhou X-F, Markx GH and Pethig R. Effect of biocide treatment on electrorotation spectra of yeast cells. Biochim. Biophys. Acta 1996; 1281: 60-64.

[10] Ortega-Vinuesa J.L., Bastos-González D. and Hidalgo-Álvarez R. Comparative studies on physically adsorbed and chemically bound IgG to carboxylated latexes, II. J. Col. Int. Sci. 1995; 176: 240-247.

11 Zhou X-F, Burt JPH and Pethig R. Automatic cell electrorotation measurements: studies of the biological effects of low-frequency magnetic fields and of heat shock. J. Phys. Med. Biol. 1998; 43: 1075-1090.

Conclusions and Recommendations for Future Work

This thesis contains the results for uncoated non-spherical latex particles, the first investigation of the coliform bacteria, namely *Escherichia coli* and *Bascillus subtilis*, and the bound biomacromolecules using primarily the dielectric technique of electrorotation. Chapter two contains a review of dielectrics and electrorotation, and, to a lesser extent dielectrophoresis and travelling wave. It was identified that, although latex particles have been used for many years in immuno-assays there have been few investigations into the affects of coating the particle surface's with biomacromolecules and bacteria on their dielectric properties.

Both *E. coli* and *B. subtilis* are of importance to human health as they can cause both food spoilage and illness. In 1999 *E. coli* O157 VTEC was confirmed as causing illness in over 1000 people in England and Wales[1]. The Standing Committee for Water Analysis high-lighted the need for improved detection of coliform bacteria, of which *E. coli* is the primary indicator, and for the reduction in the number of false positives[2].

Current techniques for the detection and viability determination of bacteria have their disadvantages, so a sensitive detection method that could do both is seen, especially by the water industry, as a useful tool. The aim of the experimental work presented in chapter 5 in this thesis was to show whether the electrorotation technique could be used as a tool for determining the physiological state of viable and non-viable bacteria and their concentration when attached to latex particles. The latex particles are used as a 'hook' to attach the bacteria of interest. As well as distinguishing those that are potentially infective (revealed through measurement of their physiological state) it is also of interest to investigate whether the technique could be used to determine different species of bacteria therefore both *E. coli* and, to a lesser extent, *B. subtilis* was investigated.

In addition, it was shown that the detection of blood analytes, such as DNA, are of importance to human health with the National Advisory Council for Human Genome Research[3] identifying the need for reliable, cheap methods of testing for blood analytes. The aim of the experimental work presented in chapter 6 in this thesis was to show

whether the electrorotation technique could be used as a tool for detecting proteins, in the form of DNA and antibodies, when attached to latex particles. As before, the latex particles are used as a 'hook' to attach the antibody of interest. As well as detecting the presence of proteins the technique was also investigated for its ability to detect the presence of specified proteins by using antibodies against the proteins of interest. It was anticipated that the addition of extra protein may not have a significant affect on the electrorotation spectra, therefore the effect of adding a third, more conductive layer , a gold conjugated antibody, was also investigated.

In Chapter 4 it was demonstrated that uncoated elliptical particles have distinct electrorotation characteristics. These characteristics were largely affected by changes in the suspending medium conductivity and pH and the surface properties of the particles. Coherent repeatable results were obtained for carboxylated elliptical particles suspended in 430 μSm^{-1} PBS solution and were therefore suitable to be used as a reliable basis for the work in the following chapters Various authors are actively investigating the dielectric properties of these particles, however, there appears to be two main subjects that require further investigation, the origin of the low frequency dispersion and the 'aging' affect. In addition, some anomalous results were observed that were not in agreement with the single-shell MatLab model, such as the affect of increasing ionic strength of the electrorotation properties of the particles and the calculation of the suspending medium conductivity. Although the MatLab modelling results were useful in helping to draw conclusions or substantiate theories, the disparity between experimental and theoretical results needs further investigation.

In Chapter 5 it was demonstrated that it was possible to detect the presence of antibodies bound to the surface of latex particles and to detect the presence of bound viable and non-viable bacteria at single organism level. At certain frequencies the direction of the rotation torque was reversed for the presence of viable bacteria. This is the first description of the effect of adherent bacteria on a non-biological particle on its electrorotational properties. Further work to elucidate the precise cause of the observed changes needs to be done, in particular to determine the differences arising due to the

loss of viability to avoid the possibility of the technique providing false-negative or false-positive viability indications. It was observed that the spectra of the bacteria could change with time. Further work is required to understand the precise physiological changes occurring within the bacteria.

The technique was shown, in principle, to be able to be able to assay both the concentration and the viability of the *E. coli*. However, it may be difficult, in a concentrated system to accurately assess the number attached and relative viability, since the spectra for viable and non-viable are similar in shape. Work is required to determine the exact state of the bacteria attached to the surface of the particle.

This work went on to demonstrate that gram positive bacteria, *B. subtilis*, can also be detected using the electrorotation assay. As with the *E. coli*, the attachment of just one bacterium to the surface of a bead produces a significant response but different to that obtained for *E. coli*. The technique provided a method for determining the difference between the two bacteria investigated here although direct comparisons of the two are difficult due to the differences in length. A more comprehensive study of the *B. subtilis*, similar to that for *E. coli* would be of interest, and a determination of the precise cause of the differences between *B. subtilis* and *E. coli* are required.

Chapter 6 demonstrated that it was possible to detect the presence of nucleic acids of the surface of the particle. It was also shown that 'layers' of antibody could be detected and distinguished. The addition of up to three 'layers' of antibody provided distinct electrorotation characteristics of their own. The addition of gold-conjugated antibodies in the system was shown to have a marked affect on the spectra and is useful as a possible dielectric-label. Further work is required to transfer this prototype system to a actual situation, such as the detection of DNA, as is discussed in this chapter.

Publications arising from this work

Hodgson CE and Pethig R. Determination of the Viability of *Escherichia coli* at the Single Organism Level by Electrorotation. Clinical Chemistry. 1998. 44(9): 2049-2051.

Hodgson CE and Pethig R. Micro-Electrode Devices for the Assay and Manipulation of Bioparticles Based on A.C. Electrokinetic Effects. Poster for Clinical Chemistry Conference, Oakridge. 1998.

Hodgson CE, Bone S and Pethig R. Electrorotation Assay for the Rapid Detection and Viability Determination of *Escherichia coli*. Poster for Electrokinetic Phenomena '98, Salzburg. 1998.

References

[1] PHLS Vero Cytotoxin-Producing *Escherichia coli* O157 Fact Sheet. Updated: 22 March 2000.

[2] Standing Committee of Analysts. An evaluation of presence-absence tests for coliform organisms and *Escherichia coli*. 1996. HMSO Publications.

[3] National Advisory Council for Human Genome Research, National Center for Human Genome Research, National Institutes of Health, U.S. Department of Health and Human Services. Published in the *Journal of the American Medical Association* 1994; 271:785.

Appendix A – Single Shell MatLab Model

```
%  barebead.m
%
% Electrorotation response for clean latex bead.
% The bead(radius a1) is assigned a bulk conductivity kb,
%  a surface conductance Ks and bulk permittivity kp1.
% The suspending medium has conductivity kc2 and permittivity
%  kp2.
%
% The anomalous low frequency dispersion is 'taken into
% account'
%
% All parameters in SI units (metres, S/m, F/m).
%
% p0: permittivity of free space.
%
% ki   (i=1,2) complex permittivity of each phase.
%
% ------------------------------------------------------------

clear;

% Depolarization factor D (=0.333 for a sphere)
 D=0.333;

 p0=8.854e-12;

% Bead surface conductance Ks, bulk conductivity kb, anomalous
% conductivity dispersion parameters A and t, with distribution
% of relaxation times given by factor "b".


 % Bead radius a1
 a1=6e-6;

 A=9e-2;
 t=50e-1;
 Ks= 0.88e-9;
 kb= 2e-8;

 f=logspace(2.9,7,80);
 zeroline=f-f;

 w=2*pi*f;
 x=i*w*t;
 b=0.61;
 y=x.^b;

 kc1=kb+(2*Ks)/a1 + A ./(1+y);
 kp1=3*p0;
```

```
% Suspending medium conductivity and permittivity
  kc2=2.35e-3;
  kp2=79*p0;

  k1=kp1-i*kc1 ./w;

  k2=kp2-i*kc2 ./w;


m=(k1-k2) ./(3*(k2+D*(k1-k2)));

rm=real(m);
im=imag(m);

plot(log10(f),-4.2e3*im,'-', log10(f),zeroline,'-');

% plot(log10(f),rm,'-', log10(f),zeroline,'-');

hold on

% Experiment date :12-6-96, lab book one, page 118-119,122-123.

% Uncoated latex beads, with carboxyl surface function groups

% in 1/10,000 PBS solution.

fexp0 = [5000 3000 1500 1000 800 600 400 200 150 100 80 60 ...
40 20 15 10 8 6 4 2 1.5 1.0 0.8 0.6 0.4 0.2 0.15   0.1]*1000;

 rot0 = [16.1 38.23 84.95 110.27 119 126.49 116.44 77.12 ...
   67.09 48.64 42.05 39.12 32.4 34.43 39.11 44.71 52.62 ...
   59.78 82.59 107.82 127.03 164.04 182.11 194.46 248.67 ...
   287.22 279.48 237.07];

plot(log10(fexp0),rot0,'o',log10(f), zeroline,'-');

hold on

xlabel('Log Frequency (Hz)')
ylabel('Rotation Rate (milli-revs/sec)')

text('position',[5.0 380], 'string','o uncoated bead')
```

Appendix B – Multi Shell MatLab Model

```
% ecoli1.m
% Latex bead with antibody coating plus viable E.coli
% The bead(radius a1) is assigned a bulk conductivity
kb,
%  a surface conductance Ks and bulk permittivity kp1.
% The antibody + E.coli coating(thickness d, radius a2)
has
% conductivity kc2, permittivity kp2.
% The suspending medium has conductivity kc3 and
% permittivity kp3.
%
% All parameters in SI units (metres, S/m, F/m).
%
% pO: permittivity of free space.
%
% ki  (i=1,2,3) complex permittivity of each phase.
%

% keff3: effective complex permittivity of bead plus
% antibody plus E.coli coating.
%
% ------------------------------------------------
----

clear;

% Antibody+E.coli layer effective thickness d; bead
radius
% a1

  d=7e-9;
  a1=3e-6;
  a2=a1+d;

% Depolarization factor D (=0.333 for a sphere)
 D=0.333;

 pO=8.854e-12;

% Bead surface conductance Ks, bulk conductivity kb,
% anomalous conductivity dispersion parameters A and t,
% with distribution of relaxation times given by factor
% "b".

A=10e-2;
t=800e-1;
Ks=1.2e-9;
kb= 1e-8;

f=logspace(2.9,7,80);
```

```
zeroline=f-f;

w=2*pi*f;
x=i*w*t;
b=0.74;
y=x.^b;

kc1=kb+(2*Ks)/a1 ;
kp1=4*p0;

% Assigned antibody+E.coli layer conductivity and
% permittivity
   kc2=0.8e-5 + A ./(1+y);
   kp2=30*p0;

% Suspending medium conductivity and permittivity
  kc3= 6.2e-3;
  kp3=79*p0;

  k1=kp1-i*kc1 ./w;
  k3=kp3-i*kc3 ./w;

  k2=kp2-i*kc2 ./w;

  am1=a1^3;
  am2=a2^3;

%  m=(k1-k3) ./(3*(k3+D*(k1-k3)));

   keff2=k2 .*(am2*(k1+2*k2)-2*am1*(k2-k1)) ...
./(am2*(k1+2*k2)+am1*(k2-k1));

  m=(keff2-k3) ./(3*(k3+D*(keff2-k3)));

  rm=real(m);
  im=imag(m);

  plot(log10(f),-1.8e3*im,'--', log10(f),zeroline,'-');

  hold on

% Experiment date :28-8-97, lab book three, page 65-66.
% Latex beads with carboxylate surface functional
% groups, with E.coli antibody coating and one viable
% E.coli on the surface in 170mM manitol with 1/10,000
% PBS solution .


fexp3 = [5000 2000 1500 1000 800 600 400 200 150 40 ...
20 15 10 6 1.5 1.0]*1000;

 rot3 = [22.15 44.3 51.02 43.33 39.55 35.62 16.71 ...
```